Reduced order modeling of nonlinear structural systems using nonlinear normal modes and invariant manifolds

Eric Pesheck

REDUCED ORDER MODELING OF NONLINEAR STRUCTURAL SYSTEMS USING NONLINEAR NORMAL MODES AND INVARIANT MANIFOLDS

by

Eric Pesheck

A dissertation submitted in partial fulfillment
of the requirements for the degree of
Doctor of Philosophy
(Mechanical Engineering)
in The University of Michigan
2000

Doctoral Committee:

Professor C. Pierre, Co-Chair
Professor S.W. Shaw, Co-Chair
Professor R. Scott
Assistant Professor Dawn Tilbury
Professor Armin Troesch

For Renée

ACKNOWLEDGEMENTS

I wish to express thanks to Professor Christophe Pierre for his generous support and guidance, to Professor Steve Shaw for his helpful insights, to Renée for her patience and motivational skills and, finally, to my parents, for getting me here.

TABLE OF CONTENTS

LIST OF FIGURES

Figure

LIST OF APPENDICES

Appendix

CHAPTER I

INTRODUCTION

In many applications, it is advantageous to achieve a thorough understanding of the dynamics of a complex structure. These structures may take many forms, including rotorcraft, buildings, bridges, vehicles, and aircraft. Modern design tools, such as Finite Element Analysis, have greatly expanded the modeling detail available for such structures. However, these techniques are limited in their abilities, especially when the structure dynamics enter a nonlinear regime. This limitation is often countered by sacrificing either time — through a large, expensive computer model, or accuracy — through the elimination of possibly significant influences. As it is of continual interest to expand the performance envelope of such structures, they are becoming lighter, more flexible and, consequently, more nonlinear. This trend points out a need for efficient, analytically rigorous, widely applicable analysis techniques for nonlinear structural systems. The primary goal of this dissertation is to address this need through the further development and implementation of model reduction through nonlinear normal modes. This work extends the invariant manifold approach developed by Shaw and Pierre [1–4], with the primary goal of obtaining accurate reduced order models of nonlinear structural systems.

1.1 Background

1.1.1 Nonlinear Structural Vibration

This work focuses on the intersection between structural dynamics and nonlinear vibrations. Of course, there has been a great deal of previous work in both the areas of nonlinear vibrations (see reference [5] for a thorough summary), and nonlinear structural analysis [6–11]. However, the two fields have typically dealt with problems of entirely different magnitudes.

Much of the literature regarding nonlinear vibrations is predicated upon simple analytic models. Generally, these models are either based on a two- or three-degree of freedom lumped mass formulation [12–15], or a Galerkin discretization of a governing partial differential equation (PDE) to similar order [16–19]. These low-order models are useful for predicting many general behaviors, and have been used with much success for the modeling of systems with few active degrees of freedom. However, many of these techniques are quite analytically involved, and not easily applicable to systems with complex PDEs or large numbers of degrees of freedom (i.e., finite element models).

Much of the literature pertaining to nonlinear structural analysis is concerned with the problem of model reduction [8, 10, 11], as modern computational techniques yield structural systems which may contain many thousands of degrees of freedom. Hence, full system analysis is both impractical and expensive. In linear systems, this difficulty may be effectively eliminated through the use of modal analysis [20], which allows motions of interest to be decoupled from the original system, and analyzed separately. This coordinate transformation enables the practical vibration analysis of most finite element systems. In nonlinear structures, there is no simple transformation which produces decoupled motions, but model reduction is still necessary for

efficient analysis. Although there are many techniques for choosing discretization functions (or vectors), some nonlinear effects are invariably ignored in the reduction process. Hence, either the reduced order model must be relatively large, so as to minimize ignored effects, or the model accuracy may suffer through lost effects. These missing effects may cause significant model errors, such as overlooking an internal resonance or ignoring critical modal interactions.

1.1.2 The "Nonlinear Mode"

The expense associated with obtaining accurate reduced-order nonlinear models has led to a considerable desire for some sort of "nonlinear modal analysis" which would be analogous to its linear counterpart. Initial work in this area was done by Rosenberg [21], Rand [13, 22], and Atkinson and Taskett [12], among others. In these works the definition of the *nonlinear normal mode* as a *vibration in unison* of the system's degrees of freedom was developed. This definition allows all generalized displacements to be expressed in terms of a single coordinate, and requires that all coordinates reach a maximum simultaneously, as well as pass through the system equilibrium position simultaneously. Furthermore, many of these results use energy methods and symmetry arguments, and thus require that the system be conservative and that the nonlinearities be of odd order. Further details may be found in reference [21], which is quite thorough. A large number of subsequent works have developed nonlinear normal modes for specific systems using these early definitions. These efforts may be divided into two general categories, those which begin with discrete, lumped mass, models [14, 23–25], and those which discretize continuous systems into – essentially – lumped mass models [17–19, 23, 26–28]. These reduced systems typically have no more than three degrees of freedom, and the nonlinear normal mode

assumptions, together with some perturbation methods, are often used to determine either the geometry of the normal mode, or the time response, or both. Often the work is simplified by either assuming that the normal mode exhibits similar motion (constant mode shape), or that the response is harmonic.

1.1.3 The Invariant Manifold

The invariant manifold approach, developed by Shaw and Pierre [1–3], and further developed in conjunction with Boivin [29–31], generalizes the previous definition of the nonlinear normal mode. Shaw and Pierre define the nonlinear normal mode as *a motion which lies on a two-dimensional invariant manifold in the systems phase space*. Here, "invariant" indicates that any motion initiated on the manifold will remain on it for all time. The invariant manifolds formulated by Shaw and Pierre were parameterized by a single position-velocity pair. This corresponds to describing all system degrees of freedom in terms of the position and velocity of one degree of freedom. This formulation lends itself naturally to the linear modal coordinates of the nonlinear system, as the invariant manifold is naturally tangent to the modes of the linearized system. This methodology is closely related to center manifold theory, which is primarily used for bifurcation analysis [32], and inertial manifold theory, in which the manifolds act as attractors for the system dynamics [33]. The invariant manifold approach produces PDEs which govern the geometry of the manifold independently of energy or symmetry considerations. This allows for the rigorous analysis of a wide variety of nonlinear systems, including systems with linear and nonlinear damping, non-symmetric nonlinearities and gyroscopic coupling. Furthermore, constraints on the velocity, such as energy conservation or harmonic motion, conceptually reduce the manifold from a surface to a curved line within the phase

space, a reduction which is consistent with the original definition of the nonlinear normal mode.

The PDEs which describe the nonlinear manifold are generally not solvable in closed form and have typically been approximated through a polynomial expansion in the manifold coordinates. This expansion produces numerous coefficients which may be obtained in a systematic fashion. This approach was utilized by Boivin for the analytical generation of the invariant manifold for a pinned-pinned beam constrained at the center by a cubic spring. Considerable detail may be found in his thesis [34].

Unlike linear modes, the nonlinear normal modes, while individually invariant, will interact during a general motion. Hence, the study of multiple-mode responses may not be achieved through the superposition of individual nonlinear normal modes. Instead, the entire set of reduced coordinates must be assumed prior to the reduction process, yielding a manifold of dimension $2M$, for M chosen modes. This approach allows for the study of true multi-mode motions of nonlinear systems, including internal resonances, without assuming periodic behavior or restricting relative magnitudes. As with the single mode case, the manifold may be approximated with a polynomial in the $2M$ manifold coordinates, where the polynomial coefficients may be determined in a complex, but systematic fashion [29]. This systematic approach enables the reduction and analysis of systems with many degrees of freedom, i.e., large structural systems.

Ultimately, the invariant manifold approach approximates all degrees of freedom, or modes, as functions of several chosen coordinate pairs. These functions may be substituted back into the original equations of motion to obtain a system which is dependent only on the chosen coordinates, yet includes the low-order effects of all

modes or degrees of freedom. The dynamics of the reduced order system may then be investigated without the uncertainty associated with modal truncation. Furthermore, all displacements and velocities may be reconstructed from the reduced dynamics.

The concept of the invariant manifold has been applied in a similar context by others [35–37], and several additional authors [38–43] have extended, approximated, and modified the formulation of Shaw and Pierre.

1.2 Dissertation Outline

The remaining chapters of this dissertation have been or are destined to be published in technical journals. Though they have been revised to achieve greater continuity, some repetition will occur. Hopefully, this repetition will underscore the main points of the work without causing undue confusion or boredom.

In Chapter II, a general formulation is symbolically reduced to yield equations which govern the free response of a set of chosen modes. The initial formulation was chosen to be in modal coordinates, and allows for all possible cubic and quadratic couplings in the modal displacements. This accounts for the most common structural nonlinearities while decoupling the system to linear order. The reduced equations and subsequent results are verified against earlier work, and further investigations on finite-element based models are carried out.

Chapter III consists of a case study: the general reduction procedure from Chapter II is employed for the study of a simple rotorcraft blade model. The equations of motion governing the transverse (flapping) and axial (extensional) motions of a rotating beam are developed and transformed into modal form. These equations are then reduced using the polynomial-based invariant manifold. Simulation results are used to evaluate the effectiveness and applicability of the reduction method.

In Chapter IV a new approach is developed which utilizes a nonlinear Galerkin formulation to overcome many of the weaknesses associated with the previous approach. The new formulation utilizes a coordinate transformation to produce modified PDEs governing the invariant manifold geometry. The new PDEs are then solved over a chosen domain using an expansion in the new manifold coordinates. This procedure requires more computational effort for each system reduction, but is both more accurate and more adaptable. Results are shown for both a simple discrete system, and a more complex finite element model.

Chapter V revisits the rotating beam case study, now applying the nonlinear Galerkin methods to produce more accurate results. The reduction procedure is modified by discretizing one dimension of the manifold domain, making the PDE solution procedure considerably more efficient. This analytical modification, and its effects on the efficiency of the method are discussed. Results are presented which build on those of both chapters III and IV.

Finally, the results are summarized in Chapter VI, and conclusions are drawn regarding the completed research, and the associated contributions to the field. Following this is a discussion of the ways in which this work may be extended. Recommendations are made regarding both theoretical and applied extensions of this work.

1.3 Contributions

The primary contributions of this work are as follows:

• The analytic solution for the asymptotic invariant manifold of a subset of structural vibrations problems. These solutions have been implemented to allow for the automatic generation of high-dimensional invariant manifolds and the corresponding

reduced-order equations of motion.

• The formulation of a transformation procedure which allows the previous analytic solutions to be applied to systems undergoing harmonic (and, in a generalized form, periodic) forcing. The practical use of this approach is also evaluated.

• An analytic formulation for the coupled flapping and extensional motions of a rotating beam with both quadratic and cubic nonlinearities. This model is placed in modal form, and reduced-order models are generated through the aforementioned analytic solutions.

• A new solution method for the manifold-governing partial differential equations is formulated. This novel approach uses a nonlinear Galerkin method to achieve reduced-order models of greater accuracy, utility and adaptability. This approach largely dispenses with the significant analytical work associated with the previous methods, allowing it to be easily applied to a vast array of nonlinear structural systems.

CHAPTER II

MODAL ANALYSIS-BASED REDUCED-ORDER MODELS FOR NONLINEAR STRUCTURES – AN INVARIANT MANIFOLD APPROACH

2.1 Introduction

2.1.1 Motivation

The vibratory response of mechanical systems in the low frequency range is typically dominated by a relatively small number of active modes. In linear systems, the reduction of a large-scale dynamic model to a smaller model consisting of these dominant modes is made mathematically precise by using the standard tools of modal analysis and superposition [20]. The use of these tools is made possible by the dynamic independence of the linear modes. However, for nonlinear systems, these tools are not directly applicable and one must use a different framework to conduct analysis and achieve insight into the dynamics. It has been known for some time that one can define individual normal modes for special classes of nonlinear systems [21], but these modes represent very special, periodic responses of conservative systems.

A repeated criticism of this approach is that it considers only these special families of solutions and, while these may be of mathematical interest, their utility is questionable, as particular initial conditions are needed in order to observe such mo-

tions in the full model. However, one can put the same criticism to linear vibration systems, the main difference being that one can cleanly separate modal dynamics in linear systems. This separability allows one to build reduced-order models by modal projection and superposition, whereby the number of modes kept is a function of the frequency range of interest. Accurate reduced-order models (ROM) can be made by ignoring modes which are known to contain only a small amount of energy, and to which energy will not flow. One goal in the present line of work has been to develop a parallel approach for a class of nonlinear systems.

Conventionally, nonlinear systems have been analyzed through projection of the governing equations onto the modes of the linearized system. This method often requires the concurrent simulation of many modes to achieve accuracy, and results in a model which is both bulky and computationally expensive. The approach presented herein allows the minor affects of many modes to be incorporated into the dynamics of a chosen subset through the addition of higher order nonlinear terms. This reduced-order model may allow for much more efficient analysis of the original system. Unlike many other methods within nonlinear dynamics, the invariant manifold approach is easily applicable for systems of arbitrary size, making it ideally suited for the analysis of real structural systems, including those described by finite element models (FEM).

2.1.2 Background

The work of Rosenberg [21] laid out the fundamental concepts for normal modes of discrete, conservative, nonlinear systems. Results on the stability and bifurcation of these modes have been the subject of many subsequent investigations; see, for example, the results and citations in [44], as well as [45]. Recent work has generalized the concept of nonlinear normal modes to a wide class of systems, including

continuous systems, systems with dissipation, gyroscopic terms, etc., as described in the works of Shaw and Pierre [2, 3]. This approach utilizes invariant manifold theory as a systematic means of generating reduced-order models. Initially, the existence and dynamics of individual nonlinear modes were investigated. Subsequently, extensions for studying the dynamics of internally resonant modes were also considered [31, 39, 44]. The introduction of multi-mode invariant manifolds that capture the dynamics of several modes and their essential interactions has allowed for a generalization of mode-based model-order reduction for nonlinear systems.

It should be noted that the approach used herein differs in some significant ways from the modes obtained by proper orthogonal decomposition, in which one uses the steady-state response of a dissipative system in order to generate a reduced-order model that is optimal in the sense that it captures the most energy possible using a predetermined number of modes. This requires that one fix the system parameters and obtain the response before generating the modes, and it uses a linear subspace as the underlying manifold ([46], and [47], describe some examples for mechanical structures). In contrast, the method described herein allows one to generate approximate manifolds directly from the equations of motion (e.g., from finite element models) in terms of the system parameters, before solving them. The method is computationally practical for large-scale, weakly nonlinear structural systems.

2.1.3 Chapter Outline

The remainder of this chapter is organized as follows. First, the definition and construction method for individual nonlinear normal modes are discussed. The extension to multi-mode manifolds is then described. Illustrative results are provided throughout the chapter, which closes with a summary of the results and the associ-

ated conclusions.

2.2 Individual Nonlinear Normal Modes

2.2.1 Invariant Manifolds

Roughly speaking, an invariant manifold for a dynamical system is a subset of the phase space on which the system behaves like a lower-dimensional dynamical system. The term invariant indicates that for motions initiated on the manifold, the corresponding solution remains on that manifold for all time. For example, in a linear, N-degree-of-freedom, undamped, non-gyroscopic, vibratory system, a single-mode motion is one in which the system behaves in a synchronous manner, essentially like a linear single degree of freedom system, and this motion is restricted to a plane in the phase space of the system (in the first-order, state-space formulation), corresponding to a given eigenvector. For systems with gyroscopic and/or dissipative terms, single mode responses also exist and correspond to motions on a single plane in the state space, but they are generally manifested by non-synchronous motions of the system components. A similar notion works for nonlinear systems as well, only the single degree of freedom response is that of a particular nonlinear differential equation, and the manifold in the state space is generally not planar. For smooth nonlinear systems, under some quite general circumstances, the manifolds are simply curved surfaces which are tangent to the manifolds of the linearized system. These geometric ideas have been put into mathematical expressions and a constructive methodology has been derived for a wide class of systems [2, 3]. This procedure, described below, is straightforward and requires only that one be able to solve the linear eigenvalue problem, followed by a series of linear equations for the coefficients that describe the nonlinear manifolds and their attendant dynamics.

2.2.2 Definition of a Nonlinear Normal Mode

A normal mode for a nonlinear system is a motion which takes place on a two-dimensional invariant manifold in the system's phase space. This manifold passes through the stable equilibrium point of interest and, at that point, is tangent to a two-dimensional eigenspace of the system linearized about that equilibrium. On this manifold the system dynamics are governed by an equation of motion involving a pair of state variables, that is, it behaves like a single degree of freedom system.

2.2.3 Construction of Nonlinear Normal Mode Manifolds

In order to determine the equations for such a nonlinear manifold and the dynamics of its associated mode, several steps are necessary. For the purposes of this derivation, it is assumed that the dynamics of an N-degree of freedom system may be expressed in the following first-order form:

$$\begin{cases} \dot{\mathbf{x}} = \mathbf{y} \\ \dot{\mathbf{y}} = \boldsymbol{f}(\mathbf{x}, \mathbf{y}) \end{cases} \tag{2.1}$$

where $\mathbf{x^T} = [x_1, ..., x_N]^T$ and $\mathbf{y^T} = [y_1, ..., y_N]^T$ represent generalized positions and velocities (either modal or physical coordinates) and $\boldsymbol{f}^T = [f_1, ..., f_N]^T$ represents the position- and velocity-dependent forces acting on the system. (Note that the inversion of an inertia operator may be required in order to express the equations in this form.) In order to search for a particular nonlinear mode, it is assumed that the manifold is parameterized by a single position-velocity pair of state variables. That is, if the dynamics of a particular position-velocity pair are known, then all other positions and velocities may be determined from them. In other words, the system degrees of freedom are "slaved" to a pair of "master" degrees of freedom. For the kth nonlinear mode, $u_k = x_k$, and $v_k = y_k$ are chosen as the "master" states and

express the remaining "slave" states as:

$$\begin{cases} x_i = X_i(u_k, v_k) \\ \qquad\qquad\qquad\qquad i = 1, \ldots, N \quad i \neq k \\ y_i = Y_i(u_k, v_k) \end{cases} \tag{2.2}$$

These are, essentially, a set of constraint equations which are to be determined. For a linear system, these relationships are linear, resulting in planar manifolds — precisely the eigenspaces. The process for obtaining solutions for the functions $(X_i(u_k, v_k), Y_i(u_k, v_k))$ begins by taking a time derivative of the constraint equations, yielding

$$\begin{cases} \dot{x}_i = \dfrac{\partial X_i}{\partial u_k}\dot{u}_k + \dfrac{\partial X_i}{\partial v_k}\dot{v}_k \\ \qquad\qquad\qquad\qquad i = 1, \ldots, N \quad i \neq k \\ \dot{y}_i = \dfrac{\partial Y_i}{\partial u_k}\dot{u}_k + \dfrac{\partial Y_i}{\partial v_k}\dot{v}_k \end{cases} \tag{2.3}$$

These equations relate the rates of change of all the state variables to those of u_k and v_k, through the constraints. They are modified by using the equations of motion, (2.1), to eliminate $\dot{x}_i$ and $\dot{y}_i$, including the case that $\dot{u}_k = v_k$ and $\dot{v}_k = f_k(\mathbf{x}, \mathbf{y})$. This eliminates all time derivatives from the equation. Next, one substitutes the constraints, equation (2.2), everywhere the state variables appear, leaving a set of partial differential equations for the functions $(X_i(u_k, v_k), Y_i(u_k, v_k))$ in terms of (u_k, v_k). These $2N - 2$, time-independent, partial differential equations govern the geometry of the kth manifold and are given by:

$$\begin{cases} \dfrac{\partial X_i}{\partial u_k}v_k + \dfrac{\partial X_i}{\partial v_k}f_k = Y_i \\ \qquad\qquad\qquad\qquad i = 1, \ldots, N \quad i \neq k \\ \dfrac{\partial Y_i}{\partial u_k}v_k + \dfrac{\partial Y_i}{\partial v_k}f_k = f_i \end{cases} \tag{2.4}$$

In general, it is not possible to determine an exact solution for the X_i's and Y_i's, since doing so is equivalent to obtaining a family of solutions to the original equations of

motion. (They can be solved exactly in some special cases involving symmetries, and these exceptional cases have received lots of attention; see *similar modes* in [44]). However, one can obtain approximate solutions in terms of series expansions for a wide class of problems. This limits the practical application of analytical techniques to weakly nonlinear systems with smooth nonlinearities. However, the development of an automated numerical scheme to solve these equations may allow for more general application. These issues have been the subject of several papers including [4, 23, 40]. Also, it should be noted that Eq. (2.4) may be collapsed into a set of $N-1$ second order partial differential equations in the X_i. These second order equations may also be produced by starting with a second order dynamic formulation, and eliminating time through similar use of the chain rule. This is detailed in Appendix A.

In order to develop approximate solutions for Eq. (2.4) which may be applied to a wide variety of nonlinear structural systems, yet remain somewhat tractable, several assumptions are necessary. In this formulation, the following assumptions are made:

• The original equations of motion (2.1)are decoupled to linear order using the N linear system modes. The system states are therefore the linear modal amplitudes and velocities. This form may be easily obtained for large structural systems, for example using modal analysis in conjunction with a finite element representation.

• Damping is not considered. However, small damping may be added to the reduced set of dynamic equations, as is commonly done in structural dynamic analysis. For large damping, one needs to include it from the outset, resulting in additional terms not encountered below.

• The nonlinearities are of second and third order only in displacement.

• The manifold is single-valued and analytic for the amplitudes under consider-

ation.

This can be generalized to include velocity-dependent linear and nonlinear terms, but again the results are more complicated.

These assumptions allow the equations of motion to be written in the following second-order form:

$$[I]\ddot{\mathbf{x}} + [\Omega]\mathbf{x} + \boldsymbol{f}^{\mathrm{nl}}(\mathbf{x}) = \mathbf{0} \tag{2.5}$$

where

$$[\Omega] = \begin{bmatrix} \omega_1^2 & 0 & 0 \\ 0 & \ddots & 0 \\ 0 & 0 & \omega_N^2 \end{bmatrix}$$

and ω_i is the ith natural frequency of the linearized system. The nonlinear forces acting on the system, $\boldsymbol{f}^{\mathrm{nl}}$, may be expressed as:

$$\boldsymbol{f}^{\mathrm{nl}} = [\alpha]\mathbf{x}^{\mathbf{2}*} + [\beta]\mathbf{x}^{\mathbf{3}*}$$

where $\mathbf{x}^{\mathbf{2}*}$ contains all unique second order combinations, and $\mathbf{x}^{\mathbf{3}*}$ contains all unique third order combinations within the vector $\mathbf{x}$. Consequently, the non-square matrices $[\alpha]$ and $[\beta]$ contain the coefficients for every possible quadratic or cubic coupling in the displacement $\mathbf{x}$. The individual elements in $[\alpha]$ and $[\beta]$ are denoted as:

$$\alpha_{j,l}^{i} \qquad\qquad \beta_{j,l,m}^{i}$$

where i indicates the row in $[\alpha]$ or $[\beta]$; and j, l, m indicate the coupled degrees of freedom. In this notation, the order of the subscripts is incidental, that is, $\alpha_{1,2}^{3} = \alpha_{2,1}^{3}$, and both refer to the same element in $[\alpha]$. Note that in order to obtain these elements, one must transform the nonlinear terms in the original equations of motion,

as expressed in terms of the physical coordinates, into the linear modal coordinates. This task, though messy, is feasible for large systems through automated procedures.

Now f_i, from equation (2.4), may be written as:

$$f_i = -\omega_i^2 X_i - \sum_{j=1}^{N}\sum_{l=j}^{N} \alpha_{j,l}^i X_j X_l - \sum_{j=1}^{N}\sum_{l=j}^{N}\sum_{m=l}^{N} \beta_{j,l,m}^i X_j X_l X_m \tag{2.6}$$

A local solution for the X_i's and Y_i's is sought in terms of u_k and v_k. This will yield all modal positions and velocities as a function of the kth modal position and velocity. An approximate local solution may be found using a polynomial expansion of X_i and Y_i in terms of u_k and v_k as:

$$\begin{cases} X_i &= a_{1,i}^k u_k + a_{2,i}^k v_k + a_{3,i}^k u_k^2 + a_{4,i}^k u_k v_k + a_{5,i}^k v_k^2 \\ & \quad + a_{6,i}^k u_k^3 + a_{7,i}^k u_k^2 v_k + a_{8,i}^k u_k v_k^2 + a_{9,i}^k v_k^3 + \ldots \\ \\ Y_i &= b_{1,i}^k u_k + b_{2,i}^k v_k + b_{3,i}^k u_k^2 + b_{4,i}^k u_k v_k + b_{5,i}^k v_k^2 \\ & \quad + b_{6,i}^k u_k^3 + b_{7,i}^k u_k^2 v_k + b_{8,i}^k u_k v_k^2 + b_{9,i}^k v_k^3 + \ldots \end{cases} \tag{2.7}$$

Thus, the expansion coefficients, $a_{j,i}^k$ and $b_{j,i}^k$, dictate the relation between the "slave" (i) and "master" (k) coordinates, and the problem now becomes that of obtaining these new unknowns.

These coefficients can be determined by substituting equations (2.6) and (2.7) into equation (2.4) and collecting like powers in u_k and v_k. This task is handled most easily by using a symbolic processor such as Mathematica^{TM}, and it yields a set of linear equations for the unknown coefficients. If this process is carried out symbolically for a small system, the results may be analyzed to extend the solution to systems if arbitrary size. Using this approach, the solution for the first order

coefficients is

$$\begin{cases} a^k_{1,i} &= \delta_{ik} \\ a^k_{2,i} &= 0 \\ b^k_{1,i} &= 0 \\ b^k_{2,i} &= \delta_{ik} \end{cases} \tag{2.8}$$

Where δ_{ik} is the Kronecker delta. This implies that the linear coefficients are zero for all $i \neq k$, while for $i = k$ one has simply $X_k = x_k = u_k$ and $Y_k = y_k = v_k$, as expected since the modes are linearly decoupled through the choice of coordinates. (If this choice is not made, the solution for the linear terms in these functions results in an alternative formulation of the eigenvalue problem [34].) The solution for the second order coefficients is:

$$\begin{aligned} a^k_{3,i} &= \frac{\alpha^i_{k,k}(2\omega_k^2 - \omega_i^2)}{\omega_i^2(\omega_i^2 - 4\omega_k^2)} \\ a^k_{5,i} &= \frac{2\alpha^i_{k,k}}{\omega_i^2(\omega_i^2 - 4\omega_k^2)} \qquad\qquad i \neq k \\ b^k_{4,i} &= \frac{-2\alpha^i_{k,k}}{\omega_i^2 - 4\omega_k^2} \end{aligned} \tag{2.9}$$

In addition, $a^k_{4,i} = b^k_{3,i} = b^k_{5,i} = 0$. At third order one obtains, $a^k_{7,i} = a^k_{9,i} = b^k_{6,i} = b^k_{8,i} = 0$, and,

$$\begin{aligned} a^k_{6,i} &= \frac{-C^{1,k}_{1,i} - \beta^i_{k,k,k} + \alpha^k_{k,k} b^k_{4,i}}{\omega_i^2} - \frac{\omega_k^2[C^{1,k}_{2,i} - C^{1,k}_{3,i}(3\omega_k^2 - \omega_i^2)]}{\omega_i^2 D^{1,k}_i} \\ a^k_{8,i} &= \frac{C^{1,k}_{3,i}}{2\omega_i^2\omega_k^2} - \frac{(3\omega_k^2 - \omega_i^2)[C^{1,k}_{2,i} - C^{1,k}_{3,i}(3\omega_k^2 - \omega_i^2)]}{2\omega_i^2\omega_k^2 D^{1,k}_i} \\ b^k_{7,i} &= \frac{-[C^{1,k}_{2,i} - C^{1,k}_{3,i}(3\omega_k^2 - \omega_i^2)]}{D^{1,k}_i} \qquad\qquad i \neq k \\ b^k_{9,i} &= a^k_{8,i} \end{aligned} \tag{2.10}$$

Where the constants $C_{p,i}^{1,k}$, and $D_i^{1,k}$ are defined as:

$$\begin{aligned} C_{1,i}^{1,k} &= \sum_{m=1}^{N} a_{3,m}^{k} \alpha_{k,m}^{i} \\ C_{2,i}^{1,k} &= 2\omega_i^2 \omega_k^2 \sum_{m=1}^{N} a_{5,m}^{k} \alpha_{k,m}^{i} \\ C_{3,i}^{1,k} &= -3(C_{1,i}^{1,k} + \beta_{k,k,k}^{i} - \alpha_{k,k}^{k} b_{4,i}^{k}) - 2\omega_i^2 \alpha_{k,k}^{k} a_{5,i}^{k} \\ D_i^{1,k} &= (\omega_k^2 - \omega_i^2)(\omega_i^2 - 9\omega_k^2) \end{aligned} \tag{2.11}$$

Note that the third-order coefficients depend on the second-order results, as is typical in perturbation expansions.

Once the expansion coefficients are calculated, all degrees of freedom are known in terms of the dynamics of a single mode, through the approximate functions X_i and Y_i.

It bears noting that this polynomial description of the manifold is only accurate in the immediate vicinity of the chosen equilibrium position, and diverges from the "exact" manifold quite rapidly beyond some critical amplitude. This amplitude depends crucially on how near the system is to an internal resonance, since this affects the magnitude of the coefficients. Currently, this amplitude is an unknown function of the system parameters, but it may be possible to determine numerically through comparison of the original and reduced equations of motion.

Also note that the coefficients of the nonlinear terms in the above expansions become singular in the cases for which 1:1, 2:1 and/or 3:1 resonances exist between the linearized frequencies of the mode of interest and one of the contributing modes. In such a case (and even near such cases) an essential modal coupling exists, and the method fails, precisely because the modes cannot be separated in the manner prescribed by the formulation. This is due to the fact that these internal resonances foster dynamic energy exchange between modes, a condition that can be handled by

using the techniques described in Section 2.3.

2.2.4 Nonlinear Normal Modal Dynamics

The expressions obtained for $X_i(u_k, v_k)$ and $Y_i(u_k, v_k)$ may be substituted into the kth equation of motion to produce a single, second order, nonlinear oscillator in u_k and v_k:

$$\dot{u}_k = v_k \tag{2.12}$$

$$\dot{v}_k = f_k(\mathbf{X}, \mathbf{Y}) \tag{2.13}$$

This oscillator governs the local dynamics on the kth nonlinear modal manifold. Due to the third-order expansion of the X_i's and Y_i's an oscillator is generated which contains terms up to ninth order in u_k and v_k. However, in the general case, all terms above fourth order (or, fifth order if $[\alpha] = 0$) would be altered by subsequent (higher order) terms in the manifold expansion, and are therefore not complete and should not be retained in a strict formulation. It should be noted, however, that the primary contributions of the "slave" coordinates to the oscillator are at third order for quadratic nonlinearities, and fifth order for cubic nonlinearities. Hence, if both quadratic and cubic nonlinearities are present, the fifth order terms, although not precise, contain vital information and should not be neglected. Similar arguments may be applied for manifold expansions of any order.

Through this process it is possible to isolate the dynamics of a single nonlinear, non-resonant mode from an N-degree of freedom, nonlinearly coupled system of equations. However, unlike linear modes, nonlinear modes are dynamically coupled, and the dynamics of the individual nonlinear modes do not form a basis for generating the response of the overall structure; that is, they cannot be superimposed.

It is highly desirable to develop a method that allows one to build accurate multi-

mode models, in order to obtain more general reduced-order models of nonlinear structural systems. These are crucial if one has internal resonances, or if it is known that several modes play a significant role in the system response of interest. This issue is tackled in Section 2.3, following the single-mode examples and discussion below.

2.2.5 Example: A Simply Supported Euler-Bernoulli Beam Constrained by a Non-Linear Spring

In order to demonstrate the ideas presented above, the method is applied to a simple problem for which the calculations can be explicitly carried out. The system is a uniform, simply supported Euler-Bernoulli beam of length 1 with a non-linear cubic spring attached at a point $\tilde{s}$ along its length —see Figure 2.1. The beam is assumed to deform in its linear range, so that the linearized system's normal modes are those of the simply supported beam alone (i.e., pure sine waves). The spring is chosen as purely cubic so that it comes into play as amplitudes grow, affecting the modal dynamics. With this choice, the influence of the individual linear modes on the non-linear modes can be computed and easily visualized. For this example $\tilde{s} = 1/2$ is chosen and, as this is a nodal point for all antisymmetric (that is, even numbered) normal modes, they remain unaffected (linear). Therefore, only the symmetric (odd numbered) normal modes are influenced by the non-linear spring and, furthermore, they feature only contributions from the other symmetric linear modes.

The beam has the following equation for transverse motion, in non-dimensional form:

$$\ddot{u} + \lambda u_{,ssss} + \mu u^3 \delta(s - \tilde{s}) = 0 \quad s \in]0, 1[\tag{2.14}$$

where $\lambda = EI/m$, $\mu = \gamma/m$, E is Young's modulus, I is the second moment of area,

m is its mass per unit length, γ is the non-linear stiffness of the spring, s represents the spatial coordinate along the beam, $u(s,t)$ is the transverse deflection of the beam, $(\cdot)_{,s}$ denotes a derivative with respect to s, an overdot represents a derivative with respect to time and $\delta(\cdot)$ is the Dirac function. The associated boundary conditions are $u(0) = u(1) = 0$, and $u_{,ss}(0) = u_{,ss}(1) = 0$. For this example, the values $\lambda = 1$, and $\mu = 10^4$ are used when numerical results are shown.

The beam deflection, $u(s,t)$, is first discretized using the natural modes of the linearized system, $\phi_j(s) = \sin(j\pi s)$,

$$u(s,t) \cong \sum_{j=1}^{N} x_j(t)\phi_j(s) \tag{2.15}$$

where N is the number of terms in the expansion, i.e., the number of terms that would be retained for a linear modal analysis of the non-linear system. Projection of equation of motion onto the ith linear mode yields

$$\ddot{x}_i + \lambda(i\pi)^4 x_i + 2\mu \left[\sum_{j=1}^{N} x_j \sin(j\frac{\pi}{2})\right]^3 \sin(i\frac{\pi}{2}) = 0 \tag{2.16}$$

for $i = 1, \ldots, N$, which can be written in first-order form as

$$\begin{cases} \dot{x}_i = y_i \\ \\ \dot{y}_i = f_i(x_1, \ldots, x_N, y_1, \ldots, y_N) \end{cases} \qquad i = 1, \ldots, N \tag{2.17}$$

where

$$f_i = -\lambda(i\pi)^4 x_i - 2\mu \left[\sum_{j=1}^{N} x_j \sin(j\frac{\pi}{2})\right]^3 \sin(i\frac{\pi}{2})$$

captures the inter-modal coupling effects. This set of differential equations, (2.17), is what is typically simulated in a study of this system's dynamics. If one wanted to know, say, the leading order frequency corrections due to the nonlinearity, one

could use a single mode ($N = 1$) and study the resulting equation of motion, using, for example, a perturbation technique, or even brute-force simulations. However, it is important to note that this approach implicitly assumes that the beam shape remains unaffected by the nonlinearity, even for moderate amplitudes of vibration.

Alternatively, the procedure described above can be applied to equation (2.17) in order to determine the third- or higher-order approximation of the non-linear normal modes of the system. As will be seen, this approach provides the corrections to the mode shapes, as well as more accurate approximations of the modal dynamics at moderate amplitudes. In the present formulation only those expansion coefficients which are present for a conservative, non-gyroscopic system are included; this is merely to simplify the presentation. If one formulates the problem by including all terms out to third order, it will be found that the terms missing here will be zero. In fact, they must be, if the modal response is to be synchronous in the sense that all points on the beam reach their extreme values simultaneously. (Note that the synchronicity condition is not imposed here, it is a consequence of the type of system being considered.)

Of course, the solution to this problem may be obtained through the explicit expressions developed earlier (Eqs. (2.9)-(2.10)), given the expressions for the individual elements of β. This approach yields expressions identical in value to those below, which were developed by Nicolas Boivin during the course of his doctoral work [34]. This work is included here because, (a), it serves to verify the more general formulation developed earlier, (b), the form of the results is relatively simple, making it conceptually informative, and (c), the results below (from [34]) are expanded upon to illustrate key concepts inherent to the invariant manifold approach.

The details of the calculations are not presented here, but they involve the so-

lution of a sequence of linear systems of equations. The kth non-linear mode is expressed by, to third order:

$$x_k = u_k \quad \dot{x}_k = v_k$$

and for $i = 1, \ldots, N$, $i \neq k$:

$$\begin{cases} x_i = \dot{x}_i = 0 & (i \text{ even}) \\ x_i = a_{6,i}^k u_k^3 + a_{8,i}^k u_k v_k^2 + \ldots & (i \text{ odd}) \\ \dot{x}_i = b_{7,i}^k u_k^2 v_k + b_{9,i}^k v_k^3 + \ldots & (i \text{ odd}) \end{cases} \tag{2.18}$$

where, if k is even, $a_{6,i}^k = a_{8,i}^k = 0$, and if k is odd, for $i = 1, \ldots, N, i \neq k$,

$$\begin{cases} a_{6,i}^k = 2\mu(-1)^{\frac{k+i}{2}} \dfrac{(i^4 - 7k^4)}{\lambda\pi^4(i^4 - k^4)(i^4 - 9k^4)} \\ \\ a_{8,i}^k = -12\mu(-1)^{\frac{k+i}{2}} \dfrac{1}{\lambda\pi^4(i^4 - k^4)(i^4 - 9k^4)} \end{cases}$$

and, for all k with $i = 1, \ldots, N, i \neq k, i$ odd:

$$\begin{cases} b_{7,i}^k = -2\lambda(\pi k)^4 a_{8,i}^k + 3a_{6,i}^k \\ \\ b_{9,i}^k = a_{8,i}^k \end{cases} \tag{2.19}$$

As mentioned above, equivalent expressions may be obtained using Eqs. (2.9)–(2.11).

Next, the deflection and velocity of the beam in the kth non-linear mode, $u^k(s,t)$ and $v^k(s,t)$, can be expressed in terms of the kth non-linear modal coordinate, $u_k(t)$, and the associated modal velocity, $v_k(t)$, as

$$u^k(s,t) = u_k \sin(k\pi s) + \sum_{\substack{i \text{ odd} \\ i \neq k}} \left[a_{6,i}^k u_k^3 + a_{8,i}^k u_k v_k^2\right] \sin(i\pi s) + \ldots \tag{2.20}$$

$$v^k(s,t) = v_k \sin(k\pi s) + \sum_{\substack{i \text{ odd} \\ i \neq k}} \left[b^k_{7,i} u_k^2 v_k + b^k_{9,i} v_k^3 \right] \sin(i\pi s) + \ldots \tag{2.21}$$

One can see that the nonlinear normal modes for this system are synchronous by noting that when the modal velocity v_k is zero, the entire velocity field is zero. Similarly, since the nonlinearities are odd (that is, symmetric about the equilibrium), all points along the beam pass through zero simultaneously — specifically, when $u_k = 0$ the entire beam has $u^k(s,t) = 0$. (For an example of a synchronous motion with even order nonlinearities present, in which case the latter observation does not hold, see [4].) Here, $u^k(s,t)$ refers to the deflection of a point located at coordinate s at time t when the system undergoes a motion in the kth non-linear normal mode. It should not to be confused with $u_k(t)$, which is the non-linear modal coordinate and is not meant to represent the motion of any particular point.

The dynamics of the non-linear mode, up to fifth order, are governed by

$$\begin{aligned} \ddot{u}_k \quad & + \lambda (k\pi)^4 u_k + 2\mu \sin^2(k\pi/2) u_k^3 \\ & + 6\mu u_k^3 \left(\sum_{\substack{i \text{ odd} \\ i \neq k}} [a^k_{6,i} u_k^2 + a^k_{8,i} v_k^2] \sin(i\pi/2) \right) \sin(k\pi/2) = 0 \end{aligned} \tag{2.22}$$

for $k = 1, \ldots, N$. Note that each non-linear mode behaves like a single degree of freedom nonlinear oscillator that is decoupled from all other system dynamics. This is a very special system motion that is constructed using dynamic invariance; only a special subset of all initial conditions can initiate such a response. These initial conditions are precisely those that lie on the two-dimensional constraint surface (manifold) in the full system phase space — that is, those which satisfy the "master-slave" relationships between the dynamic variables.

Figures 2.2 and 2.3 show the position and velocity of the beam at 7 equal time intervals during a purely first mode response, as generated by equations (2.20)–(2.22).

Note that the peak velocity distribution in Figure 2.3, and the zero displacement field in Figure 2.2 correspond to the initial configuration. Also note that as the beam undergoes its oscillation, the shape does not remain fixed, and that the spring influence increases with displacement amplitude. Figure 2.4 depicts the most important projection of the modal manifold, showing how the third linear modal amplitude (X_3) depends on the amplitude and velocity of the first mode. (Note that there are corresponding surfaces for all odd order linear modes, but they are less important in this example; the even order modal surfaces lie exactly on the $u_1 - v_1$ plane, confirming that no even modes participate, due to the symmetry of the spring placement) A nonlinear modal response is initiated by using a set of initial conditions that lie on these surfaces, that is, by relating the linear modes in precisely the manner dictated by the "master-slave" invariance constraints. This relation is, of course, amplitude dependent. In particular, for this example, a periodic trajectory is traced out on the manifold, corresponding to the initial conditions in Figures 2.2 and 2.3. Once such a motion is initiated, it will persist for all time.

Figure 2.5 illustrates the error associated with modal truncation. If only the first mode shape is used to discretize the system, all dynamics are constrained to the plane shown. The three-dimensional closed curve (identical to that in Figure 2.4) is not realizable, and its projection (dashed curve) may only be approximated. Both solutions correspond to a single differential equation, but truncation overly constrains the system.

Figure 2.6 shows the peak beam configurations for a set of beam motions with distinct initial energies. (This is not the same as Figure 2.2, which shows a single response at different times.) These are obtained by considering equation (2.20) and taking the zero velocity ($v_k = 0$) configuration for different values of u_k. For the

low amplitude case, the beam shape is nearly that of the linear case, while the beam distorts exactly as expected as the amplitude grows. Note that this is also consistent with the nature of the manifold depicted in Figure 2.4 (at $v_k = 0$).

Figures 2.7–2.8 (also from the thesis of Nicolas Boivin [34]) display simulation results obtained using this procedure, along with results obtained with classical linear modal analyses of the non-linear system performed with various numbers of modeled linear modes. In both figures, the "exact" solution was determined using a linear modal analysis with 25 linear modes; that is, by simulating the 25 degree of freedom system obtained by projecting the equations of motion onto 25 of the linear modes, using initial conditions which lie on the third-order approximation of the nonlinear normal mode manifold in the 50-dimensional phase space. In this particular case it is seen that at least three to five linear modes are necessary to achieve an accuracy comparable to that obtained with a single fifth-order non-linear mode as obtained above. The nonlinear mode results are obtained by simulation of a single second-order differential equation (equation (2.22)), which includes the influence of the other linear modes. In the case where one uses a single linear mode through the entire analysis, the influence of the other linear modes is completely missing, whereas it is naturally embedded in the non-linear normal mode. See Figure 2.8 which compares several simulations, all utilizing only one ODE, to the "exact" solution. It should be noted that the initial displacements shown in these figures include contributions from the "master" mode (u_1), as well as the "slave" modes. Consequently, the initial displacement will vary as additional modes are included i.e., as the manifold is projected into a larger configuration space.

2.2.6 Systematic Implementation

The above example is presented here due to its analytic simplicity. It should be noted that the analytic solutions presented in equations (2.9) and (2.10) are much more general, allowing generation of the manifold and modal equations for any mode given $[\alpha]$, $[\beta]$, and the linear natural frequencies (ω's). This process has been computationally implemented such that no analytic work is necessary once the necessary parameters are known, allowing the analysis of very general structural systems including finite element models and complex analytic systems.

2.2.7 Example: Finite Element-Based Beam

The computer program mentioned above was used for the analysis of the system shown in Figure 2.9. PATRAN was used to create a 200 element beam with free ends and discrete linear springs at nodes 57 and 117. Once the linear modes of this model were known, discrete nonlinear springs were added (analytically) to the endpoints. The characteristics of the springs (purely cubic) and the eigenvectors were then used to construct the $[\beta]$ matrix (here $[\alpha] = 0$). Using these, the general analytic solutions, Eqs. (2.9)-(2.10), may be used to easily generate any individual nonlinear normal mode of the system. Due to the number of coefficients involved, this task would be exceedingly tedious without the explicit solution provided. Figure 2.10 displays some results for the fourth nonlinear normal mode of the system. These results indicate that a single nonlinear normal mode is more accurate than a model which uses four linear modes. The "exact" results (25 linear modes) slowly diverge from the nonlinear normal mode results due to higher-order effects which cannot be captured by a third-order manifold. A more meaningful result would include a comparison between the approximate manifold dynamics and the exact manifold

(currently unknown) dynamics. Further work is underway in this area.

2.3 Reduced-Order Modeling Using Multi-Mode Models

2.3.1 Definition of a Nonlinear Multi-Mode Model

In order to generalize the ideas developed above to the case of multi-mode invariant manifolds, one must make a further departure from the linear case. For a linear system, a multi-mode model is built simply by employing superposition of individual modes. In the nonlinear case, the individual modes are coupled, sometimes in an essential manner, and generally cannot be superimposed (especially in the case of internal resonance). In terms of the phase space, this means that even if one could select initial conditions that somehow contained only two nonlinear modes, the resulting dynamics would not simply be a combination of the two individual modal responses.

A nonlinear M-mode invariant motion of a system is a response which takes place on a $2M$-dimensional invariant manifold in the system's phase space; the manifold passes through the stable equilibrium point of interest and, at that point, it is tangent to a $2N$-dimensional eigenspace of the system linearized about that equilibrium (representing N linear modes). On this manifold the system dynamics are governed by M pairs of state variables, that is, it behaves like an M-degree of freedom system.

2.3.2 Construction of a Multi-Mode Manifold

One must reformulate the problem for this case by starting with a multi-mode form that contains the individual modes of interest as a "seed" upon which the reduced-order model is built. The method proceeds by assuming that all system degrees of freedom are slaved to a subset of the overall system degrees of freedom, where the subset has the desired size of the reduced-order model and corresponds

to a desired set of modes. This is expressed by a set of to-be-determined constraint equations among the dynamic variables, just as is done in for individual nonlinear modes. As before, these constraint equations are required to satisfy the differential equations of motion. This again yields a set of partial differential equations that capture desired relationships, without involving any time derivatives, which are solved using series expansions. If one includes all the resonant modes at a given order in the "seed" modes, no singularities will arise in the equations for the coefficients, at least up to that order. Restriction of the equations of motion to the resulting manifold yields a reduced-order dynamical system that systematically and correctly captures the coupled dynamics of the included modes. By keeping only those modes that play a significant role in the system response, one obtains an accurate reduced-order model, just as is done in linear vibration theory.

The modes of interest, or the modeled, or master, modes are described by a set of indices denoted as S_M. For example, if one is interested in a reduced-order model that contains extensions of the second, third and fifth linear modes, $S_M = \{2, 3, 5\}$. The displacements and velocities of the modeled modes can be expressed by the vectors $\mathbf{u_M}$ and $\mathbf{v_M}$, which contain elements $(u_i, v_i),\ i \in S_M$. Consequently, the associated manifold exists as a $2M$-dimensional "surface" in the $2N$-dimensional phase space. The dynamics of the reduced M-degree of freedom system will be constrained to lie on this surface, and all interactions with the non-modeled, or "slave", linear modes are incorporated into the resultant dynamics. That is, motions that take place directly on the multi-mode manifold correctly account for effects due to the non-modeled linear modes, while still eliminating the dynamic coupling to them. (Again, this is true only when the motion is initiated on the manifold.) This contrasts with the conventional methodology of simply disregarding those linear modes which are not

of interest or thought to be unimportant, or simulating a large number of additional degrees of freedom in order to achieve accuracy within the modes of interest. In other words, this approach allows one to work with only the number of modes of direct interest without concern for dynamic contamination from any modes that are not included. Further theoretical discussion of these topics may be found in [29].

The approach for determining the multi-mode manifold is similar to that described in the previous section, except that the manifolds are now parameterized by $2M$ variables. (Of course, the process reduces to the individual mode case for $M = 1$.) This may be expressed as:

$$\begin{cases} x_k = u_k \\ \qquad\qquad \text{for} \quad k \in S_M \\ y_k = v_k \end{cases} \tag{2.23}$$

$$\begin{cases} x_j = X_j(\mathbf{u_M}, \mathbf{v_M}) \\ \qquad\qquad\qquad\qquad \text{for} \quad j \notin S_M \\ y_j = Y_j(\mathbf{u_M}, \mathbf{v_M}) \end{cases} \tag{2.24}$$

As in the single mode case, equations (2.23) and (2.24) are substituted into the governing equation, (2.1), the equations of motion are employed, and all slave variables are expressed in terms of the constraints, yielding:

$$\begin{cases} Y_j = \dot{X}_j = \displaystyle\sum_{k \in S_M} \frac{\partial X_j}{\partial u_k} v_k + \frac{\partial X_j}{\partial v_k} f_k \\ f_j = \dot{Y}_j = \displaystyle\sum_{k \in S_M} \frac{\partial Y_j}{\partial u_k} v_k + \frac{\partial Y_j}{\partial v_k} f_k \end{cases} \tag{2.25}$$

Here, as in the previous case, exact solutions are not generally available and approximate solutions are sought in the form of series expansions. Due to the additional degrees of freedom, the number of terms in these expansions grows considerably with

the number of modeled modes, M. The general form is given by,

$$\begin{aligned} X_j(\mathbf{u_M}, \mathbf{v_M}) &= \sum_{k \in S_M} a^k_{1,j} u_k + a^k_{2,j} v_k + \sum_{k \in S_M} \sum_{l \in S_M} a^{k,l}_{3,j} u_k u_l + a^{k,l}_{4,j} u_k v_l + a^{k,l}_{5,j} v_k v_l \\ &+ \sum_{k \in S_M} \sum_{l \in S_M} \sum_{q \in S_M} a^{k,l,q}_{6,j} u_k u_l u_q + a^{k,l,q}_{7,j} u_k u_l v_q \\ &+ a^{k,l,q}_{8,j} u_k v_l v_q + a^{k,l,q}_{9,j} v_k v_l v_q + \ldots \end{aligned} \tag{2.26}$$

$$\begin{aligned} Y_j(\mathbf{u_M}, \mathbf{v_M}) &= \sum_{k \in S_M} b^k_{1,j} u_k + b^k_{2,j} v_k + \sum_{k \in S_M} \sum_{l \in S_M} b^{k,l}_{3,j} u_k u_l + b^{k,l}_{4,j} u_k v_l + b^{k,l}_{5,j} v_k v_l \\ &+ \sum_{k \in S_M} \sum_{l \in S_M} \sum_{q \in S_M} b^{k,l,q}_{6,j} u_k u_l u_q + b^{k,l,q}_{7,j} u_k u_l v_q \\ &+ b^{k,l,q}_{8,j} u_k v_l v_q + b^{k,l,q}_{9,j} v_k v_l v_q + \ldots \end{aligned} \tag{2.27}$$

Again, if ones uses linear modal coordinates to express the equations of motion, the linear terms in the above expansions are zero for $j \notin S_M$, and the higher order terms vanish when $j \in S_M$. It should be noted that the terms in this expansion are not unique. For example, there are two coefficients for the term $u_k u_l v_q$ when k and l are different. In order to produce a unique solution, it is assumed that these, non-unique, coefficients are equal. That is, because

$$u_k u_l v_q = u_l u_k v_q \neq u_k u_q v_l$$

the relation

$$a^{k,l,q}_{7,j} = a^{l,k,q}_{7,j}$$

is enforced, but

$$a^{k,l,q}_{7,j} \neq a^{k,q,l}_{7,j}$$

is allowed. Also, as in the single mode case, these are local results, and their fidelity depends on the amplitude of motion as well as the proximity to internal resonances between master and slave modes.

If equations (2.26) and (2.27) are substituted into equation (2.25), a large set of linear equations is produced for the coefficients. As in the single mode case, these equations may be solved by equating the coefficients of like powers in the u's and v's. This process may be simplified by dividing it into several subproblems according to the number of distinct modes contained in the coefficient superscripts. That is, one first solves for terms like $a_{6,i}^{k,k,k}$, then the terms like $a_{6,i}^{k,k,l}$, where $k \neq l$, and finally those like $a_{6,i}^{k,l,q}$ where k, l and q are all distinct. These are referred to as the one-mode, two-mode, and three-mode coefficients, respectively. The one-mode problem is almost identical to that of the single mode manifold, and the same solutions may be used. However, the numerical answers are not identical, as the inclusion of more modes eliminates some of the expansion coefficients (e.g., $a_{3,j}^{k,k} = 0$ if $j \in S_m$), and the values of the constants $C_{p,i}^{1,k}$'s, as defined in Eq. (2.11) are consequently altered. That is, certain constraints are eliminated when an additional mode is included in S_m, and this change is reflected in the reduced equations of motion.

The two-mode problem may be solved first for the second-order expansion coefficients, and then for the appropriate third-order coefficients. The problems are both linear, but due to the size and complexity of the explicit solutions, they are presented here in matrix form only. In addition, the coefficients which are zero have been eliminated from the matrix formulation. It is found that in the one-, two- and three-mode problems the expansion coefficients $a_4, a_7, a_9, b_3, b_5, b_6, b_8$ are all zero. Again, this is due to the fact that only conservative, non-gyroscopic systems

are considered, which eliminates the possibility of such terms appearing (although one cannot use a simple synchronicity argument in this case, since several modes are present). The second-order coefficients may be determined by solving:

$$\begin{bmatrix} -2 & 2\omega_k^2 & 1 & 0 \\ -2 & 2\omega_l^2 & 0 & 1 \\ -2\omega_i^2 & 0 & \omega_l^2 & \omega_k^2 \\ 0 & 2\omega_i^2 & 1 & 1 \end{bmatrix} \begin{bmatrix} a_{3,i}^{k,l} \\ a_{5,i}^{k,l} \\ b_{4,i}^{k,l} \\ b_{4,i}^{l,k} \end{bmatrix} = \begin{bmatrix} 0 \\ 0 \\ \alpha_{k,l}^{i} \\ 0 \end{bmatrix} \tag{2.28}$$

while the third-order coefficients are obtained by solving:

$$\begin{bmatrix} -3 & 2\omega_k^2 & 0 & 1 & 0 & 0 \\ -6 & 2\omega_l^2 & 2\omega_k^2 & 0 & 2 & 0 \\ 0 & -2 & -1 & 0 & 0 & 3 \\ -3\omega_i^2 & 0 & 0 & \omega_l^2 & 2\omega_k^2 & 0 \\ 0 & -2\omega_i^2 & 0 & -2 & -2 & 6\omega_k^2 \\ 0 & 0 & -\omega_i^2 & 0 & -2 & 3\omega_l^2 \end{bmatrix} \begin{bmatrix} a_{6,i}^{k,k,l} \\ a_{8,i}^{k,k,l} \\ a_{8,i}^{l,k,k} \\ b_{7,i}^{k,k,l} \\ b_{7,i}^{l,k,k} \\ b_{9,i}^{k,k,l} \end{bmatrix} = \begin{bmatrix} -C_{1,i}^{3,k,l} \\ -C_{2,i}^{3,k,l} \\ 0 \\ C_{7,i}^{3,k,l} \\ C_{5,i}^{3,k,l} \\ C_{6,i}^{3,k,l} \end{bmatrix} \tag{2.29}$$

for the two-mode problem, and

$$\begin{bmatrix} -6 & 2\omega_k^2 & 2\omega_l^2 & 0 & 2 & 0 & 0 & 0 \\ -6 & 0 & 2\omega_m^2 & 2\omega_k^2 & 0 & 2 & 0 & 0 \\ -6 & 2\omega_m^2 & 0 & 2\omega_l^2 & 0 & 0 & 2 & 0 \\ 0 & -1 & -1 & -1 & 0 & 0 & 0 & 3 \\ -3\omega_i^2 & 0 & 0 & 0 & \omega_m^2 & \omega_l^2 & \omega_k^2 & 0 \\ 0 & -2\omega_i^2 & 0 & 0 & -2 & 0 & -2 & 6\omega_l^2 \\ 0 & 0 & -2\omega_i^2 & 0 & -2 & -2 & 0 & 6\omega_k^2 \\ 0 & 0 & 0 & -2\omega_i^2 & 0 & -2 & -2 & 6\omega_m^2 \end{bmatrix} \begin{bmatrix} a_{6,i}^{k,l,m} \\ a_{8,i}^{l,m,k} \\ a_{8,i}^{k,l,m} \\ a_{8,i}^{m,l,k} \\ b_{7,i}^{k,l,m} \\ b_{7,i}^{k,m,l} \\ b_{7,i}^{l,m,k} \\ b_{9,i}^{k,l,m} \end{bmatrix} = \begin{bmatrix} C_{8,i}^{3,k,l,m} \\ C_{8,i}^{3,k,m,l} \\ C_{8,i}^{3,l,m,k} \\ 0 \\ C_{9,i}^{3,k,l,m} \\ C_{10,i}^{3,l,m,k} \\ C_{10,i}^{3,k,l,m} \\ C_{10,i}^{3,m,l,k} \end{bmatrix} \tag{2.30}$$

for the three-mode problem. Each equation depends on a specific $i \notin S_M$ and $k, l, m \in S_M$. The constants $C_{p,i}^{3,k,l}$ depend on the first- and second-order results, and are shown explicitly in Appendix B. These matrix expressions were initially formulated by hand, and then checked using the symbolic processor Mathematica^{TM}. Due to the relatively sparse nature of these matrices, they may be symbolically inverted to yield analytic expressions for the expansion coefficients which depend only on $[\alpha], [\beta]$, the ω's and the lower-order expansion coefficients. Though these expressions are rather large and unwieldy, they may be implemented in a computer code and used to systematically calculate all of the expansion coefficients. It should be noted that the symbolic approach used here allows k, l, m in equations (2.28)–(2.30) to represent any three modeled modes, and the corresponding (symbolic) solutions will be valid for any three modeled modes. Alternatively, numbers may be used in equations (2.28)–(2.30), and inversion may be repeated for each combination of modeled modes. If several modes are chosen, this may entail considerable work each time a solution is sought. The symbolic approach avoids this by producing a single, explicit, general purpose solution. However, due to its complexity, this approach may no longer be practical if additional nonlinear terms or expansion coefficients are included in the formulation (for example, arising from gyroscopic terms).

While internal resonances between modeled modes are automatically accounted for, internal resonances between modeled and unmodeled modes will cause singularities in the analytic solutions. There are many possible internal resonances. Through third order, they are:

$$\begin{array}{ll} \omega_i = \omega_k & \omega_i = 3\omega_k \\ \omega_i = 2\omega_k & \omega_i = |2\omega_k \pm \omega_l| \\ \omega_i = |\omega_k \pm \omega_l| & \omega_i = |\omega_k \pm \omega_l \pm \omega_m| \end{array} \tag{2.31}$$

where $(i,k,l,m) \in S_M$, if singularities are to be avoided in the manifold coefficients.

Once the expansion coefficients are known, the unmodeled (slave) degrees of freedom can be expressed as approximate functions of the modeled (master) coordinates. These functions may be substituted back into the equations of motion corresponding to the modeled modes. In this manner, the unmodeled modes are eliminated from the original set of second order differential equations. This reduction process may be automated, producing a set of equations with polynomial nonlinearities in the master coordinates. As in the single-mode case, a third-order expansion of the unmodeled coordinates produces equations which are precise through fourth order if $[\alpha]$ is nonzero, and fifth order if $[\alpha] = 0$. These fifth-order terms are retained in all cases, even when they are incomplete at that order, as it is found that their inclusion improves simulation accuracy.

As discussed in Section 2.2.6 for the single-mode case, a computer program has been developed for the multi-mode case which – given $[\alpha]$, $[\beta]$, and the system's linear natural frequencies – can reduce a system of N equations which are formulated in the linear modal coordinates, down to a system of M equations of motion, in M chosen modal coordinates i.e., a reduced-order model. This program generates the complete, third-order, M-mode manifold via the analytic solutions to equations (2.28)–(2.30), enabling the M equations of motion to be expressed to fifth order. However, N third-order equations have been "reduced" to M fifth-order equations and, as such, some examination is necessary to determine when this approach will result in significant time savings; this matter is considered next.

2.3.3 Some Computational Considerations

Depending on the ratio of M/N, the simplification obtained from this approach may be significant. One indication of the complexity of a given system is the total number of nonlinear terms in the model. This is a measure of both the number of computations necessary at a given time step in a numerical simulation, and the overall size and complexity of the system. In the original system, there are N equations, with

$$\frac{1}{6}(N^3 + 6N^2 + 5N)$$

possible nonlinear terms in each equation (this and the following results are obtained by counting the terms at each order). By comparison, in the reduced system there are M equations with

$$\frac{M}{30}(4M^4 + 30M^3 + 85M^2 + 105M + 46)$$

terms each, when all generated fifth-order terms are retained (in order to be conservative). At the highest order, this difference reduces to an $M \times (4/5)M^5$ versus an $N \times N^3$ set of nonlinear terms. Consequently, there is not significant reduction in the number of terms if

$$M \geq\approx N^{2/3}$$

in the limiting case of the fifth-order result. It can be shown that for $N > 4$, reduction will always occur if $M \leq \sqrt{N}$. This is not a distinct boundary, but it may be used as a general guide when applying this technique. These criteria are indicative of the most nonlinear cases. In simpler cases, when the $[\alpha]$ and $[\beta]$ matrices are sparse, the resulting reduced set may contain many terms which are also zero or of negligible

magnitude. Due to these effects, an absolute description of the efficiency of this technique is not possible, and each case must be evaluated individually. For example, if $N = 20$, and $[\alpha]$ and $[\beta]$ are full, there will be $20 \times 1750 = 35000$ original nonlinear terms. If this is reduced to $M = 4$ equations, there will be, at most, $4 \times 636 = 2544$ nonlinear terms in the reduced set, a reduction of 93%!

In many structural systems, it is primarily the low frequency modes which are of interest. However, when nonlinearities are present, it is often necessary to simulate the high frequency modes as well in order to achieve the desired accuracy in the modes of interest. This requires that the time steps of any integration scheme be small enough to reproduce the high frequency dynamics accurately. When these systems are reduced to their low frequency modes using a multi-mode manifold, the effects of the high frequency modes are captured in the reduced equations, and it is no longer necessary to simulate them explicitly, hence allowing for a time step governed by the low frequency modes. When this time savings is compounded with that due to the size reduction of the equations, the necessary computer time may be reduced by several orders of magnitude. In addition, it should be noted that the size of the reduced equations does not grow with N. Consequently, it is possible to produce models which are reduced from many more modes than would have previously been practical. Also, as N is increased, the convergence of the reduced equations (with M held constant) may be studied to guarantee their accuracy.

2.3.4 Example: A Second Finite Element-Based Beam

The computer program mentioned above was used for the analysis of the system shown in Fig. 2.11. The finite element code PATRAN was used to create a beam model with 200 two-noded beam finite elements. The beam in Fig. 2.11 is pinned

at one end, with the other constrained by a linear spring. A nonlinear torsional spring is located at the pinned end. As with the previous finite element example, the characteristics of the nonlinear spring and the linear eigenvectors were used to construct the $[\alpha]$ and $[\beta]$ matrices. Using these, reduced equations for any chosen set of nonlinear normal modes may easily be generated. Once the reduced modal dynamics have been determined (here, through fourth-order Runge-Kutta numerical integration) the manifold coefficients may be used to reconstruct the non-modeled modal displacements, and the corresponding physical displacements. Two results are shown: in the first, the system is not internally resonant and the torsional spring contains both quadratic and cubic nonlinearities, and in the second, the linear spring is tuned such that a 2:1 internal resonance in generated between the second and third linear modes, and the torsional spring is purely quadratic.

The results for the first case, shown in Fig. 2.12, illustrate the displacements at the beam's quarter span, predicted by an "exact" solution (25 linear modes), a three-mode nonlinear manifold, and a three-linear-mode truncation. The first three modes were used in both three-mode models. For this case it can be seen that the linearly truncated model yields results which slowly diverge, while the other two match quite well. However, these small errors hardly seem to justify the effort necessary to generate the 6-dimensional manifold, and the reduced equations it yields. One must keep in mind that the small errors shown here simply indicate that for this system, at this amplitude, with these initial conditions, the contributions of the non-modeled modes are not very significant. Changes in any of these parameters may affect the results in unexpected ways.

In the second case, Fig. 2.13, the displacements at half span predicted by the "exact" solution, the two-mode manifold, and a two-linear-mode truncation are shown.

Both two-mode solutions use the second and third (internally resonant) linear modes. Here, a significant error, in the form of a nearly constant offset, is present from the outset. Analysis shows that this offset is due to contributions from the first mode, a phenomenon which deserves some exploration.

The two-mode manifold solution explicitly simulates the second and third modes, and then assembles the contributions of the remaining modes, including the first, to obtain the dynamics of the entire system. Hence, the obtained offset is a polynomial function of u_2, u_3, v_2, and v_3. The "exact" solution is initiated on the manifold, so the initial conditions in the second and third modes, together with the manifold coefficients, specify the initial conditions of all the modes, which are then simulated. For this solution, all 25 modes interact dynamically to maintain the offset. The two-mode truncation simply assumes that all other modes remain quiescent and do not contribute, an approach with no hope of yielding accurate results in this situation. For this case it is apparent that modes two and three are not easily separable from the system. That is, that mode one (at least!) must be accounted for or contamination is ensured. Also, the manifold solution reproduces the "exact" one exceptionally well, indicating considerable manifold accuracy.

The two examples above illustrate that, while exceptional results are not guaranteed, important (and unexpected) effects, when present, may be captured. Indeed, it is these unpredictable modal interactions which prove the utility of this approach for large scale systems. Due to its finite element origin, and the systematic reduction procedure, the above example could just as easily have been a plate, shell, or aircraft frame, and the reduction procedure would remain unchanged. As such, though the reduction process is analytically complex, its automation enables the generation of rigorous, uncontaminated, reduced-order models of a large variety of nonlinear

structural systems.

2.4 The Case of Harmonic Excitation

In linear systems, one typically ignores external forcing when generating the reduced-order model, then applies the forcing through projection onto the retained modes. In such cases, the other modes are also forced and active, but are simply ignored. Similarly, in the nonlinear case, if one simply adds forcing to the reduced equations produced by the multi-mode manifold method, the invariance of the manifold is violated, and some effects may be lost. This has been attempted and has met with moderate success, see [48], especially near primary resonances, where small forces produce large responses.

Alternatively, the forcing can be incorporated directly into the formulation of the manifold. This is accomplished through state space augmentation of the original system, and it requires that the forcing can be expressed as a set of first or second order differential equations. This approach, which makes the system appear autonomous, is sometimes used in the study of control systems, but was originally suggested for this application by Richard Rand [49]. Here, pure harmonic forcing is discussed in detail, as it is both the simplest and most common type of time-dependent forcing, and it can be exactly captured by a simple additional, artificially introduced "mode."

Consider the addition of harmonic excitation to equation (2.5), that is, the right hand side is replaced by:

$$-\mathbf{F}\cos\omega_f t$$

where $\mathbf{F}^T = [F_1, F_2, \ldots F_N]^T$ is the forcing amplitude vector, and ω_f is the forcing frequency. A new "degree of freedom," x_f is introduced to represent this time varying term. Since this new coordinate is a known, harmonic function of time, it can be

represented by a second order differential equation:

$$\ddot{x}_f + \omega_f^2 x_f = 0$$

where $x_f(0) = 1$, and $\dot{x_f}(0) = 0$. Now, this information may be used to incorporate the forcing into the matrix formulation, transforming equation (2.5) into:

$$[I]\ddot{\mathbf{x}}^+ + [,\,]\mathbf{x}^+ + f^{nl}(\mathbf{x}) = \mathbf{0} \tag{2.32}$$

where

$$[,\,] = \begin{bmatrix} \omega_1^2 & 0 & 0 & F_1 \\ 0 & \ddots & 0 & \vdots \\ 0 & 0 & \omega_N^2 & F_N \\ 0 & 0 & 0 & \omega_f^2 \end{bmatrix}$$

and $\mathbf{x}^{+T} = [x_1, ..., x_N, x_f]^T$. This system of equations may be diagonalized through a linear transformation. If the definition $\mathbf{x}^+ = [U]\boldsymbol{\eta}$ is applied, where $\boldsymbol{\eta}$ is a new coordinate vector, and

$$[U] = \begin{bmatrix} 1 & 0 & \cdots & 0 & \gamma_1 \\ 0 & 1 & \cdots & 0 & \gamma_2 \\ \vdots & \vdots & \ddots & \vdots & \vdots \\ 0 & 0 & \cdots & 1 & \gamma_N \\ 0 & 0 & \cdots & 0 & 1 \end{bmatrix}$$

and

$$\gamma_i = \frac{F_i}{\omega_f^2 - \omega_i^2}$$

then premultiply equation (2.32), by the matrix:

$$[V]^T = \begin{bmatrix} 1 & 0 & \cdots & 0 & -\gamma_1 \\ 0 & 1 & \cdots & 0 & -\gamma_2 \\ \vdots & \vdots & \ddots & \vdots & \vdots \\ 0 & 0 & \cdots & 1 & -\gamma_N \\ 0 & 0 & \cdots & 0 & 1 \end{bmatrix}$$

the equations are transformed to:

$$[I]\ddot{\boldsymbol{\eta}} + [\Omega']\boldsymbol{\eta} + [\alpha']\boldsymbol{\eta}^{2*} + [\beta']\boldsymbol{\eta}^{3*} = 0 \tag{2.33}$$

Here, $[\Omega']$ is an $(N+1)\times(N+1)$ diagonal matrix where the first N diagonal elements are the ω_i^2, and the $(N+1)$th element is ω_f^2. Also, the $(N+1)$th element of the vector $\boldsymbol{\eta}$ is unaffected by the transformation, and remains as x_f. Some manipulation is necessary to produce the new $[\alpha']$ and $[\beta']$ matrices. This can be done using the original $[\alpha]$ and $[\beta]$ and substituting for x_i as:

$$x_i = \eta_i + \gamma_i x_f \qquad\qquad i = 1 \ldots N \tag{2.34}$$

The new matrices will have several more columns, and one additional row at the bottom. However, this last row represents a linear equation, so both $[\alpha']$ and $[\beta']$ will have a final row of zeros. It should be noted that this transformation is not valid at a (linear) resonance, as one or more of the γ_i's will become undefined.

Equation (2.33) is now in exactly the same form as that used for the multi-mode manifold formulation, equation (2.5). Consequently, manifolds may be sought in terms of the modes of interest ($\eta_k, k \in S_M$), as well as the forcing "coordinates," ($x_f, \dot{x_f}$), using the solutions developed previously. This will produce a reduced set of differential equations in $\eta_k, \dot{\eta_k}, x_f$, and $\dot{x_f}$ where $k \in S_M$. Equation (2.34) may

be used to re-express these equations in terms of the original coordinates (a non-trivial process for high-order terms). Finally, x_f may be replaced by its known, time-dependent value — producing an equation which will generally include various powers of $\cos \omega_f t$ and $\sin \omega_f t$, in the form of both direct and parametric excitation.

Computational implementation of this method has been realized. This program is able to reduce an N-mode structural system which is forced by a single harmonic, to an M-mode model which is also forced. However, several factors complicate the practical use of this approach. First, since the forcing is treated as an additional degree-of-freedom, and the original approach required small displacements, the forcing must be of the order of the displacements. To some degree, this may be accomplished through rescaling the original equations of motion, although this approach is limited in scope. Furthermore significant participation from the "slave" modes typically requires light damping, and the light damping encourages multiple steady state solutions. The existence of many solutions makes it difficult to compare the reduced and original equations of motion, as there is usually little or no known information about the number of solutions for either system. Hence a correspondence between exact and approximate results often may not be reached, and the approach may not be verified. However, the transformation outlined above may be useful in the event that additional (non-asymptotic) techniques are developed for solving the manifold-governing partial differential equations.

2.5 Discussion

Some of the most interesting features and results of this approach are the following: (1) The individual modes do not correspond to motions with a fixed system shape that obeys a nonlinear differential equation of motion; rather, the relative dis-

placements and velocities of the system degrees of freedom vary during the response in a manner that depends on the total energy in that mode. (2) This implies that one cannot simply use a nonlinear displacement field in order to generate an invariant nonlinear mode — a combined displacement/velocity field is required. In some examples, such as the simple cantilevered beam (see [50]), the velocity field can be ignored without much loss of accuracy, and the invariant manifold formulation allows for a systematic evaluation of the importance of the terms associated with these effects. (3) These shape distortions in the displacement and velocity fields are one of the keys to the utility of the reduced-order models, in that the effects of several linear modes are captured by a single nonlinear mode, thereby reducing the number of dynamic variables needed for an accurate system description. (4) As described in the review by Nayfeh, [51], and the book by Vakakis *et al.*, [44], results for nonlinear normal modes can be obtained by a number of different approaches, including perturbation and energy methods. (5) One main advantage of the invariant manifold approach is that it uses coordinates that are naturally suited to computational implementation. (6) The extensions to multi-mode manifolds and periodic excitation are straightforward and easily implemented in an automated computational procedure. (7) The method is analytically intensive in the formulation stage, but offers savings in computational time for simulations, due to the small number of degrees of freedom in the reduced-order model obtained. (8) A general theory for reducing large-scale systems with periodic excitation to reduced-order invariant models has been worked out and coded into an computer program that automatically generates the required coefficients for the manifolds and the dynamic model. (9) These results effectively extend the reach of modal analysis to weakly nonlinear systems.

Ongoing efforts by the author and others are directed along the following lines:

(1) the automatic generation of reduced-order models from nonlinear finite-element based descriptions of a structure; some results along these lines have been produced by the author as well as by Mazzilli and co-workers [52]; (2) the use of these reduced-order models as component modes for substructures of large-scale systems; (3) testing of these methods on simple, idealized structures; and, (4) application to more complex structures such as systems of rotating beams and coupled-beam systems.

It is hoped that the results of these investigations will lead to more effective model reduction techniques for large-scale engineering structures.

2.6 Figures

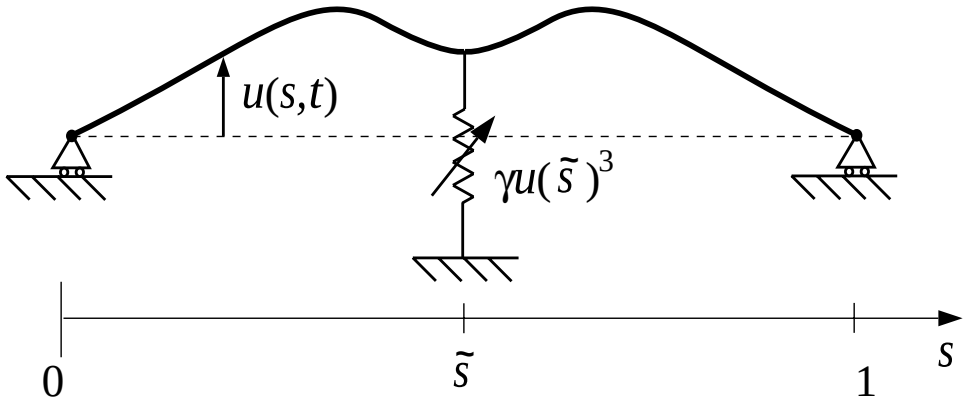

Figure 2.1: Simply-Supported Euler-Bernoulli (linear) beam connected to a purely cubic spring.

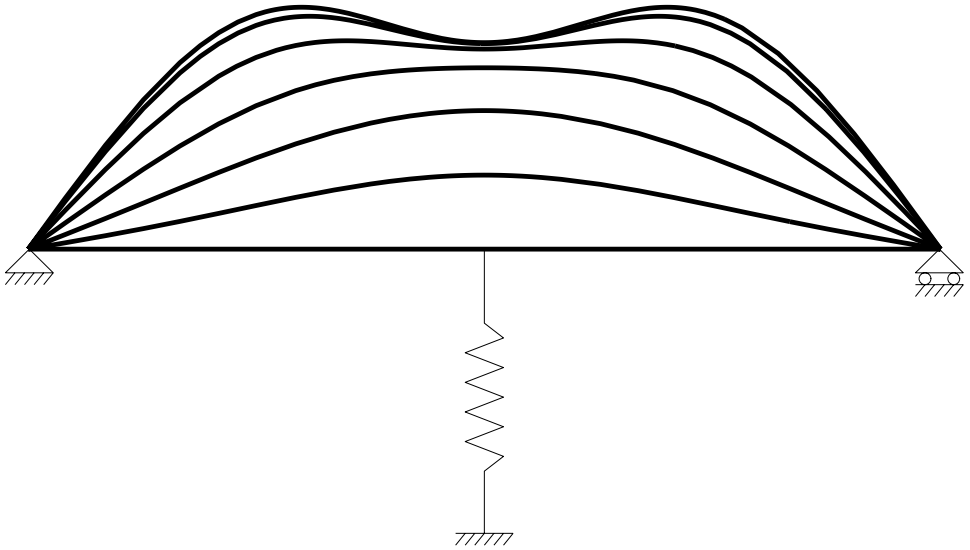

Figure 2.2: Beam displacement through a quarter-period of motion in the first nonlinear normal mode, sampled at seven equal time intervals. $u_1(0) = 0, v_1(0) = 6.93$

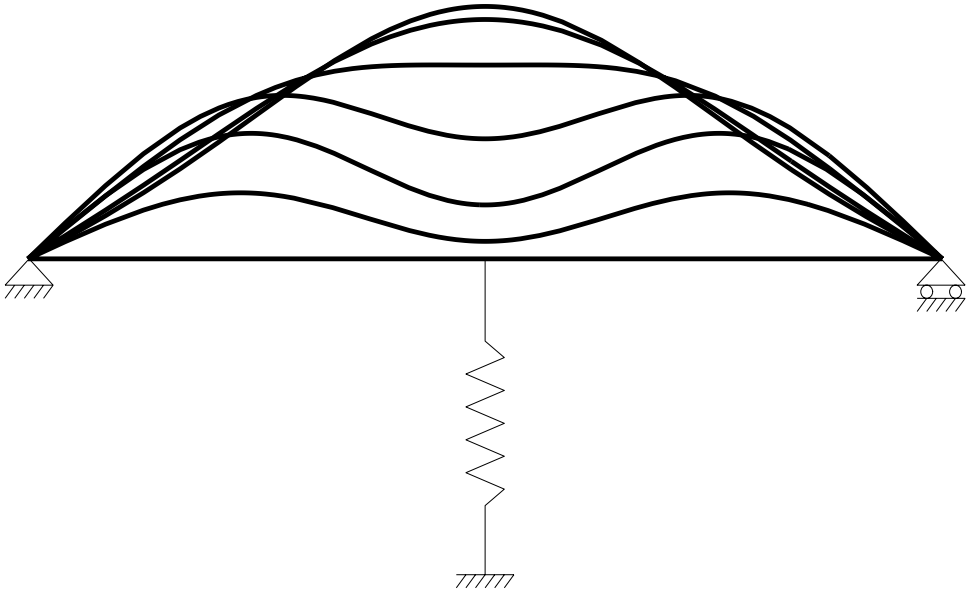

Figure 2.3: Beam velocity profile through a quarter-period of motion in the first nonlinear normal mode, sampled at seven equal time intervals. $u_1(0) = 0, v_1(0) = 6.93$

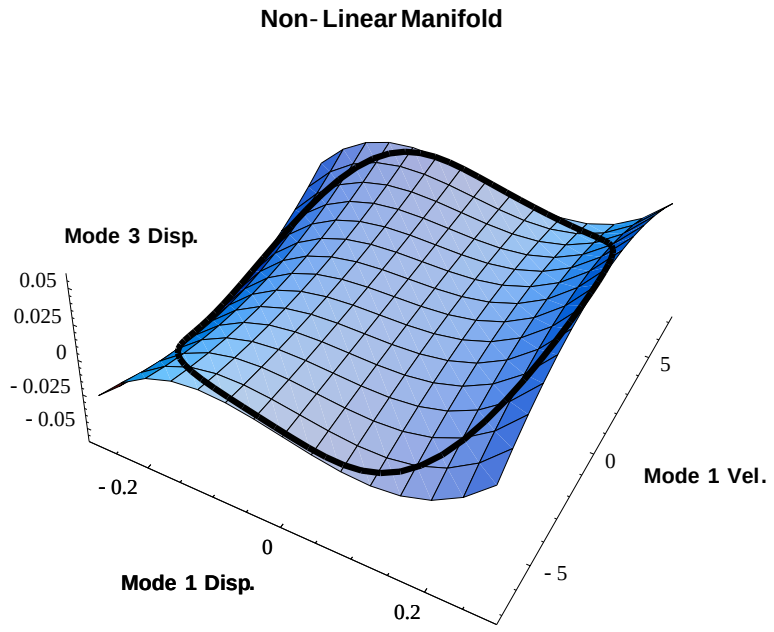

Figure 2.4: Modal manifold projected into the u_1, v_1, u_3 subspace. The closed curve corresponds to the initial conditions in Figures 2.2 and 2.3

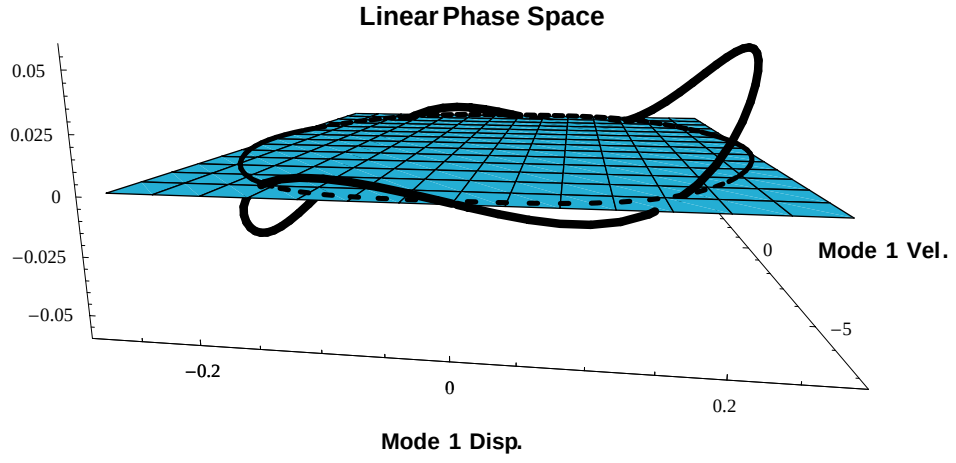

Figure 2.5: Linear phase space corresponding to a single mode truncation. The solid curve lies on the manifold in Figure 2.4, while its projection (dashed line) may only be approximated.

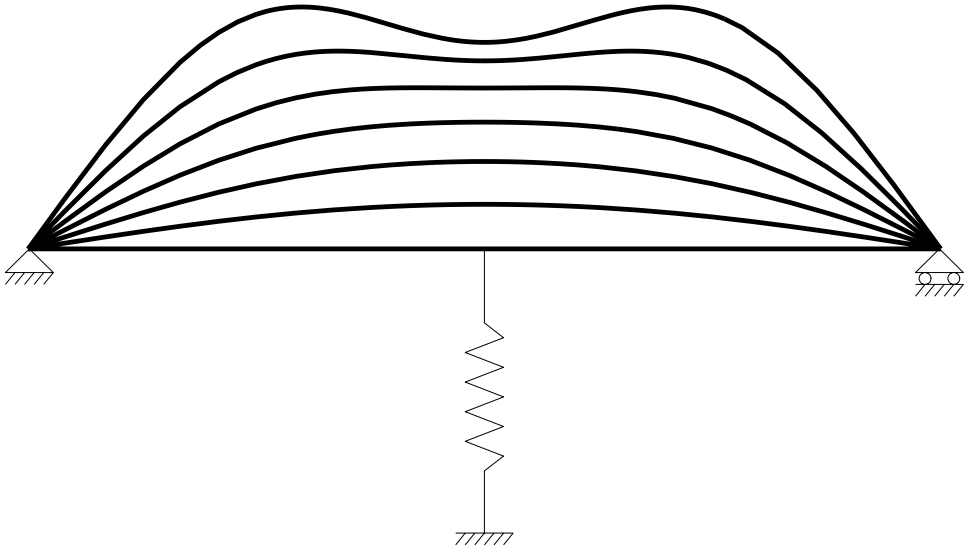

Figure 2.6: Peak configurations (zero velocity) for equal intervals in u_1.

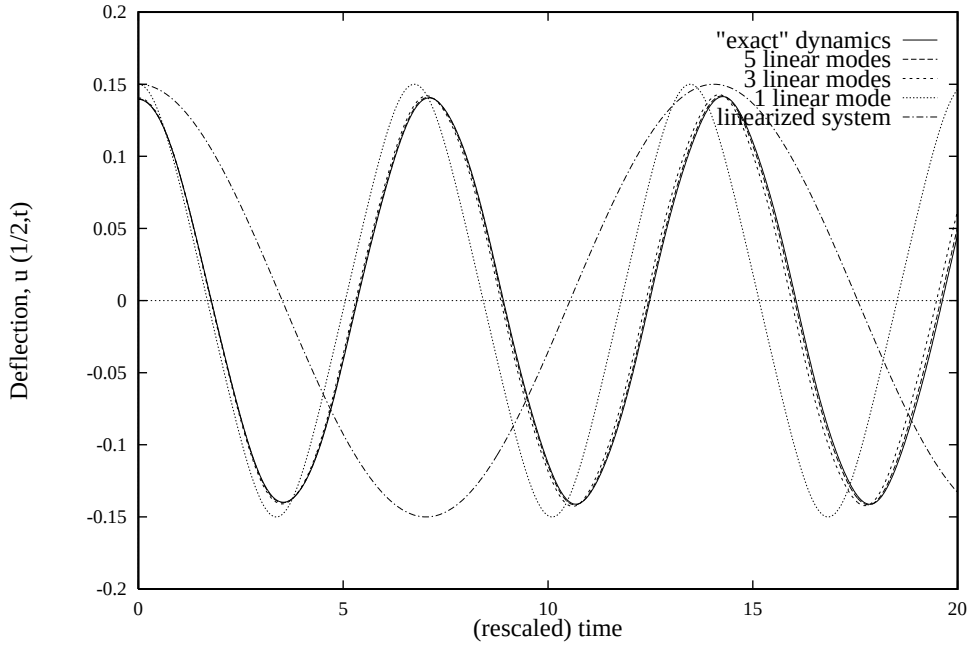

Figure 2.7: Deflection of the middle-point of the beam as obtained by various linear modal analysis simulations initiated on the first nonlinear normal mode manifold. $u_1(0) = 0.15$, $v_1(0) = 0$.

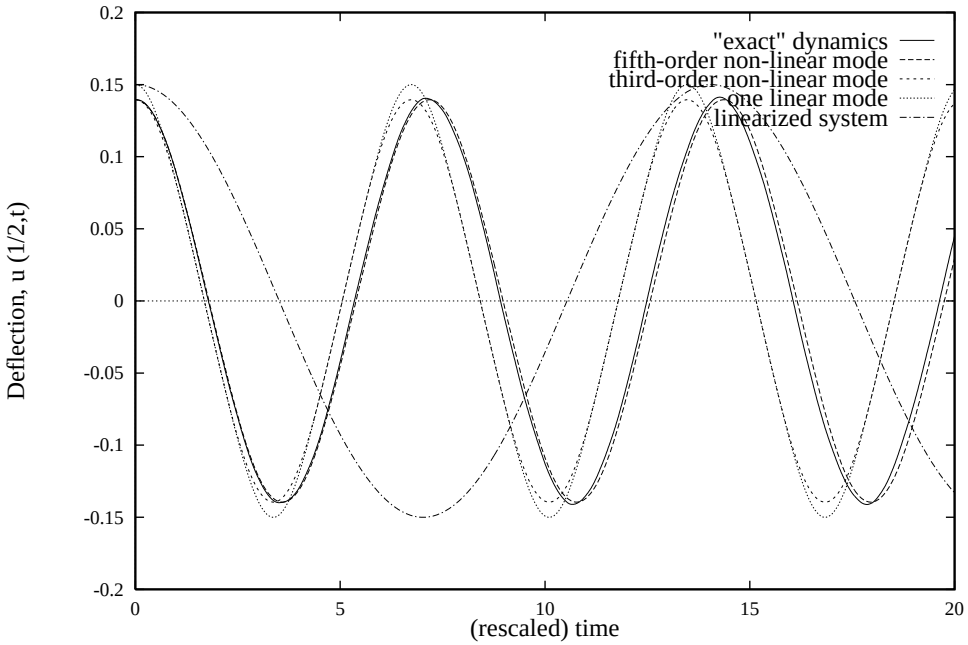

Figure 2.8: Deflection of the middle-point of the beam as obtained by various simulations initiated on the first nonlinear normal mode manifold. $u_1(0) = 0.15$, $v_1(0) = 0$.

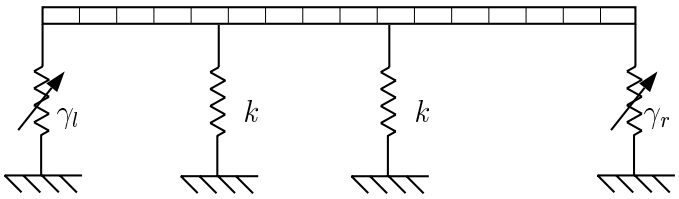

Figure 2.9: Schematic of finite element model. 200 beam elements were used to construct a beam with: $L = 1$ m, $\rho = 7860\text{kg/m}^3$, $E = 2 \times 10^{11}\text{N/m}^2$, $I = 5 \times 10^{-8}\text{m}^4$, $k = 10^5\text{N/m}$, $\gamma_l = 10^{12}\text{N/m}^3$, $\gamma_r = 5 \times 10^{11}\text{N/m}^3$

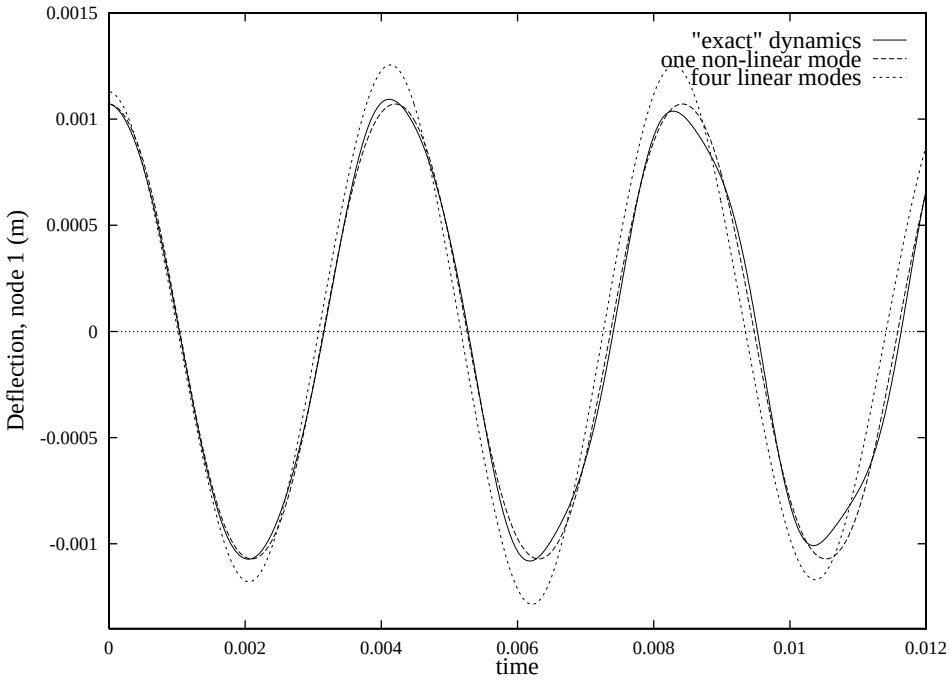

Figure 2.10: Deflection of the left end of a 200-element finite element beam using several different models initiated on the fourth-mode invariant manifold.

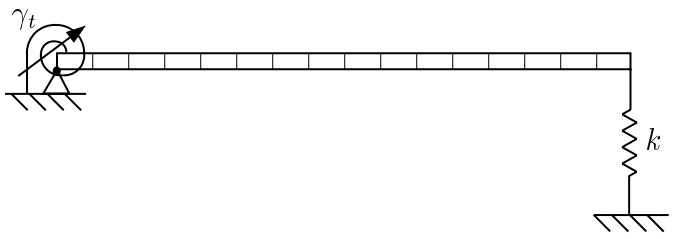

Figure 2.11: Schematic of finite element model: 200 beam elements were used to construct a beam with: $L = 1$ m, $\rho = 7860\text{kg/m}^3$, $E = 2 \times 10^{11}\text{N/m}^2$, $I = 5 \times 10^{-8}\text{m}^4$. The parameters k and γ_t vary by case.

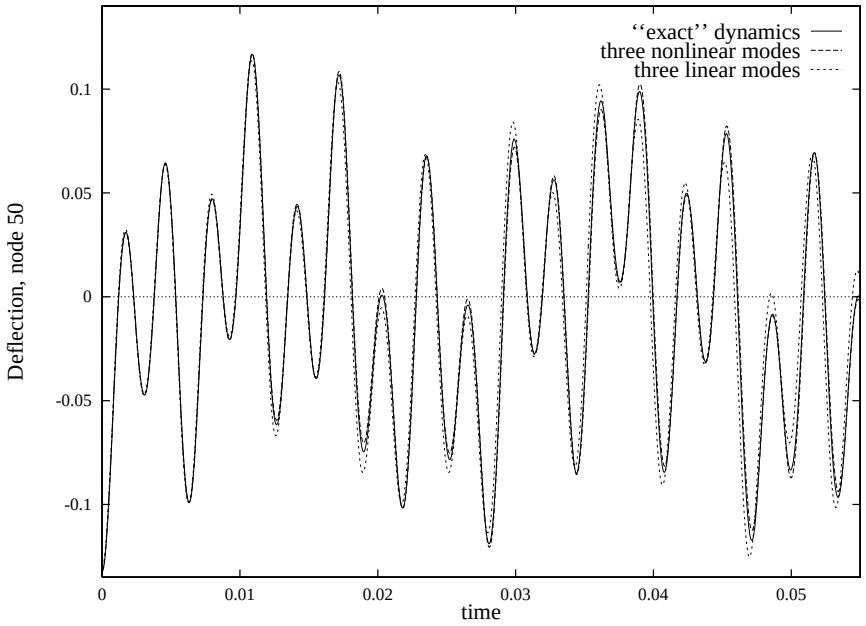

Figure 2.12: Deflection of node 50 (quarter span of beam) versus time using various methods. Here, $k = 10^8$, and the nonlinear spring strength is $\gamma_t = 5000u'(0)^2 + 20000u'(0)^3$, with initial conditions: $u_1(t=0) = -0.15, u_2(t=0) = 0.12, u_3(t=0) = 0.25, v_1(t=0) = v_2(t=0) = v_3(t=0) = 0$.

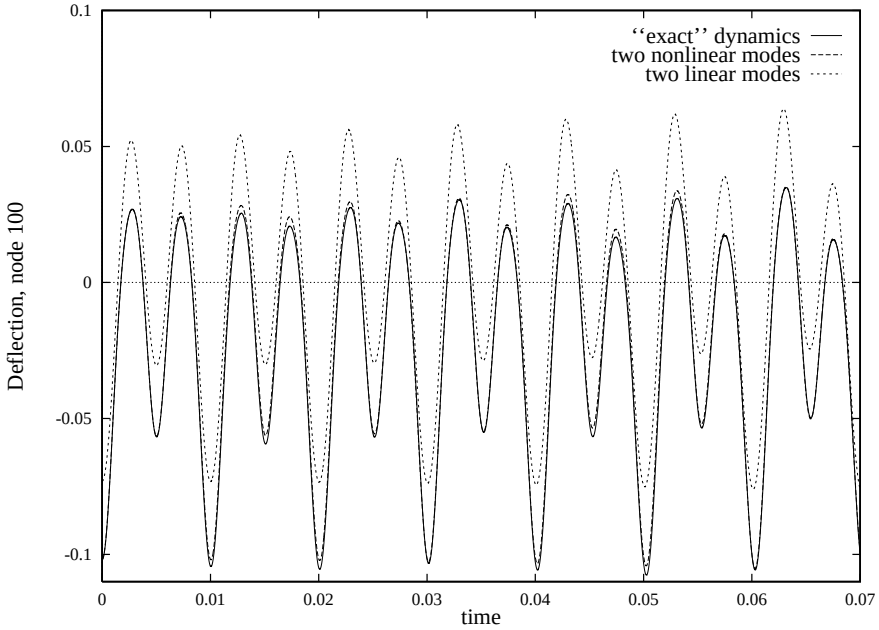

Figure 2.13: Deflection of node 100 (half span of beam) versus time using various methods. Here, $k = 1.185 \times 10^6$, and the nonlinear spring strength is $\gamma_t = 10000u'(0)^2$, with initial conditions:$u_2(t=0) = 0.2, u_3(t=0) = -0.35, v_2(t=0) = v_3(t=0) = 0$.

CHAPTER III

MODAL REDUCTION OF A NONLINEAR ROTATING BEAM THROUGH NONLINEAR NORMAL MODES

3.1 Introduction

The determination of rotorcraft blade dynamics has been the subject of considerable study. These dynamics are difficult to obtain accurately, as the rotation, together with the blade geometry, produces significant nonlinear effects, including multi-directional coupling and centrifugal stiffening through bending-induced axial foreshortening. Understanding these dynamics is critical in order to ensure stability and achieve optimal designs.

Much work has been done to create nonlinear finite element schemes which are capable of accurate analysis [53–55]. However, this approach yields extremely large models which often render complete nonlinear analysis impractical. Consequently, it is typical to use the full model to determine the nonlinear equilibrium solution, and then linearize about this solution. This approach ignores many nonlinear dynamic terms, and may predict inaccurate results.

Alternatively, several general analytic formulations have been developed [56–58]. These formulations, though applicable for a wide variety of parameters and blade

geometries, are difficult to use, as they are quite complex. Ultimately, this approach yields equations which are no more transparent than those from the finite element approach.

Consequently, many studies of these systems are done on highly idealized models [59–62], as results are more easily obtained, and new strategies and methods may be evaluated more effectively. The nonlinearities obtained in such cases are more manageable, and the qualitative behavior may often be extrapolated to more realistic systems.

In this study, such an idealized model is used. A uniform cantilevered Euler-Bernoulli beam, rotating at constant velocity, and constrained to deform in the transverse (flapping) and axial directions is considered. The resulting equations are discretized using the linear modes of the rotating beam, and nonlinearities in slope and displacement are retained through third order, yielding a set of modal equations which are linearly uncoupled, but coupled at second and third order. The modal convergence of this system is then evaluated to ensure a reference model of sufficient accuracy.

This model is then reduced using several different approaches, including the use of multi-mode invariant manifolds [63], a direct extension of the manifold-based nonlinear normal modes (NNMs) first developed by Shaw and Pierre [2,3]. This approach results in reduced-order models which include the most prominent effects of all non-modeled modes, while allowing arbitrary sets of modes to be chosen as the modeled subset. These reduced models are efficient, and formulated such that they may easily be extended to considerably more complex rotor blade models—both analytic and finite-element based.

The results indicate that, though the transverse dynamics are of primary interest,

it is necessary to account for the influence of extensional motions. The NNM-based reduction procedure embeds these axial-transverse interactions (and more) without requiring the explicit simulation necessitated by the traditional (linear modal analysis) approach. Consequently, the NNM-based reduced models are considerably more accurate than other models of equivalent size.

3.2 Formulation

The uniform rotating Euler-Bernoulli beam shown in Fig. 3.1 is considered. Rotatory inertia is neglected, motion is restricted to a rotating plane (thus eliminating lead-lag motion), and nonlinear axial strain is allowed. Hence, the potential energy, U, and kinetic energy, T, may be expressed as follows:

$$T = \frac{1}{2}\int_0^L m(\dot{u}^2 + \dot{w}^2) + m\Omega^2(h+x+u)^2 dx \tag{3.1}$$

$$U = \frac{1}{2}\int_0^L EI(w_{,xx})^2 + EA(u_{,x} + \frac{1}{2}(w_{,x})^2)^2 dx \tag{3.2}$$

where $u(x,t)$ and $w(x,t)$ are the axial and transverse displacements within the rotating reference frame, $(\cdot)_{,x}$ is a derivative with respect to the spatial variable x, an overdot represents a time derivative, h is the hub radius, Ω is the constant angular velocity of the beam, m is the mass per unit length, and E, A, I, and L are the typical beam parameters — Young's modulus, cross sectional area, moment of inertia, and length, respectively. These expressions, and Hamilton's principle, may be used to develop the following weak formulation for the equations of motion:

$$\int_{t_1}^{t_2}\int_0^L \Big\{[-m\ddot{w}\delta w - EIw_{,xx}\delta w_{,xx} - EA(u_{,x} + \frac{1}{2}(w_{,x})^2)w_{,x}\delta w_{,x}] + [-m\ddot{u}\delta u + m\Omega^2(x+h+u)\delta u - EA(u_{,x} + \frac{1}{2}(w_{,x})^2)\delta u_{,x}]\Big\} dx dt = 0 \tag{3.3}$$

where $\delta(\cdot)$ denotes the variation of a quantity.

With the foreknowledge that these equations will be discretized using the fixed-free axial bar modes and fixed-free transverse modes of the nonrotating linear beam (and their corresponding boundary conditions), these expressions may be reduced through integration by parts to:

$$\int_{t_1}^{t_2}\int_0^L \Big\{[-m\ddot{w} - EIw_{,xxxx}]\delta w - [EA(u_{,x} + \frac{1}{2}(w_{,x})^2)w_{,x}]\delta w_{,x} + [-m\ddot{u} + m\Omega^2(x+h+u) + EAu_{,xx}]\delta u - [EA\frac{1}{2}(w_{,x})^2]\delta u_{,x}\Big\} dxdt = 0 \tag{3.4}$$

At this point it is convenient to separate $u(x,t)$ into static and dynamic components, as follows:

$$u(x,t) = u_s(x) + u_d(x,t) \tag{3.5}$$

where $u_s(x)$ satisfies:

$$u_{s,xx} + \lambda^2 u = -\lambda^2(h+x)$$

and $\lambda^2 = m\Omega^2/EA$. Using the appropriate boundary conditions, it is found that

$$u_s(x) = \frac{1 + \lambda h \sin(\lambda L)}{\lambda \cos(\lambda L)} \sin(\lambda x) + h\cos(\lambda x) - (h+x)$$

which represents the static elongation of the beam due to rotation. If Eq. (3.5) is substituted into Eq. (3.4) and the nonlinear terms are neglected (for now), two linear partial differential equations remain, whose modal solutions will decouple the fully nonlinear equations of motion to linear order. These are:

$$m\ddot{u}_d - m\Omega^2 u_d - EAu_{d,xx} = 0 \tag{3.6}$$

$$m\ddot{w} + EIw_{,xxxx} - EA(u_{s,x}w_{,xx} + u_{s,xx}w_{,x}) = 0 \tag{3.7}$$

In the axial direction, the modes of the rotating beam, $\phi_i(x)$, are simply the well known axial mode shapes for a uniform (fixed-free) nonrotating beam. However, the transverse mode shapes of the rotating beam, $\psi_i(x)$, are approximated using a Rayleigh-Ritz procedure [20], as:

$$\psi_i(x) = \sum_{j=1}^{N_c} \eta_{(i,j)} \theta_j(x)$$

where the $\theta_j(x)$ are the familiar modes of a (nonrotating) fixed-free beam. Once the modes of the linearized rotating beam are determined, modal solutions to the nonlinear equations are sought in the form:

$$u_d = \sum_{i=1}^{N_a} a_i(t)\phi_i(x) \qquad\qquad w = \sum_{i=1}^{N_t} c_i(t)\psi_i(x). \tag{3.8}$$

The integers N_a, N_t, and N_c are used to denote the number of modes included in each of the above expansions.

If these discretizations are substituted into the weak formulation, Eq. (3.4), projected onto the linear modes, and orthogonality is invoked, the resultant discretized nonlinear equations are:

$$\ddot{a_j} + (\omega_{a,j})^2 a_j + \frac{EA}{2} \sum_{k=1}^{N_t} \sum_{l=k}^{N_t} c_k c_l \int_0^L \gamma(k,l,x)\phi_{j,x} dx = 0 \tag{3.9}$$

$$\text{for } j = 1 \ldots N_a$$

$$\ddot{c_j} + (\omega_{t,j})^2 c_j + EA \Bigg[\sum_{k=1}^{N_a} \sum_{l=1}^{N_t} a_k c_l \int_0^L \phi_{k,x}\psi_{l,x}\psi_{j,x} dx + \frac{1}{2} \sum_{k=1}^{N_t} \sum_{l=k}^{N_t} \sum_{i=l}^{N_t} c_k c_l c_i \int_0^L \sigma(k,l,i,x)\psi_{j,x} dx \Bigg] = 0 \tag{3.10}$$

$$\text{for } j = 1 \ldots N_t$$

Here, γ and σ are defined as

$$\gamma(i,j,x) = \begin{cases} \psi_{i,x}^2 & i = j \\ 2\psi_{i,x}\psi_{j,x} & i \neq j \end{cases} \tag{3.11}$$

$$\sigma(k,l,i,x) = \begin{cases} \psi_{k,x}^3 & k = l = i \\ 3\psi_{k,x}^2\psi_{i,x} & k = l \neq i \\ 3\psi_{l,x}^2\psi_{k,x} & k \neq l = i \\ 6\psi_{k,x}\psi_{l,x}\psi_{i,x} & k \neq l \neq i \end{cases} \tag{3.12}$$

and $\omega_a{}_{,j}$ and $\omega_t{}_{,j}$ are the natural frequencies associated with the jth mode in the axial and transverse directions, respectively. The transverse natural frequencies, $\omega_t{}_{,j}$, were compared against those in [59] and found to be in good agreement. Small differences ($\approx .05\%$) were traced to different extensibility assumptions. Note that the nonlinearities dictate a particular form of nonlinear coupling between the two sets of differential equations. It is this nonlinear interaction which produces axial shortening as a consequence of transverse bending, as well as the cubic stiffening due to nonlinear strains.

The accuracy of this reduced system of equations depends primarily upon three parameters: N_c, the number of component (nonrotating fixed-free beam) modes used to assemble each transverse rotating mode; N_t, the number of transverse rotating modes in $w(x,t)$; and N_a, the number of axial modes in $u_d(x,t)$. In order to effectively evaluate the proposed model reduction methods, it is necessary to obtain an accurate discretized reference model. As such, the convergence of the system properties and dynamics must by investigated in order to determine acceptable values for N_c, N_t, and N_a.

Often, in systems such as this, quasi-static assumptions are employed. In this case, the accelerations in the axial direction, ($\ddot{a}_j$ in Eq. (3.9)), would be neglected, allowing each a_j to be determined as a quadratic function of the c_k's. These expressions would then be inserted into Eq. (3.10) to achieve a purely cubic system model, which governs dynamics in the transverse direction. Though some results are shown in which this approach was used, it is not emphasized here, as rotorcraft systems contain coupling terms and inertial effects which may not be accounted for through quasi-static assumptions.

3.3 System Convergence

Several properties of the system may be evaluated as the numbers of included modes are varied, and the convergence of these properties will be used here as a general guide in determining a minimal model size for accurate results. In this study, the primary focus is on the dynamics of the lower frequency transverse modes of an approximate helicopter rotor blade model. The nominal parameters used to study the system convergence are as follows: $L = 9\,\mathrm{m}$, $m = 10\,\mathrm{kg/m}$, $EI = 3.99 \times 10^5\,\mathrm{N \cdot m^2}$, $EA = 2.23 \times 10^8\,\mathrm{N}$, $\Omega = 30$ rad/s, and $h = 0.5\,\mathrm{m}$. It is assumed that reasonable deviations from these parameters will have little effect on the system convergence. For the reader's reference, the first several transverse and axial natural frequencies are shown in Table 3.1, using the nominal parameters above, with rotation rates of $\Omega = 0$ and $\Omega = 30$ rad/s (nearly transonic blade tip velocity).

It is necessary to investigate the convergence behavior relative to N_c (the number of stationary transverse component modes) first, as this will dictate both the accuracy of the transverse modes, and the system dynamics as a whole. This convergence may be evaluated through examination of the properties of the assembled rotating modes

of the system for various values of N_c. The assembled mode shapes ($\psi_j(x)$) converge quite quickly, showing very little difference for $N_c > 4$. However, the associated rotating beam natural frequencies ($\omega_{t,j}$) converge considerably slower. It has been found that for $N_c = 11$ the first three natural frequencies are correct through four decimal places. For higher modes, the effects of rotation are less prominent, and $\psi_j(x)$ approaches the corresponding non-rotating component mode, $\theta_j(x)$. Therefore, higher transverse modes ($j > 10$) may be well approximated by only including several component modes above and below j. Based on these results, it was decided to use the empirical formula: $N_c = N_t + 9$ to determine N_c. Again, this guideline is tailored to the model parameters and modes of interest considered herein.

Next, the effects of N_a, the number of axial modes, are evaluated. This is done two ways: first, through examination of the axial deformation, $u_d(x)$, due to a static transverse deflection, $w(x)$; second, through numerical integration of the discretized equations of motion, Eqs. (3.9) and (3.10), for a fixed N_t, and various values of N_a.

Figure 3.2 depicts a particular static transverse deflection, $w(x)$, and the corresponding axial deformation for various values of N_a. These results are produced by choosing a deformation, $w(x)$, and the corresponding c_j's, substituting into Eq. (3.9), assuming a static solution, solving for the N_a a_j's, and reconstructing the final axial deformation shape. This illustrates the ability of the axial deformation to react properly to deformations in the transverse direction. In Fig. 3.2, $w(x)$ is the second transverse mode, $\psi_2(x)$, and it is easily seen that the convergence of $u_x(x)$ is quite slow, requiring at least six axial modes to capture the general character of the deformation. It should be noted that convergence near $x = L$ will be particularly slow, due to the choice of axial modal functions, $\phi_j(x)$, which do not satisfy the actual boundary conditions at the blade tip. However, this error is confined to the beam

tip, and as such, its effects are expected to be small.

As the dynamics in the transverse direction are of primary interest, it is worthwhile to examine directly the transverse motions and the resulting axial deflections for various values of N_a. Figures 3.3 and 3.4 depict the dynamics of the beam tip in the transverse and axial directions, respectively, for $N_a = 1$, 3, 6, and 9, with an initial deflection in the second transverse mode. All simulations are carried out using a fourth order Runga-Kutta integration scheme, and six transverse (rotating) modes ($N_t = 6$). The results indicate that the primary effects of N_a on the transverse dynamics, $w(x,t)$, are in the response frequency, with secondary effects in amplitude. It may be seen that the transverse dynamics are well captured by six axial modes, although nine axial modes yield an additional frequency correction. Figure 3.4 highlights the nonlinear dynamics in the axial direction. Here, the dynamic participation of the additional axial modes is apparent, as increases in N_a clearly produce higher frequency components in the response. It should be noticed that Figs. 3.3 and 3.4 show considerably different time frames, with approximately one period of the oscillations of Fig. 3.3 apparent as a slow harmonic component of Fig. 3.4. The high frequency dynamics visible in Fig. 3.4 are largely a result of the "ringing" of the axial modes due to nonlinear internal stresses which result from the initial conditions. That is, the initial conditions assume deflections in $w(x)$ only, without the corresponding (equilibrium producing) deflections in $u(x)$. However, the high frequency content of these dynamics aids in the accurate evaluation of model convergence. Once again, small differences may be observed between the dynamics produced using six and nine axial modes. Hence nine axial modes ($N_a = 9$) are used for the final system model.

Next, it is necessary to determine the number of transverse rotating modes, N_t,

to be used. As with the axial modes, this is done by comparing the dynamic beam response for various values of N_t. Figure 3.5 shows the transverse response at the beam tip, $w(L,t)$, for an initial condition in the second transverse mode, with $N_t = 3$, 6, and 9. The last two responses are quite close, but as small differences may still be observed between $N_t = 6$ and $N_t = 9$, and since the transverse dynamics are of greatest interest, the higher value was chosen.

Through these procedures, the final model was chosen to contain $N_c = 18$ stationary fixed-free beam modes, which are used to generate $N_t = 9$ transverse rotating modes. These transverse modes are then coupled to $N_a = 9$ axial modes, for a final model size of $N = N_t + N_a = 18$ modes. It is recognized that, due to the limited nature of this convergence study, and the well documented convergence difficulties for similar rotating systems, this model is somewhat minimal. However, it is of sufficient size to effectively demonstrate the nonlinear normal mode-based reduction procedure, and it will henceforth be referred to as the "exact" model.

An additional check of this model is illustrated in Fig. 3.6, which shows the periodic response frequency of the first mode as a function of the number of total model modes for a given motion amplitude. For this example, equal numbers of axial and transverse modes were used, so the abscissa corresponds to $N_a + N_t$. One can see that, at this amplitude, the response frequency is accurately determined by an 18 mode model. The periodic solutions used for this figure were obtained computationally by locating initial conditions in the vicinity of the first mode which yield a periodic solution. These solutions will, in fact, lie on the invariant manifold which is the basis of our reduction technique.

3.4 Nonlinear Mode-Based Model Reduction

The approach used here to generate reduced order models of Eqs. (3.9) and (3.10) was originally developed by Shaw and Pierre [2]. It utilizes invariant manifolds in the system's phase space to generate constraint equations which dynamically "enslave" nonessential modal degrees of freedom (DOF) to those of interest. The resulting reduced equations capture many of the nonlinear influences of the enslaved DOFs without requiring explicit simulation. A general exposition of the procedure and systematic implementation used here may be found in [64]. For this system, the transverse motions are of primary interest. Therefore, one or more of the transverse modal coordinates (c's), along with any internally resonant modal coordinates will be chosen as "master" coordinates, and the remaining coordinates will be enslaved. For example, if the set of "master" modal positions and velocities is denoted by $(\mathbf{u_M}, \mathbf{v_M})$, the reduced differential equation for a chosen transverse mode is of the following form:

$$\ddot{c_j} + \omega_{t,j}^2 \, c_j + f_{nl}(\mathbf{u_M}, \mathbf{v_M}) = \mathbf{0} \qquad \text{where } c_j \in \mathbf{u_M} \tag{3.13}$$

with the associated constraint equations,

$$c_k = X_{t,k}\,(\mathbf{u_M}, \mathbf{v_M}) \quad \dot{c_k} = Y_{t,k}\,(\mathbf{u_M}, \mathbf{v_M})$$
$$\text{where } k = 1 \ldots N_t, c_k \notin \mathbf{u_M}$$

$$a_k = X_{a,k}\,(\mathbf{u_M}, \mathbf{v_M}) \quad \dot{a_k} = Y_{a,k}\,(\mathbf{u_M}, \mathbf{v_M})$$
$$\text{where } k = 1 \ldots N_a, a_k \notin \mathbf{u_M}$$

Here, the function f_{nl} depends on the properties of the original system and is up to fifth order in the elements of $(\mathbf{u_M}, \mathbf{v_M})$, and the constraint equations (the X's and Y's) are third order polynomials in the elements of $(\mathbf{u_M}, \mathbf{v_M})$. The key to choosing

these constraints properly is that they are forced to satisfy the equations of motion. As an illustration, if $(\mathbf{u_M}, \mathbf{v_M})$ consists of only the position and velocity of the third mode, $(c_3, \dot{c_3})$, the resulting NNM-reduced differential equation is of the form:

$$\ddot{c_3} + \omega_{t,3}^2\, c_3 + A_1\, c_3^3 + A_2\, c_3\, \dot{c_3}^2 + A_3\, c_3^5 + A_4\, c_3^3\, \dot{c_3}^2 + A_5\, c_3\, \dot{c_3}^4 = 0 \qquad (3.14)$$

where the constants, A_i, are analytical functions of the system parameters. Hence, only the coordinates in $(\mathbf{u_M}, \mathbf{v_M})$ need to be simulated (using equations such as Eq.(3.13)), while the constraint equations are used to reconstruct the response of the enslaved modes. This reduction procedure has been computationally automated for a certain subclass of nonlinear structural systems—including Eqs. (3.9) and (3.10), where the nonlinear coefficients have been evaluated—such that one merely has to choose the desired "master" coordinate set, and the reduced equations of motion and constraint equations are automatically generated. In cases of internal resonance, non-removable coupling between resonant modes requires augmenting the set of "master" modes to include all modes which are internally resonant with the original set. That is, internally resonant groups of modes must lie entirely in either the "master" or "slave" subgroups. More complete expositions of this material may be found in [63, 64]

The rotating beam system is particularly well suited for this reduction procedure for two reasons. First, the axial nonlinearities—see Eq. (3.9)—are only functions of the c_j's. This improves the accuracy of the constraint equations, as several higher order (error generating) effects are eliminated. Secondly, the nature of the nonlinearity results in nonlinear coefficients (such as σ and γ) which grow with the modal wave number. Therefore, nonlinear effects from higher modes are likely to be important for these systems. Nonlinearities which are "translational" (such as nonlinear

springs between adjacent masses) do not share this property, and yield systems which approach linearity as the mode number is increased.

3.5 Results

Results are given for several cases. First, the time-dependent shape of the deformed beam is illustrated for motions occurring in the third nonlinear mode, and the relationship between modal amplitude and response frequency is discussed for the first three modes. Second, the rotation rate, Ω, is tuned to create a 3:1 internal resonance between the first two transverse modes. Results generated from the reduced, 2-DOF models of this system are then compared to those of the "exact" model. Lastly, system parameters are adjusted to create an internal resonance between an axial and transverse mode. As before, the proposed NNM approach is compared with other reduction methods.

One feature of the nonlinear normal mode method is that, although only one mode is simulated, the others can be reconstructed through the constraint equations. This results in nonlinear modes which change shape with amplitude and velocity (also known as non-similar NNMs [44]). This property is illustrated in Fig. 3.7, where the functions $w(x,t)$ and $u(x,t)$ are reconstructed from a simulation time-history and the relevant constraint equations. Mode shapes are shown for several instants of time, spaced evenly within a quarter-period of motion. The non-similar nature of $w(x,t)$ is not especially noticeable, although the peak displacement of the first lobe does move to the right as the amplitude decreases. Note that, for $u(x)$, the static solution is included (dashed line), and that all departures from this are non-similar, as the axial and transverse motions are linearly uncoupled. Also, for $u(x,t)$, the shapes shown are representative of the entire periodic behavior. That is, while

$w(x,t)$ would become symmetric about the x-axis with further time sampling, the corresponding axial motion, $u(x,t)$, would simply repeat (at twice the frequency of $w(x,t)$).

Further insight may be obtained through examination of Fig. 3.8, which illustrates the relation between the response frequency and amplitude for the first three nonlinear modes, using various models. Here, the "Exact Model" indicates the frequency of a periodic solution for the full (18-DOF) model, found through numerical methods. This solution lies on the "exact" invariant manifold, and is successfully approximated by our nonlinear mode approach over a range particular to each mode. The quasi-static results shown here illustrate the effects of eliminating axial independence through quasi-static assumptions. This approach relies on the distinct separation between the axial and transverse modes. Hence, while effective here, it is not readily extendible to realistic blade geometries, as the modes of these models contain no such distinct categories. The "One Linear Mode: Nonlinear" result eliminates the influence of all other modes, and consequently diverges quite quickly. The divergence observed between the nonlinear mode and exact solutions is due to higher order effects which cannot be captured by the third-order manifold employed here. Model fidelity could be improved through the use of higher-order manifolds. As an aid for physical interpretation, a tip displacement of .2m approximately corresponds to a transverse modal amplitude of 1.0 (for all transverse modes).

A 3:1 internal resonance between the first two transverse modes was created by adjusting the rotation rate, Ω, from 30 to 23.85 rad/s. Conditions such as this may easily occur during typical operations. As with the single-mode results above, Fig. 3.9 depicts results from various two-DOF reduced systems, and their comparison with the "exact" results. Here, the "exact" (Eighteen Linear Modes) model dynamics

are initiated on the approximate invariant manifold. That is, the initial conditions in the mode(s) of interest are chosen, and then the remaining degrees of freedom are assigned their initial values according to the constraint equations, Eq. (3.4). For this case, the coupling between the two resonant modes is well captured by the nonlinear normal mode approach, which requires the calculation of a two-mode (four-dimensional) invariant manifold, and yields a fully coupled, two-DOF, reduced model. The "Two Linear Modes: Nonlinear" response includes the two internally resonant modes, and their nonlinear coupling terms, but fails to achieve the proper qualitative or quantitative results. Under these circumstances, the proposed reduction procedure is particularly attractive. Figure 3.10 illustrates the effectiveness of the manifold constraint equations for predicting the motion of non-modeled modes. The two curves shown depict the displacement of the ninth transverse mode for the motion shown in Fig. 3.9, and compare the dynamics obtained through numerical integration of the entire system, with those predicted by the manifold constraint equations. That is, the "Simulated" curve is a product of the dynamic interactions of a 18-DOF system, while the "Reconstructed" curve is a polynomial combination of the positions and velocities of the first and second transverse modes. It is precisely this motion which must occur if this mode is not to contaminate the reduced dynamics.

Lastly, a 2:1 internal resonance between the first axial mode and the fourth transverse mode exists for following parameter values: $m = 11.84\,\mathrm{kg/m}$, $EI = 4.73 \times 10^5\,\mathrm{N\,m^2}$, $EA = 1.89 \times 10^8\,\mathrm{N}$, $\Omega = 30\,\mathrm{rad/s}$, and $h = 0\,\mathrm{m}$. As before, the results in Fig. 3.11 show considerable error when additional modes are not accounted for. The "Two Linear Modes: Nonlinear" results, though internally resonant, exhibit a period of modulation which is entirely wrong. Of course, if more linear modes are simply added, these results will improve, but in cases such as this it is difficult to

deduce which modes would yield the most improvement. That is, should one add the third transverse, fifth transverse, or second axial modes to the model to achieve the best three-mode model for the study of this internal resonance? These questions are automatically resolved through the use of nonlinear normal modes by properly accounting for all other modes, thus avoiding guesswork and oversized models.

3.6 Conclusions

The above results illustrate the utility of the invariant manifold-based approach for generating nonlinear normal modes. For the rotating beam system considered, there are critical nonlinear couplings between the system's linear modes which must be accounted for if accurate results are to be obtained. Specifically, the coupling between the transverse and axial modes, due to bending induced foreshortening effects, is essential. The NNM approach accurately estimates the influence of this coupling for moderate amplitude motions, generating minimal models which retain considerable accuracy.

In addition, the systematic nature of the reduction process makes it applicable to more complex blade models. In geometrically correct blade models, the system modes no longer occur in easily separable categories. Likewise, the nonlinearities do not share the ordered structure of our model. However, if the linear modes are known, and the nonlinear coupling terms have been determined, the reduction process remains unchanged. Hence, the methods proposed herein may readily be extended to more realistic rotorcraft blade models—ultimately yielding optimal reduced models with minimal guesswork.

With this goal in mind, there are some particular issues which require further attention. The blade model must be shifted from analytical to finite-element based,

allowing the generation of models with complex geometry and material properties. This generalization requires work at the element level, due to the nature of the nonlinearities involved, but will enable the inclusion of more general motions, such as torsion and lead-lag. In addition, with the goal of improving manifold accuracy, some refinements to the reduction procedure may be possible. Such refinements will significantly extend the valid amplitude range of NNM-based models.

3.7 Figures

	$\omega_{t,1}$	$\omega_{t,2}$	$\omega_{t,3}$	$\omega_{t,4}$	$\omega_{a,1}$	$\omega_{a,2}$
$\Omega = 0$	8.672	54.35	152.2	298.2	824.7	2474.0
$\Omega = 30$	34.03	95.84	200.5	351.5	824.1	2473.9

Table 3.1: The transverse and axial natural frequencies (in rad/s) for the first several modes both at rest ($\Omega = 0$) and at the nominal rotation rate ($\Omega = 30$ rad/s).

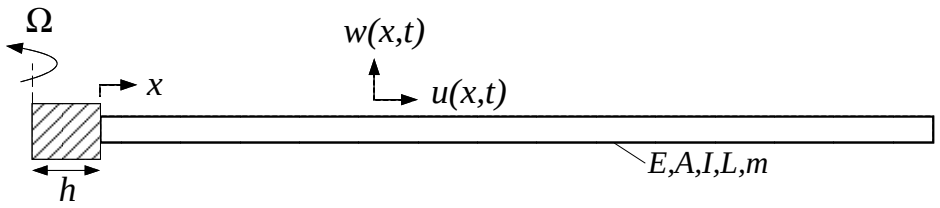

Figure 3.1: Rotating beam system, Ω =Constant

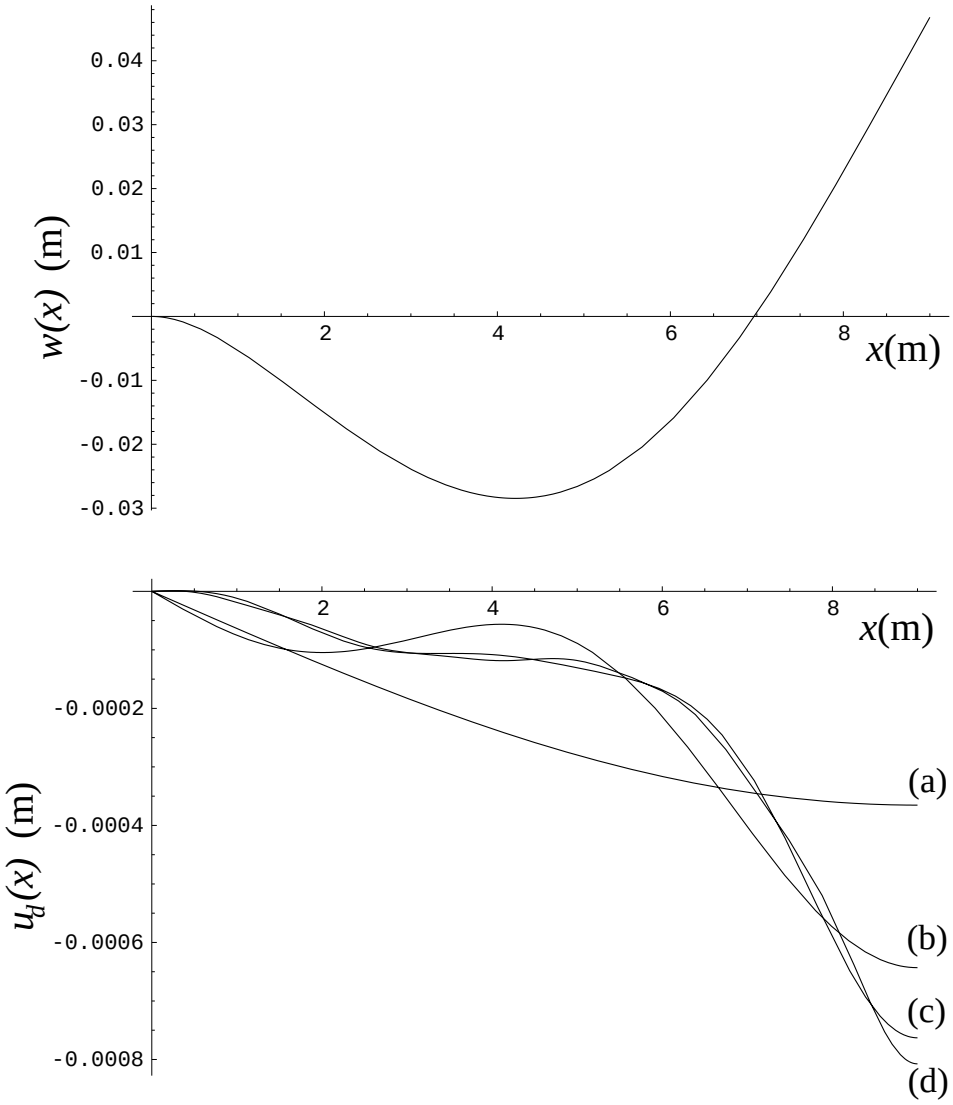

Figure 3.2: Axial deflection, $u_d(x)$, due to a static transverse deflection, $w(x)$, for various values of N_a; (a) $N_a = 1$, (b) $N_a = 3$, (c) $N_a = 6$, (d) $N_a = 12$.

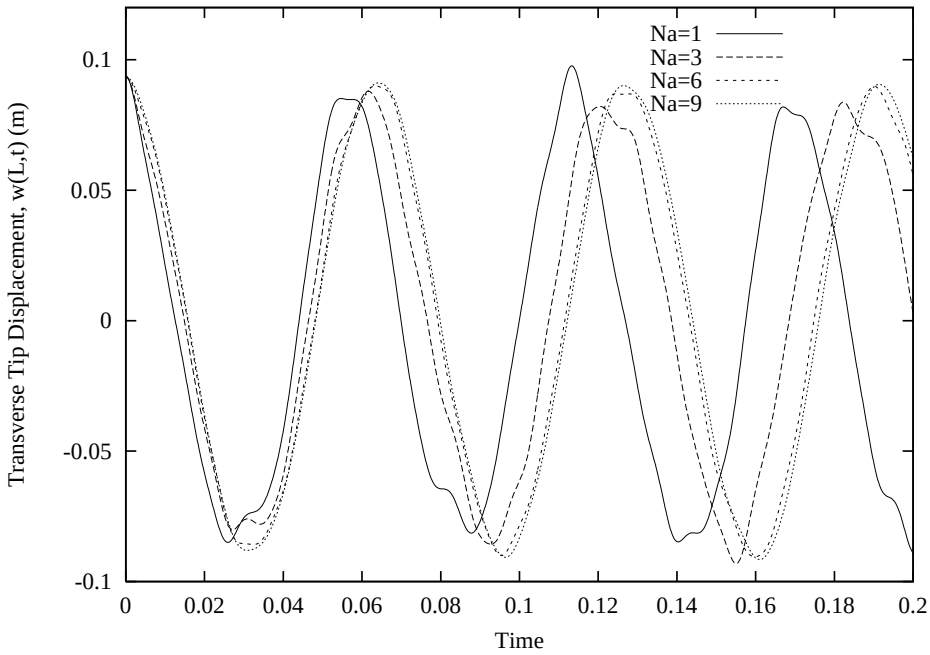

Figure 3.3: Transverse dynamics initiated in the second transverse mode, shown at the beam tip, for various values of N_a.

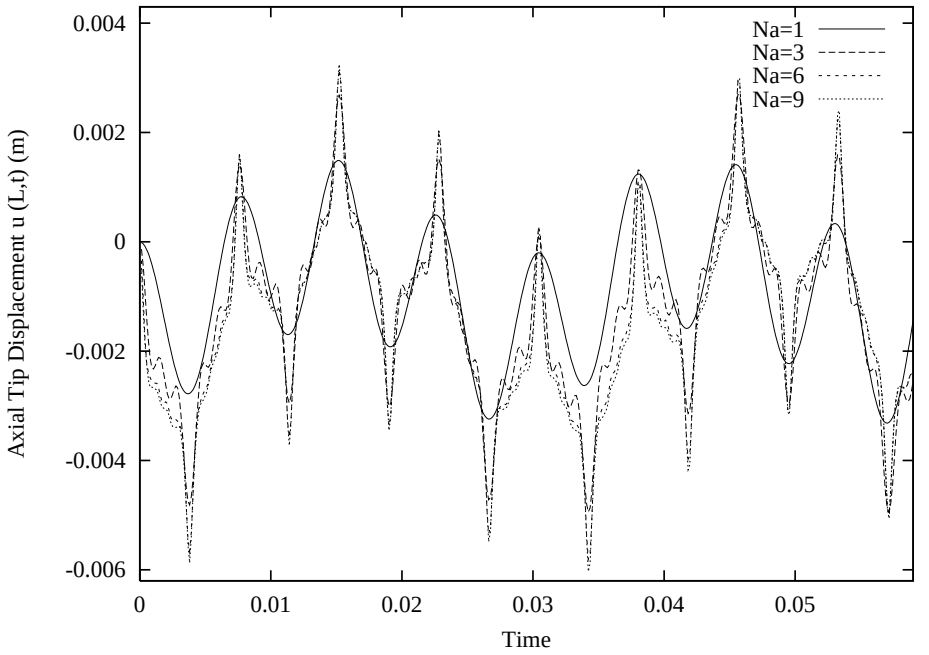

Figure 3.4: Axial dynamics due to initial conditions in the second transverse mode, shown at the beam tip, for various values of N_a.

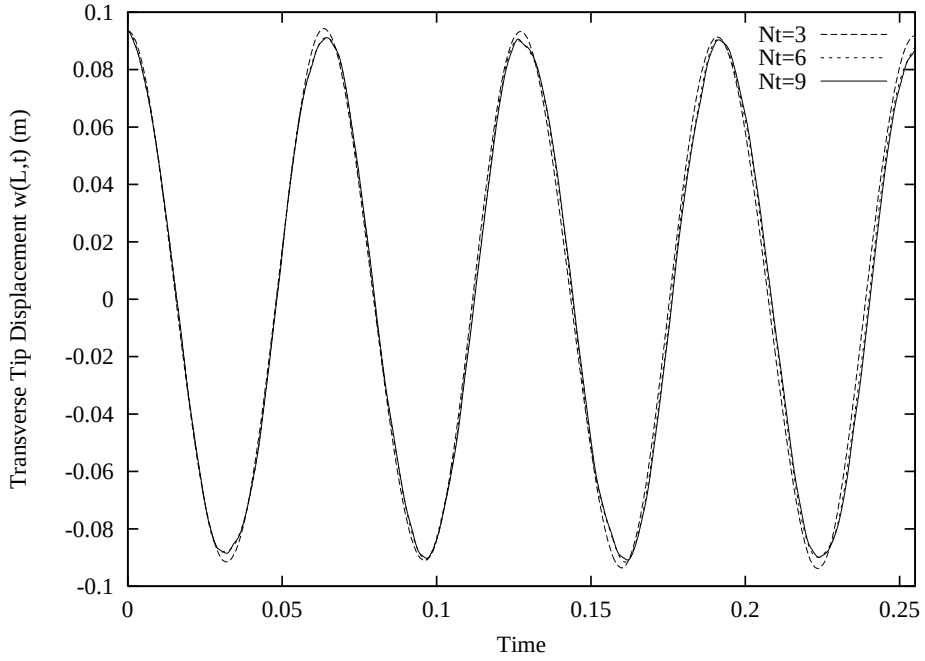

Figure 3.5: Transverse dynamics initiated in the second transverse mode, shown at the beam tip, for various values of N_t.

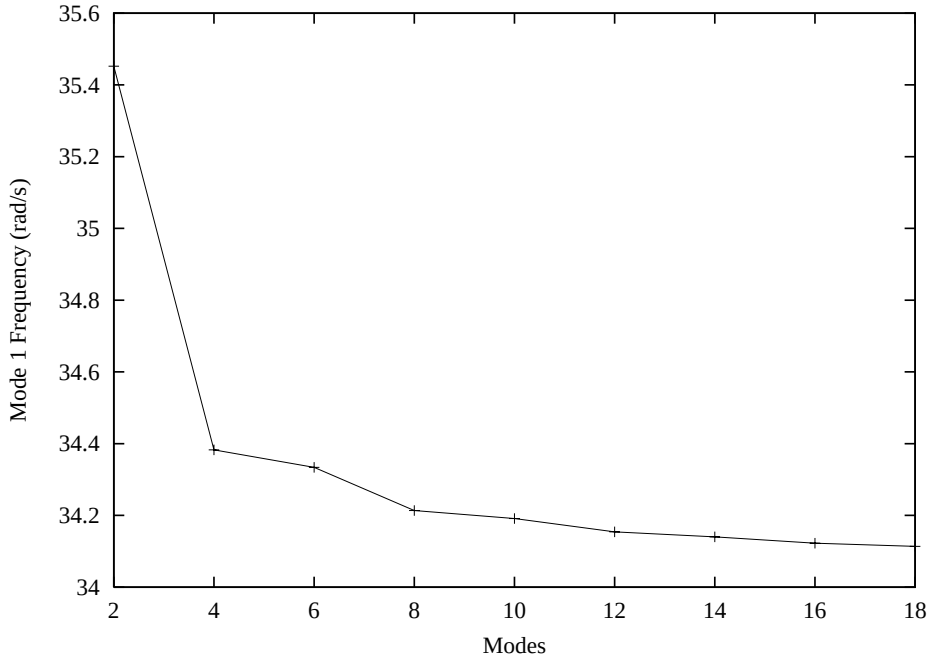

Figure 3.6: Mode 1 frequency versus number of modes. here, $N_a = N_t$, and $c_1(0) = 1.0$, corresponding to an end deflection of $w(L) \approx 0.2$m.

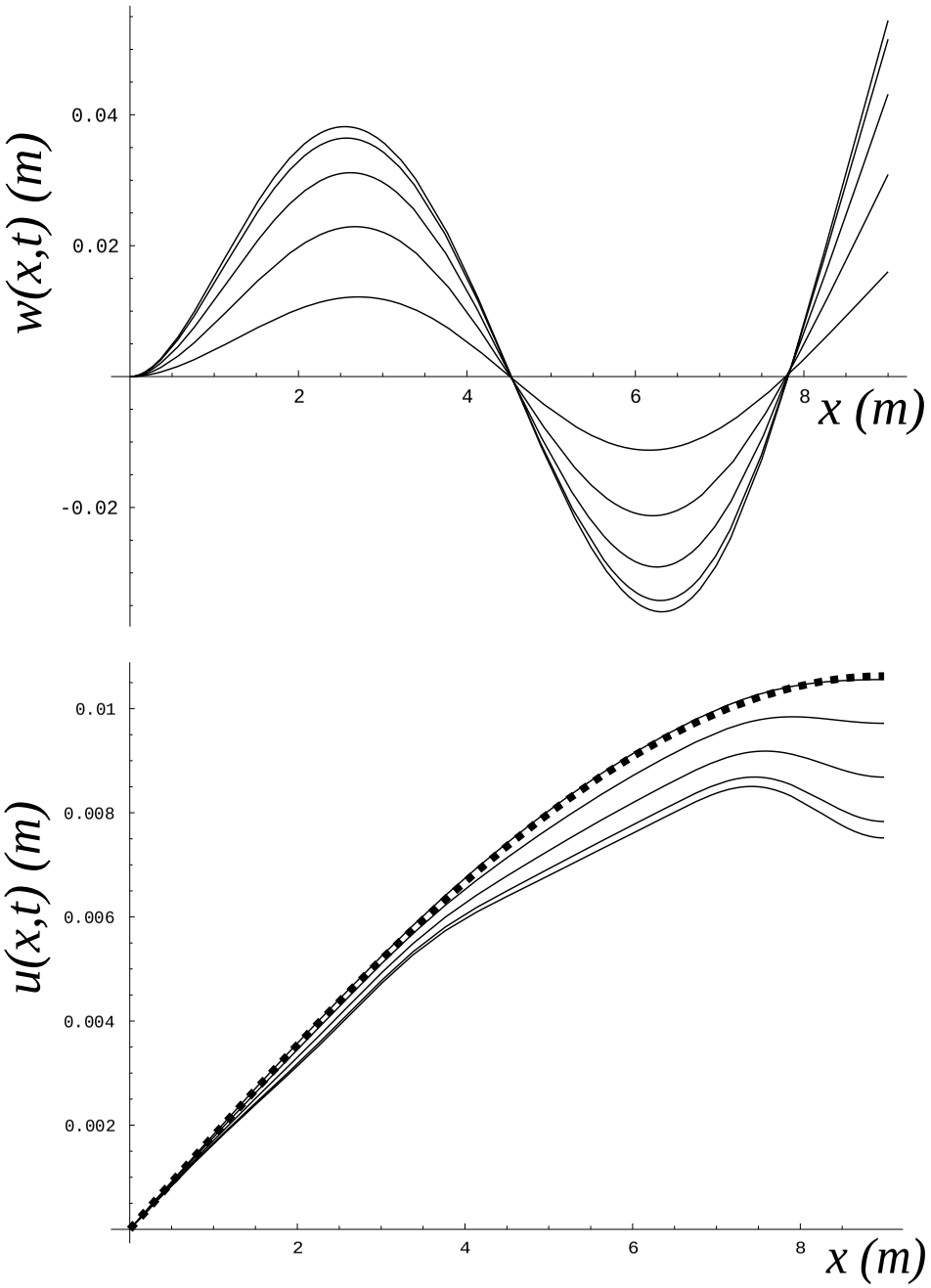

Figure 3.7: Transverse and axial deflections, $w(x,t)$ and $u(x,t)$, for a quarter-period of motion in the third nonlinear mode. The dashed line denotes the static deflection, $u_s(x)$.

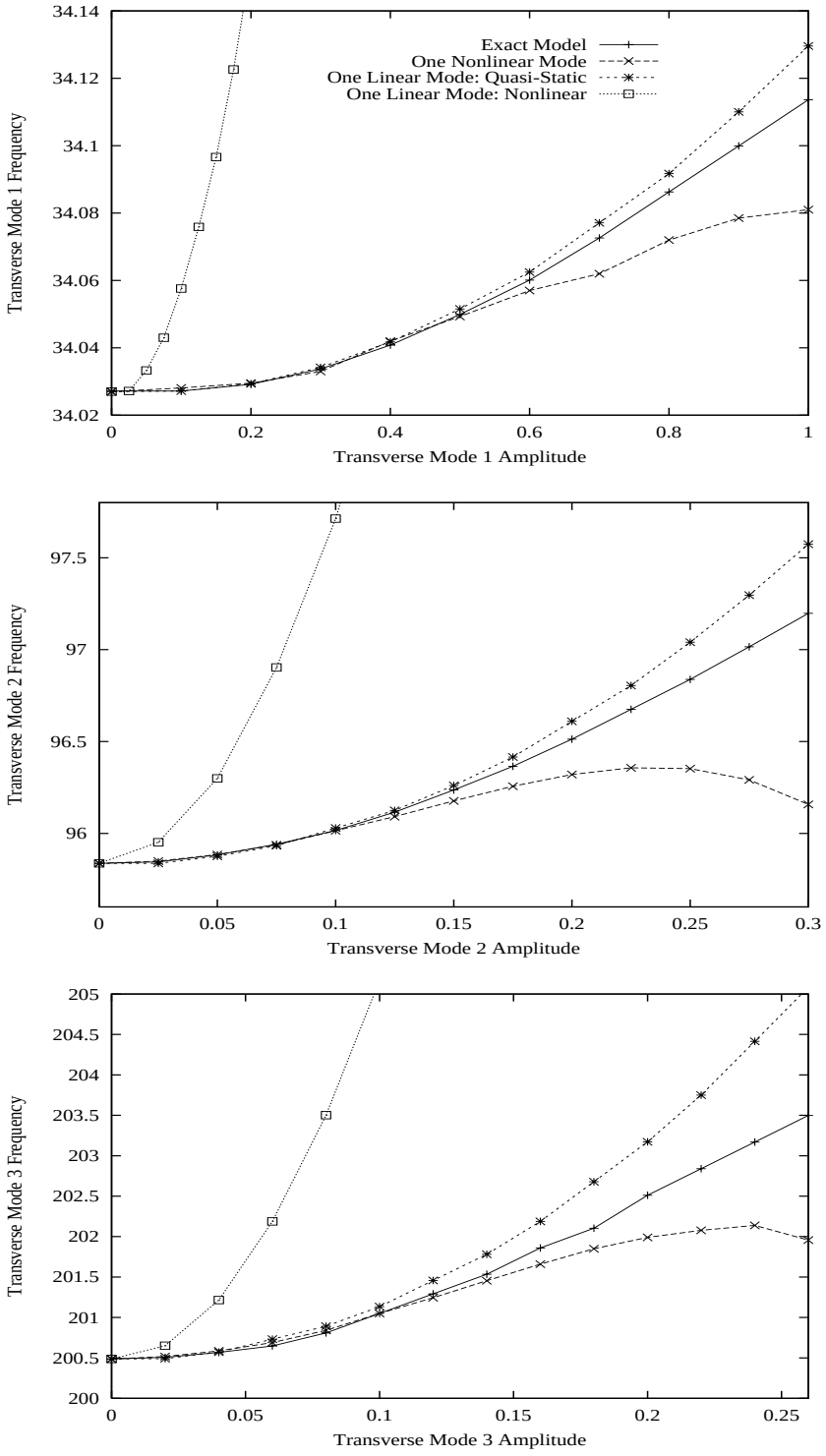

Figure 3.8: Response frequency as a function of modal amplitude for several one-mode models, as well as the exact solution, for the first three transverse modes.

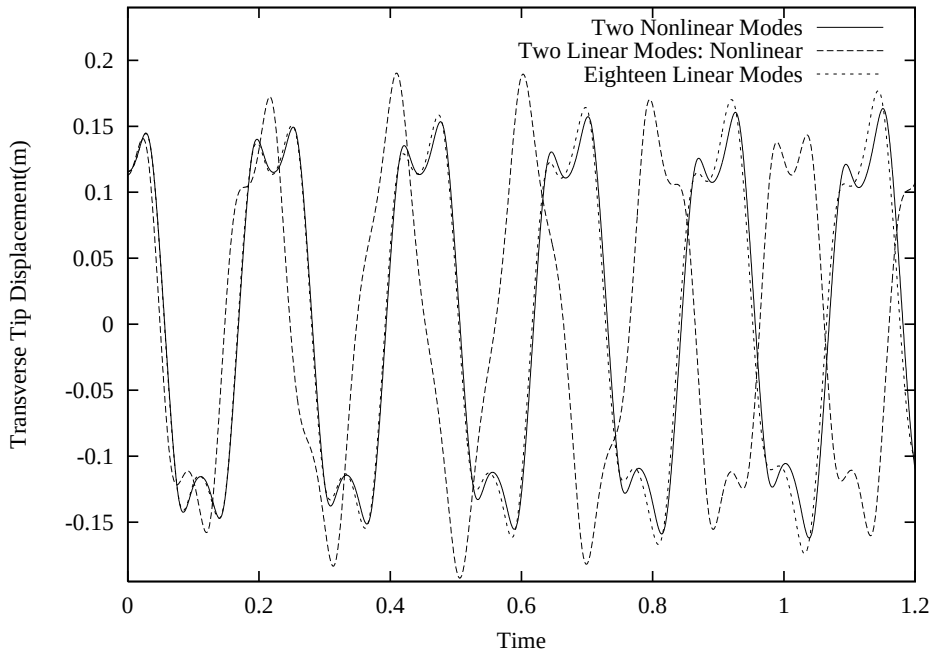

Figure 3.9: Transverse deflection, $w(L,t)$, initiated on a two-mode (first and second transverse) nonlinear manifold with $3\omega_{t,1} \approx \omega_{t,2}$, for the "Exact" and various reduced (2-DOF) models.

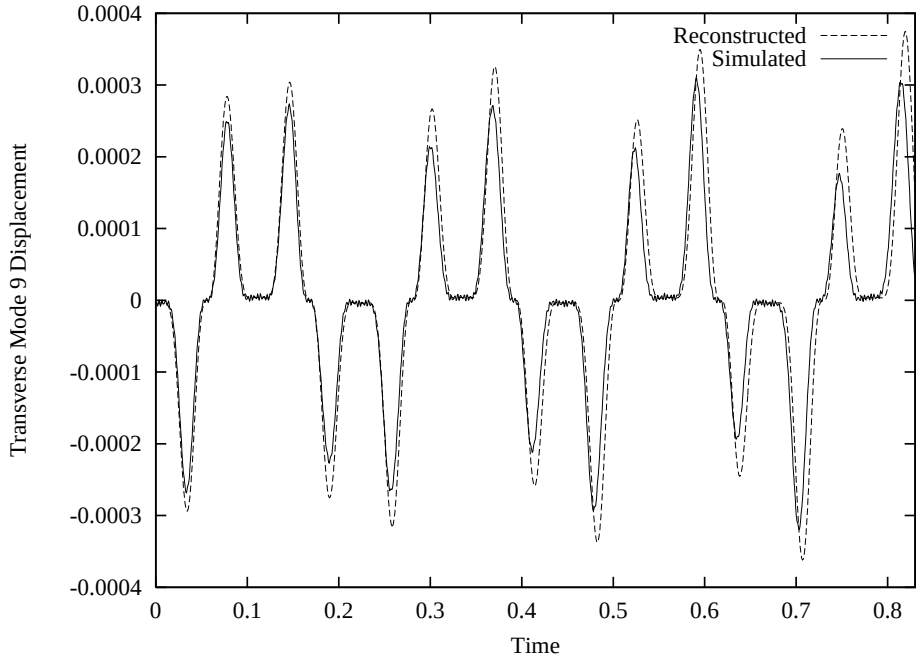

Figure 3.10: Modal deflection of the ninth transverse mode, $c_9(t)$, initiated on a two-mode (first and second transverse) nonlinear manifold with $3\omega_{t,1} \approx \omega_{t,2}$ as predicted by simulation, and reconstructed using the constraint equations, Eq. (3.4).

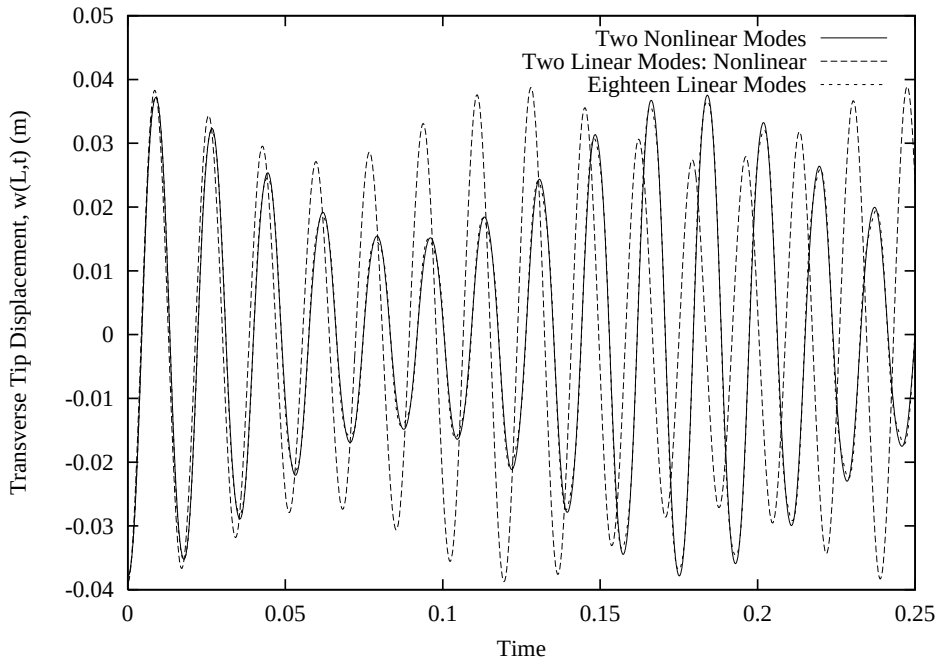

Figure 3.11: Transverse deflection, $w(L,t)$, initiated on a two-mode (fourth transverse and first axial) nonlinear manifold with $2\omega_{t,4} \approx \omega_{a,1}$, for the "Exact" and various reduced (2-DOF) models.

CHAPTER IV

A NEW GALERKIN-BASED APPROACH FOR ACCURATE NONLINEAR NORMAL MODES THROUGH INVARIANT MANIFOLDS

4.1 Introduction

The generation of effective reduced order models for nonlinear dynamic systems is difficult, due to the complex interactions between system components. These nonlinear interactions typically couple the system dynamics such that accurate results may only be achieved through the inclusion of many modes or degrees of freedom (DOFs). Such large models are cumbersome, making analysis both difficult and slow, as well as physically nonintuitive. Alternatively, smaller models often sacrifice accuracy, ultimately yielding questionable results. Ideally a minimal model is sought, which accurately accounts for the nonlinear interactions between components, without requiring their explicit simulation. In pursuit of this goal, there has been considerable work on the development of reduced-order models (ROMs) of nonlinear dynamic systems.

Some early work along these lines concentrated on the definition and existence of nonlinear normal modes (NNMs), their properties, and illustrative examples [12, 21]. These concepts were further extended by Rand [13, 22], and more recently by King

and Vakakis [23, 26] among others. The present work builds upon the invariant manifold formulation developed by Shaw and Pierre [2, 3] and extended in reference [63]. This nonlinear extension of modal analysis allows one to generate reduced-order models by restricting non-essential modes (or DOFs) to an invariant manifold parameterized by a set of retained modes (or DOFs). This invariant manifold allows the corresponding ROM to account for the participation of all DOFs without requiring their explicit simulation. Although some work has been done using periodicity constraints to locate the invariant manifold numerically [40], most approaches use asymptotic methods to generate polynomials which approximate the manifold locally. This approach has been used successfully for the analysis of systems within the local nonlinear regime [39, 64, 65]. However, as is typical of asymptotic methods, the resultant dynamics are only accurate for small motions, and the upper bound for these motions is not known *a priori*. In addition, due to the nature of the polynomial approximation, the divergence of the asymptotic approximation and the actual manifold may occur at small amplitudes — yielding entirely inaccurate results at amplitudes only slightly beyond the domain of convergence. Hence, though the invariant manifold formulation of the NNM is sound, the asymptotic solution method sometimes yields results with limited applicability.

If nonlinear modal analysis is to become a practical tool, it must be accurate, reliable, and general. Earlier efforts have not fully met these criteria. The various asymptotic methods are locally accurate, but the unknown extent of this accuracy, restrictions on the types of nonlinearities that can be handled, and the effort necessary result in limited reliability and generality. Other analytical methods have typically restricted either the temporal or spatial behavior of the model, ultimately compromising both accuracy and generality. Lastly, numerical simulations may be

used to locate the invariant manifold, and generate ROMs, but this requires extensive simulation and relies upon the periodicity of the system response. Hence, this approach is cumbersome and lacks generality.

The approach developed herein eliminates many of these problems. As with the asymptotic approach, the nonlinear partial differential equations governing the manifold are solved approximately. However, instead of the local polynomial approximation, a series approximation is employed over a chosen domain. Nonlinear equations in the expansion coefficients are obtained through a Galerkin projection and then solved to achieve an approximation of the manifold which minimizes the error for the selected set of basis functions, i.e., the error is minimized in the domain spanned by the chosen basis functions. Typical results are shown in Fig. 4.1, which illustrates the difference between the asymptotic and Galerkin-based manifolds. The curves shown correspond to cross sections of the second-mode manifold for the ten-mode finite element beam model discussed in Section 4.4. This approach allows one to determine the manifold geometry to a chosen accuracy through a given (and possibly large) amplitude. Furthermore, the chosen formulation and computational nature of this approach allow it to be used for the analysis of a large variety of nonlinear dynamic systems. Some similar work on the reduction of dynamic systems using Galerkin methods has been conducted by Steindl *et al.* [46].

The application of the nonlinear Galerkin method, as well as the coordinate transformation of the manifold-governing partial differential equations (PDEs) developed herein constitute unique contributions to the field. Their utility is illustrated through the examination of two example systems. First, a two degree of freedom system with cubic nonlinearities is analyzed. The convergence and geometry of the two (numerically obtained) approximate invariant manifolds are discussed, and the

Galerkin-based reduced model is shown to accurately predict the system response. These results are compared against those from the asymptotic approach. Second, a finite element based beam model with a quadratic/cubic nonlinear torsional spring at one end is examined. Results are presented which correspond to the second and fifth nonlinear normal modes of the beam. As with the simpler system, these results indicate that the Galerkin-based reduced-order model retains accuracy throughout the chosen amplitude domain, without requiring the nonlinear effects to remain weak. This accuracy enables one to use the reduced order model with confidence in its validity, even for amplitudes corresponding to large nonlinear effects.

These examples serve to illustrate the potential of this approach. The formulation may be extended to determine manifolds of higher dimension, yielding reduced-order, multi-DOF, models for motions occurring within multiple, interacting modes. In addition, considerable insight may be obtained through the application of this process to existing problems within the area of nonlinear dynamics. Ultimately, this approach promises to be a valuable new tool for the analysis and understanding of nonlinear dynamic systems.

4.2 Formulation

This approach assumes that a reduced-order model is sought for a set of nonlinear coupled oscillators. Whether from a system of discrete masses, finite element model, or discretized continuous system, these may be expressed in the form:

$$\ddot{\boldsymbol{\eta}} + [Z]\dot{\boldsymbol{\eta}} + [\Omega]\boldsymbol{\eta} = \boldsymbol{f}(\boldsymbol{\eta}, \dot{\boldsymbol{\eta}}) \tag{4.1}$$

where $\boldsymbol{\eta}$ is a vector of normalized modal coordinates, $[Z]$ and $[\Omega]$ are diagonal damping and stiffness matrices, respectively, $\boldsymbol{f}(\boldsymbol{\eta}, \dot{\boldsymbol{\eta}})$ contains any additional linear or

nonlinear terms, and each overdot indicates a time derivative. The individual elements of $[Z]$ and $[\Omega]$ are written as $2\zeta_i\omega_i$, and ω_i^2, respectively, for the ith equation. This form is selected for analytical convenience, and does not reflect a necessary restriction of the approach.

From this point, previous single-mode invariant manifold formulations [2] have constrained all degrees of freedom to be functions of a chosen coordinate pair, as:

$$\begin{aligned} \eta_i &= X_i(\eta_k, \dot{\eta}_k) \\ &\qquad\qquad \text{for } i = 1 \ldots N, i \neq k \\ \dot{\eta}_i &= Y_i(\eta_k, \dot{\eta}_k) \end{aligned} \tag{4.2}$$

for N original modal coordinates. Here, an alternative set of coordinates is defined using the transformation:

$$\begin{aligned} \eta_k &= a\cos\phi \\ \dot{\eta}_k &= -a\omega_k \sin\phi \end{aligned} \tag{4.3}$$

and, the original constraints, Eq. (4.2) become:

$$\begin{aligned} \eta_i &= P_i(a, \phi) \\ &\qquad\qquad \text{for } i = 1 \ldots N, i \neq k \\ \dot{\eta}_i &= Q_i(a, \phi) \end{aligned} \tag{4.4}$$

The resulting system uses this hybrid coordinate system. That is, all modal positions and velocities are expressed in terms of a "master" amplitude and phase corresponding to the motions of the kth mode. These constraint relations are dictated for the kth mode (by Eq. (4.3)), and remain unknown for all others. Determining these

unknown relations, that is, P_i and Q_i, will ultimately yield reduced dynamic equations in $a(t)$ and $\phi(t)$ only. Unlike earlier methods, this approach is not conducive to solutions through polynomial expansions. However, it does offer the following advantages:

- The dynamics in the transformed coordinates are elementary for $\boldsymbol{f} = 0$.
- The new constraint equations, (P_i, Q_i) must be periodic in ϕ, and thus may be expressed with harmonic functions in ϕ.
- The bounding values for the manifold are reduced from four values $(\pm u_k, \pm v_k)$ to one — the upper bound of a.

As an alternative to modal positions and velocities, the entire system may be transformed to an amplitude–phase representation. However, this approach is unnecessarily complex, as it is more cumbersome to represent one set of amplitudes and phases in terms a "master set," and such a system is further removed from the original coordinates.

The original equation of motion governing η_k may be transformed into two first order equations in a and ϕ [5]:

$$\begin{aligned} \dot{a} &= \left(\frac{-f_k}{\omega_k} - 2\zeta_k \omega_k a \sin\phi\right) \sin\phi \\ \dot{\phi} &= \omega_k - \left(\frac{f_k}{a\omega_k} + 2\zeta_k \omega_k a \sin\phi\right) \cos\phi \end{aligned} \tag{4.5}$$

and the remaining differential equations may be written in first order form as:

$$\begin{aligned} \dot{P}_i(a,\phi) &= Q_i(a,\phi) \\ \dot{Q}_i(a,\phi) &= -2\zeta_i \omega_i Q_i(a,\phi) - \omega_i^2 P_i(a,\phi) + f_i \end{aligned} \qquad \text{for } i = 1 \ldots N, i \neq k \tag{4.6}$$

The time derivatives on the left hand side of Eq. (4.6) may be expanded using the chain rule to obtain

$$\dot{P}_i(a,\phi) = \frac{\partial P_i}{\partial a}\dot{a} + \frac{\partial P_i}{\partial \phi}\dot{\phi}$$

$$\text{for } i = 1 \ldots N, i \neq k \tag{4.7}$$

$$\dot{Q}_i(a,\phi) = \frac{\partial Q_i}{\partial a}\dot{a} + \frac{\partial Q_i}{\partial \phi}\dot{\phi}$$

Equations (4.5–4.7) are combined to yield a set of partial differential equations (PDEs) that are independent of time and govern the invariant manifold geometry:

$$Q_i = \frac{\partial P_i}{\partial a}\left(\frac{-f_k}{\omega_k} - 2\zeta_k\omega_k a\sin\phi\right)\sin\phi + \frac{\partial P_i}{\partial \phi}\left[\omega_k - \left(\frac{f_k}{a\omega_k} + 2\zeta_k\omega_k a\sin\phi\right)\cos\phi\right] \tag{4.8}$$

$$\text{for } i = 1 \ldots N, i \neq k$$

$$\begin{aligned} -2\zeta_i\omega_i Q_i - \omega_i^2 P_i + f_i \;\; = \;\; & \frac{\partial Q_i}{\partial a}\left(\frac{-f_k}{\omega_k} - 2\zeta_k\omega_k a\sin\phi\right)\sin\phi \\ & + \frac{\partial Q_i}{\partial \phi}\left[\omega_k - \left(\frac{f_k}{a\omega_k} + 2\zeta_k\omega_k a\sin\phi\right)\cos\phi\right] \end{aligned} \tag{4.9}$$

$$\text{for } i = 1 \ldots N, i \neq k.$$

In previous works, a similar process is used to yield manifold-governing equations in terms of a master position and velocity, (u_k, v_k). A polynomial expansion in u_k and v_k is then used to asymptotically approximate the local solution to a given order. Herein, the asymptotic approach is replaced by a Galerkin method. As before, the solution is achieved through a function series with unknown coefficients, but here the functions of amplitude and phase (a and ϕ), are defined over a preselected amplitude domain. The solution of the resulting discretized equations minimizes the error over the chosen domain, yielding manifolds of considerably greater accuracy and range.

The unknown position and velocity constraint relations are expanded as a double series in the amplitude and phase as:

$$P_i(a,\phi) = \sum_{l=1}^{N_a}\sum_{m=1}^{N_\phi} C_i^{l,m}\, T_{l,m}(a,\phi)$$

$$\text{for } i = 1\ldots N, i \neq k \qquad (4.10)$$

$$Q_i(a,\phi) = \sum_{l=1}^{N_a}\sum_{m=1}^{N_\phi} D_i^{l,m}\, U_{l,m}(a,\phi)$$

where the C's and D's are the unknown expansion coefficients and the $T_{l,m}$ and $U_{l,m}$ are known shape functions, typically composed of products of functions in a, and ϕ. For example, a given $T_{l,m}$ might be a product of a harmonic function in ϕ and a polynomial function in a, defined over the domain $a \in [0, a_o]$, $\phi \in [0, 2\pi]$. N_a and N_ϕ are used to denote the number of expansion functions used in a and ϕ, respectively. This expansion is substituted into the manifold-governing equations (Eqs. (4.8) and (4.9)), which are multiplied through by a to remove the singularity at $a = 0$. Finally, all terms are moved to the right side of the equation, and a Galerkin projection [5] is carried out using the individual shape functions over the chosen domain. This leaves:

$$0 = \int_{a,\phi} U_{p,q}\left[-a\sum_{l,m} D_i^{l,m}U_{l,m} + \sum_{l,m} C_i^{l,m}\frac{\partial T_{l,m}}{\partial a}\left(\frac{-f_k}{\omega_k} - 2\zeta_k\omega_k a\sin\phi\right)a\sin\phi\right.$$

$$\left. + \sum_{l,m} C_i^{l,m}\frac{\partial T_{l,m}}{\partial \phi}\left[a\omega_k - \left(\frac{f_k}{\omega_k} + 2\zeta_k\omega_k a^2\sin\phi\right)\cos\phi\right]\right] da\, d\phi \qquad (4.11)$$

$$0 = \int_{a,\phi} T_{p,q} \Bigg[2\zeta_i \omega_i a \sum_{l,m} D_i^{l,m} U_{l,m} + \omega_i^2 a \sum_{l,m} C_i^{l,m} T_{l,m} - a f_i$$

$$+ \sum_{l,m} D_i^{l,m} \frac{\partial U_{l,m}}{\partial a} \left(\frac{-f_k}{\omega_k} - 2\zeta_k \omega_k a \sin\phi \right) a \sin\phi \tag{4.12}$$

$$+ \sum_{l,m} D_i^{l,m} \frac{\partial U_{l,m}}{\partial \phi} \left[a\omega_k - \left(\frac{f_k}{\omega_k} + 2\zeta_k \omega_k a^2 \sin\phi \right) \cos\phi \right] \Bigg] da\, d\phi$$

for $i = 1 \ldots N, i \neq k, p = 1 \ldots N_a$, and $q = 1 \ldots N_\phi$. This represents a set of $2(N-1)N_a N_\phi$ nonlinear equations in the C's and D's, the solution of which will be optimal (in a least squares sense) for the chosen basis functions and domain.

In principle, this integration could be completed analytically, leaving a set of explicit nonlinear equations. However, as the system size and number of expansion functions increase, this quickly becomes impractical. The alternative is to use numerical integration for each function evaluation. Though it is considerably slower than an explicit formulation, this approach requires very little additional analytic work, and the generality of $\boldsymbol{f}$ makes it applicable to a wide variety of nonlinear systems. Regardless of the evaluation method, Eqs. (4.11) and (4.12) may be solved using an algorithm for the solution of multi-variable nonlinear systems of equations. This solution yields the series coefficients for each $P_i(a,\phi), Q_i(a,\phi)$ pair over the chosen domain, e.g., $\phi \in [0, 2\pi], a \in [0, a_o]$.

Unlike the asymptotic approach, here the expansion order may be increased to produce more accurate results without requiring additional analytical work. Hence manifold accuracy is reduced to an issue of computational effort. Also, the domain of convergence is known *a priori*, and the results obtained may be used with confidence throughout that region, once the desired convergence is achieved.

Once the P_i and Q_i have reached the desired accuracy, f_k, in Eq. (4.5), may be

evaluated for any given (a, ϕ), and the dynamics within the chosen mode may be determined. The resultant time histories, $a(t)$ and $\phi(t)$, allow the evaluation of all linear modal positions and velocities (through the P's and Q's — Eq. (4.10)), and the global system response may be assembled.

It should be noted that there are other solution methods which may be applied to obtain the coefficients. For example, an incremental approach which separates each C and D as $C_i = C_i^o + \delta C_i$, and $D_i = D_i^o + \delta D_i$ could be linearized locally (in the δC's and δD's) and used iteratively until a solution was reached. However, as above, the integration for each step must be done either analytically (using a general formulation) or numerically, and the resulting solution will apply over the chosen domain.

Thus the nonlinear Galerkin method described above allows one to generate accurate reduced-order models for many types of nonlinear structures, without restrictions on the form or magnitude of the nonlinearity, and these models are expected to maintain fidelity throughout a predetermined domain.

In the next two sections, this formulation is applied to generate reduced-order models of two example systems. The first, a two-mass system with purely cubic nonlinearities, serves to solidify the concepts developed above and uses a single function set to represent the amplitude dependence of the manifold. The second system is intended to showcase the power and benefits associated with the nonlinear Galerkin approach. A nonlinear finite element beam model is used to generate a set of equations which are then reduced to a single-mode ROM. Due to the model size, this reduction is carried out by solving the manifold equations over several local domains. This composite manifold is then used for the ensuing analysis.

4.3 Application: A Nonlinear Two-mass System

As an illustrative example, the nonlinear undamped two-mass system shown in Fig. 4.2 is used. The corresponding equations of motion in q_1 and q_2 are:

$$\begin{aligned} \ddot{q_1} + q_1 + 5(q_1 - q_2) &= -2q_1^3 - (q_1 - q_2)^3 \\ \ddot{q_2} + 5(q_2 - q_1) &= -(q_2 - q_1)^3 \end{aligned} \tag{4.13}$$

A linear eigenanalysis is carried out, and the natural frequencies are found to be:

$$\omega_1 = 0.689 \qquad \omega_2 = 3.244$$

and a transformation matrix of the form:

$$\left\{ \begin{array}{c} q_1 \\ q_2 \end{array} \right\} = \left[\begin{array}{cc} 0.671 & 0.741 \\ 0.741 & -0.671 \end{array} \right] \left\{ \begin{array}{c} \eta_1 \\ \eta_2 \end{array} \right\}$$

may be used to decouple the two equations to linear order. The resulting modal equations are:

$$\begin{aligned} \ddot{\eta_1} + \omega_1^2 \eta_1 &= f_1(\eta_1, \eta_2) \\ \ddot{\eta_2} + \omega_2^2 \eta_2 &= f_2(\eta_1, \eta_2) \end{aligned} \tag{4.14}$$

where the nonlinear terms may be written as:

$$\begin{aligned} f_1 &= -0.405\,\eta_1^3 - 1.34\,\eta_1^2\eta_2 - 1.51\,\eta_1\eta_2^2 - 0.349\,\eta_2^3 \\ f_2 &= -0.448\,\eta_1^3 - 1.51\,\eta_1^2\eta_2 - 1.05\,\eta_1\eta_2^2 - 4.58\,\eta_2^3 \end{aligned} \tag{4.15}$$

The equations are now of the form assumed in Eq. (4.1) and, given a set of expansion functions, Eqs. (4.11) and (4.12) may be employed to yield the system of nonlinear equations whose solution will produce the manifold coefficients. Many different sets of basis functions may be used to describe the manifold geometry. Here we use the following double expansion in a and ϕ:

$$T_{l,m}(a,\phi) = L_l(a)\cos((m-1)\phi)$$

$$U_{l,m}(a,\phi) = L_l(a)\sin((m)\phi)$$

The harmonic functions are a natural choice for expanding the ϕ dependence over $[0, 2\pi]$, and the use of cosine functions for T (corresponding to a modal position), and sine functions for U (corresponding to a modal velocity) is predicated upon the synchronous motions expected for a conservative non-gyroscopic system. That is, in a periodic motion, all degrees of freedom must simultaneously reach zero velocity (at a corresponding maximum or minimum displacement). In other systems, this property may not be present, and a more general expansion in ϕ may be necessary. The functions $L_l(a)$ were chosen to be a set of polynomials defined over the domain $[0, a_o]$, with zero slope at $a = 0$, and which satisfy the orthogonality property:

$$\int_0^{a_o} aL_i(a)L_j(a) = \begin{cases} 1 & \text{for } i = j \\ 0 & \text{for } i \neq j \end{cases}$$

The analytical expressions for the first seven $L_i(a)$ are shown in Appendix C, and are illustrated in Figure 4.3. The restriction of the slope at $a = 0$ is a reflection of the modal form of the original equations of motion. That is, the independence of the governing equations at linear order precludes linear contributions to the manifold at $a = 0$. If the equations of motion were in another coordinate system, e.g., physical

coordinates or non-orthogonal component modes, the $L_i(a)$ should allow for linear contributions to the invariant manifold at $a = 0$.

The orthogonality property above, along with the orthogonal properties of the harmonic functions and the absence of velocity-dependent forces, allows Eq. (4.11) to be reduced to:

$$D_i^{p,q} = F(\boldsymbol{C})$$

where $\boldsymbol{C}$ represents a vector containing all the $C_i^{l,m}$. Hence, given a guess for the C's, the D's may be determined, and Eq. (4.12) may be evaluated. As a consequence, only the C's need to be considered as independent variables.

The resulting set of nonlinear equations can be solved computationally. Here, the Galerkin projection was carried out numerically at each iteration, and Powell's Hybrid method [66] was implemented via the NAG (Numerical Algorithms Group) routines to achieve a solution. This numerical algorithm uses successive function evaluations to approximate the Jacobian and progress toward a solution.

4.3.1 The First Nonlinear Normal Mode

The first nonlinear normal mode of this system may be examined by solving Eqs. (4.11) and (4.12) using the above expansions, for $k = 1$, to determine $P_2(a, \phi)$ and $Q_2(a, \phi)$. Two cross sections of P_2, $\phi = 0$, and $a = a_o = 2.22$, are illustrated in Figure 4.4 (a) and (b), respectively, for a number of different expansion orders, depicted in the form (N_a, N_ϕ), as well as the asymptotic solution and the exact solution. The asymptotic solution corresponds to a third order manifold in $(\eta_1, \dot{\eta_1})$, generated according to the analytical formulas presented in reference [63], and then transformed into the (a, ϕ) coordinates. The conservative nature of this problem requires that the individual nonlinear normal modes be periodic, and this may be

exploited to obtain the exact solution by searching the configuration space for initial conditions which yield a periodic response, and consequently must lie on the invariant manifold. This search is carried out within the plane depicted in Fig. 4.4(a) and the exact results are shown. However, these results are not shown in Fig. 4.4(b), as the amplitude does not remain constant through a given motion, and the exact solution is not easily transferred to the plane of constant amplitude. The results indicate that three polynomial functions and eight harmonics are necessary to out-perform the asymptotic results, and that even with five polynomials and twelve harmonics, there is still some small error near a_o. This error appears to be confined to a few regions of ϕ, as plot (b) indicates convergence over most of the domain. It should be noted that, due to the symmetric nature of the manifold, the ϕ expansion only yields contributions from the odd harmonics. Note that further increases in the number of harmonics or polynomials would result in improved convergence, albeit at higher computational cost.

The invariant manifolds for $P_2(a, \phi)$ and $Q_2(a, \phi)$ are shown in Fig. 4.5, for the solution corresponding to $N_a = 5$, and $N_\phi = 12$. These surfaces represent an approximate solution to Eqs. (4.8) and (4.9), and allow the accurate extension of the first linear mode into the nonlinear realm. Given these constraint relations, $f_1(\eta_1, \eta_2)$ in Eq. (4.15) becomes $f_1(a, \phi)$, and the amplitude-phase differential equations — Eq. (4.5) — may be integrated to find the correct single-mode motion. These manifolds go well beyond the domain of "small motions" and "first order effects," allowing one to generate results which may be limited by the fidelity of the mathematical model, rather than that of the reduction technique. Here, at $a = 2.22$ and $\phi = 0$ the calculated nonlinear force, $f_1(a, \phi)$, is slightly greater in magnitude than the linear force, $\omega_1^2 a$, corresponding to a large nonlinear effect.

The degree of nonlinearity is easily observed in Figure 4.6, wherein the response frequency can be seen to change significantly with amplitude. Though not initially apparent, the known manifold does not allow this curve to be extended to an amplitude of $a_o(= 2.22)$, as the peak amplitude for a given motion is not at $\phi = 0$, but at $\phi = \pi/2$. Motions with initial amplitudes greater than 1.5 will eventually exceed $a_o = 2.22$, thereby leaving the known invariant manifold. The plot indicates that both the asymptotic and Galerkin-based manifolds accurately capture the response frequency, while ignoring the effects of the second mode (shown as the "One Mode Solution") leads to considerable error at the larger amplitudes. The asymptotic and Galerkin-based manifolds yield nearly equivalent response frequencies through an initial amplitude of 1.0, after which some divergence of the asymptotic result may be seen.

Time histories for these four periodic solutions are shown in Fig. 4.7. Each trajectory is produced through a different analytical route. The "Galerkin Manifold" results are produced by simulating Eq. (4.5), using the $(N_a = 5, N_\phi = 12)$ manifold to evaluate f_1, then using the manifold equations to compute the modal displaments for each (a, ϕ), and finally using the eigenvectors to compute the physical displacement. The "Asymptotic Manifold" uses the analytical solutions from reference [63] to determine $\eta_2 = g(\eta_1, \dot{\eta}_1)$, simulates Eq. (4.14) (retaining terms of the proper order), determines the modal deflections and, finally, the physical deflections. The "One Mode Solution" simply assumes $\eta_2(t) = 0$, simulates Eq. (4.14), and uses only the first mode shape to determine physical motion. Lastly, the "Exact" solution corresponds to the numerically determined initial conditions which result in periodic behavior of both degrees of freedom. Hence, although each simulation has an initial condition corresponding to $\eta_1 = 1.5$ and $\dot{\eta}_1 = 0$, the different mode-two

constraints yield different initial conditions. The results indicate that, at this amplitude, the Galerkin-based results are indistinguishable from the "Exact," whereas the asymptotic manifold results are nearly correct, and the "One Mode Solution" has considerable errors in both amplitude and frequency. These results clearly show that the nonlinear Galerkin approach has produced a model which utilizes the full potential of the invariant manifold to reduce the system to a single oscillator whose motions would not incite contamination from the rest of the system. Of course, as this first NNM is simply an extension of the first linear mode into the nonlinear realm, a corresponding extension must exist for the system's second linear mode.

4.3.2 The Second Nonlinear Normal Mode

The convergence of manifold corresponding to the second nonlinear normal mode is illustrated in Figure 4.8, for the cross sections $\phi = 0$ (a), and $a = a_o = 3.0$ (b). For this mode the asymptotic manifold diverges quite quickly from the exact solution, making even the $N_a = 1, N_\phi = 2$ solution a considerable improvement. Plot (b) illustrates that the harmonic content of the manifold is simpler than that of the first normal mode, and this observation is consistent with the fact that only half as many harmonics are necessary to reach convergence. As with the first mode, the convergence appears to be the slowest near a_o. However, as was discussed above, the motions which begin at $\phi = 0$, and near a_o, will exceed a_o during the course of their motion (this is characteristic of systems which stiffen with increased amplitude). Consequently, convergence near the points $(a, \phi) = (a_o, 0), (a_o, \pi)$ and $(a_o, 2\pi)$ is not necessary for practical use of the manifold. Unfortunately, the question of "how near?," must be evaluated for any given problem.

The invariant manifolds corresponding to $P_1(a, \phi)$ and $Q_1(a, \phi)$ are shown in

plots (a) and (b) of Fig. 4.9, for an expansion with $N_a = 4$ polynomials, and $N_\phi = 6$ harmonics. As before, the expansions which describe these surfaces may be used to eliminate η_1 from the system, leaving equations of motion in only the amplitude and phase of the second linear mode. As was apparent from the cross sections shown in Fig. 4.8, the qualitative shape of these surfaces is considerably different than those in Fig. 4.5. The presence of fewer (and lower) harmonics in the surface indicates a closer tie between the phases of the two modes. That is, for motions occurring on this invariant manifold, the two modes are closer to moving in unison than for motions on the mode-one invariant manifold.

As with the first nonlinear normal mode, simulations may be carried out using this invariant manifold, as well as the other reduction techniques, and the amplitude-frequency relation may be determined. For the second mode, as Fig. 4.10 illustrates, all approaches yield nearly the correct response frequency, indicating that the participation of the first mode has little effect. However, an accurate response frequency does not guarantee an accurate description of the system motion. Figure 4.11 illustrates that, though the frequencies are all close, both the "One Mode Solution," and the "Asymptotic Manifold" contain errors in the response magnitude stemming from their treatment of the first mode. As is apparent in Fig. 4.8, the asymptotic solution over-predicts the mode-one participation, while the "One Mode Solution" assumes no mode-one participation at all. Once again, the "Exact" solution is indistinguishable from the nonlinear Galerkin results, highlighting the exceptional accuracy of the approach.

4.4 Application: Nonlinear Finite Element Beam

In order to illustrate the general applicability of this approach for the generation of reduced-order models, a more realistic structural model is examined. The finite element code PATRAN was used to create a linear model of a beam with transverse deflection $u(x,t)$ using 200 two-noded beam finite elements. The beam, shown in Fig. 4.12, is pinned at one end, while the other is constrained by a linear spring. A nonlinear torsional spring with quadratic and cubic components is located at the pinned end. Given the characteristics of the nonlinear spring and the eigenvectors of the linearized system, one may determine the coupled nonlinear forces for each mode due to the torsional spring. For illustration purposes, the lowest 10 (of 400 possible) linear modes are chosen to represent the "complete" model, from which a NNM-based reduced-order model will be generated. Note that this 10-DOF model contains nonlinear coupling between all linear modes through the nonlinear spring.

The increase in example system size from two modes to 10 modes requires a shift in tactics. For the previous example, each nonlinear mode was associated with a single (P,Q) pair — representing the contributions of the other linear mode. For the finite element system, each nonlinear mode is associated with *nine* (P,Q) pairs. Consequently, a manifold with expansions of order $N_a = 5$, and $N_\phi = 12$, now requires a solution of 540 coupled nonlinear equations for 540 coefficients. The computational effort necessary for the solution scales approximately with $(N_a N_\phi (N-1))^2$, indicating that, for a shift from two to ten DOF, the solution time would increase by approximately a factor of 81.

In order to achieve a more efficient solution, the domain in a may be discretized into several smaller intervals. These intervals may then be described as linear in a

(fixing N_a at two — one coefficient for each segment endpoint) and solved as individual sub-problems. The harmonic dependence is retained, so that each expansion now contains $2N_\phi$ coefficients, and corresponds to a thin annular strip of the manifold ($a \in [a_i, a_{i+1}]$ while $\phi \in [0, 2\pi]$). As with the polynomial approach, the velocity coefficients (the D's) may be condensed out, leaving only the C's as variables. This is only slightly more complex without the orthogonal properties of the previous polynomial functions.

Besides the reduction of problem size, there are several other benefits to this piecewise amplitude approach. The linear dependence on a simplifies the evaluation of each sub-problem by eliminating the higher order polynomials, and the smaller domain allows fewer points to be used in the numerical integration. In addition, discrete linear segments may capture details or features which would require an impractical number of polynomials. Finally, in the event that numerical difficulties are encountered (e.g. from a bifurcation in the manifold, or a nonremovable modal interaction), the anomaly is localized to the sub-problem level, whereas the global solutions used for the first example simply may not converge at all.

This piecewise strategy was used to examine the second and fifth NNMs of transverse vibration for the finite element beam system shown in Fig. 4.12. Both solutions used $N_\phi = 8$ harmonics and the second NNM solution used 80 piecewise segments in a, while the fifth NNM solution used 40. Both manifolds were obtained for modal amplitudes of $a \in [0, 2]$, which corresponds to a maximum deflection of approximately 0.65 meters. If these amplitudes seem unreasonably large for the 1 meter long beam model, it should be realized that entirely equivalent results may be obtained through a simple rescaling of parameters. That is, if the slope/moment relationship from the nonlinear torsional spring, γ_t, is adjusted from $[5000u'(0)^2 + (2 \times 10^4)u'(0)^3]$ to

$[(5\times10^4)u'(0)^2+(2\times10^6)u'(0)^3]$, (where a $'$ indicates a spatial derivative with respect to x) the results from $a\in[0,2]$ are mapped onto the domain $a\in[0,0.2]$.

The sections of the second-mode invariant manifold which correspond to the slaved displacements of the first and third linear modes, at $\phi=0$, are displayed in Fig. 4.1. As with the first example, the asymptotic manifolds used here are calculated to third order according to the analytical solutions presented in reference [63]. Here, the deficiency of the asymptotic approach is quite apparent. Though the initial behavior is captured by both methods, the polynomial basis of the asymptotic approach inevitably leads to a rapid departure from the correct solution as the amplitude increases. This tendency is magnified by the fact that for strong nonlinear effects the exact invariant manifold often approaches linearity in a (the behavior seen in Fig. 4.1(a) is typical, and similar results may be seen in reference [12]). The asymptotic approximation in Fig. 4.1(b) does seem to capture some basic properties of the manifold. However, at the intermediate amplitudes, the relative error is considerable. In addition, the asymptotic solution is considerably worse at other values of ϕ. Figure 4.13 shows both the calculated Galerkin invariant manifold and the corresponding asymptotic solution. The curve shown in Fig. 4.1(b) corresponds to the $\phi=0$ edge of Fig. 4.13, although there is some difference in scale. Clearly, the asymptotic solution is quite limited in its applicability, although it is qualitatively consistent with the Galerkin solution.

In systems such as this, with many DOFs, a poor asymptotic approximation of a single mode's contribution (as in Fig. 4.1(a)) is likely. Even when the remaining modes are accurately approximated, this type of error may quickly dominate the associated reduced-order model. The Galerkin-based approach avoids this error by allowing one to ensure the accuracy of each mode's constraint relations throughout

the full domain.

Figure 4.14 illustrates the time response of the various periodic second-mode solutions. The Galerkin Manifold and Exact solutions are indistinguishable, while the One Mode Solution and Asymptotic Manifold yield inaccurate results. The deflections shown illustrate both the power of this approach, and the inadequacy of the other methods. The ability to accurately account for the dynamic contribution of the other system modes allows the corresponding reduced-order model to be nearly exact. Of course, the Galerkin manifold only approaches the exact, and small errors are likely to remain. The degree of these errors (for the present solution) may be seen in Fig. 4.15, which illustrates the periodic mode-six contribution to the motions seen in Fig. 4.14. It is apparent that although the exact solution is quite well approximated, some higher order effects are still not entirely accounted for. This could be remedied by increasing the number of harmonics and piecewise linear segments.

In Fig. 4.16, the fifth NNM is depicted to highlight the non-similar nature of the mode shape predicted by the Galerkin approach. The two curves show the small and large amplitude displacement configurations for motions within the normal mode (at $\phi = 0$). They are normalized for plotting purposes by the amplitude of the first lobe of the mode shape. One should note that this shape not only changes with amplitude, but also will change dynamically throughout the course of a periodic motion. This information may be useful in a number of contexts, such as control algorithms or sensor location. Of particular interest here is the increased participation of the end spring at larger amplitudes.

Figure 4.17 depicts a worst-case scenario for the asymptotic approach. Not only is the domain of convergence small but, slightly outside this domain, the error grows extremely rapidly. For this case (the mode-one contribution to the fifth NNM), these

errors quickly overwhelm any benefits of the asymptotic approach. In addition, this type of amplitude dependence is quite difficult to capture using the orthogonal basis functions from the first example (as seen in Fig. 4.3). The piecewise linear amplitude approach, however, performs very well, yielding an accurate reduced-order model.

The amplitude-frequency relation for the fifth NNM is shown in Fig. 4.18. Several features of this plot are worth discussing. First, the asymptotic results obviously suffer greatly from the aforementioned errors. Second, the exact periodic response frequency appears to be approaching a limit with increased amplitude. This is to be expected as, for larger amplitudes, the nonlinear torsional spring begins to resemble a clamped boundary condition, and the NNM should document this transition from pinned to clamped-like conditions at the left end for increased amplitudes. Third, this transition requires modal interaction and, consequently, may not be captured through a single-mode truncation. Here, unlike the first example, the one-mode model leads to frequency predictions which are qualitatively wrong.

4.5 Further Considerations

The model fidelity which can be attained using this approach is compelling. However, as with all methods, there are limitations to its application. In particular, further study is necessary to determine what occurs when NNMs become unstable and bifurcate. Some work has been done in this area [45], and further development is necessary to ensure that the reduced-order models developed herein represent unique and stable motions of the original system. Another limitation of this technique is that it relies on accurate modeling of the nonlinearities within the original system. That is, if cubic nonlinearities were included in the original model as a means of capturing the leading-order nonlinear effects, but higher order terms were neglected,

the reduced-order model may only be accurate to leading order. An exact reduction of an approximate system is limited in its applicability. This is in contrast to the asymptotic approaches, where the domain of validity for the reduced model generally does not exceed that of the original model. The consequence of this may be that relatively simple, low-order manifold solutions are sufficient for most real systems due to the uncertainties involved in the measurement and modeling of nonlinear effects.

The individual NNMs discussed here are only useful when used independently. As with the asymptotic nonlinear normal modes developed earlier, and unlike linear modes, simultaneous motions within two or more nonlinear normal modes are bound to interact. The two primary consequences of this are that (a) larger reduced-order models may not be assembled from the individual NNMs, and (b) sometimes these interactions are not removable (e.g., due to an internal resonance) and certain individual NNMs may not be generated individually. The ability to approximate the invariant manifold for a range of different amplitudes also raises a host of issues. Internal resonances which are present at very low amplitudes may be avoided at higher amplitudes (due to amplitude-dependent frequency changes). Conversely, systems which have no internal resonances at low amplitudes may have significant interactions at greater amplitudes. An instance of this effect was observed during the study of the second linear mode for the finite element beam system. These results are illustrated in Fig. 4.19, which depicts the mode five contribution to the second NNM manifold (at $\phi = 0$). The anomaly occurs close to a 6:1 frequency relation between the second and fifth modes, and the Galerkin manifold contains significant contributions from the sixth harmonic in ϕ. Though a complete study of this interaction is beyond the scope of this work, it should be noted that the Galerkin solution indicates its presence, while the asymptotic solution does not, and that the overall

effect is quite weak. These issues may be addressed through a generalization of the present formulation, to develop multi-mode invariant manifolds using the nonlinear Galerkin methodology where several pairs of modal amplitudes and phases are chosen as "master" coordinates. For the case above, this would entail adding the amplitude and phase of the fifth mode to those of the second, and conducting an expansion in four variables. Of course, this requires considerably more expansion coefficients, and the computational effort will become correspondingly more larger. However, this is the next logical step for this line of work.

4.6 Conclusion

This work expands upon the invariant manifold formulation of Shaw and Pierre [2], utilizing a coordinate transformation and nonlinear Galerkin solution to produce reduced order models for nonlinear systems which are accurate, reliable, general, and analytically rigorous. The use of the Galerkin projection enables an unprecedented solution accuracy for the manifold-governing equations. This accuracy allows the corresponding reduced-order models to take full advantage of the potential inherent in the original invariant manifold formulation. The examples discussed clearly illustrate the accuracy attainable through this approach, with nearly all results showing little or no discrepancy from the numerically determined exact solution. As indicated by the finite-element beam example, the method is not restricted to simple mass/spring systems. In addition, the computational foundation of the solution procedure allows the system nonlinearities to take on a wide variety of forms with little or no additional analytic work. Furthermore, the formulation may be extended to produce reduced-order models which contain several modes or DOFs, allowing the study of more general, multi-mode motions, as well as internal resonances. The method shows

great promise for the development and understanding of reduced-order models for nonlinear dynamic systems.

4.7 Figures

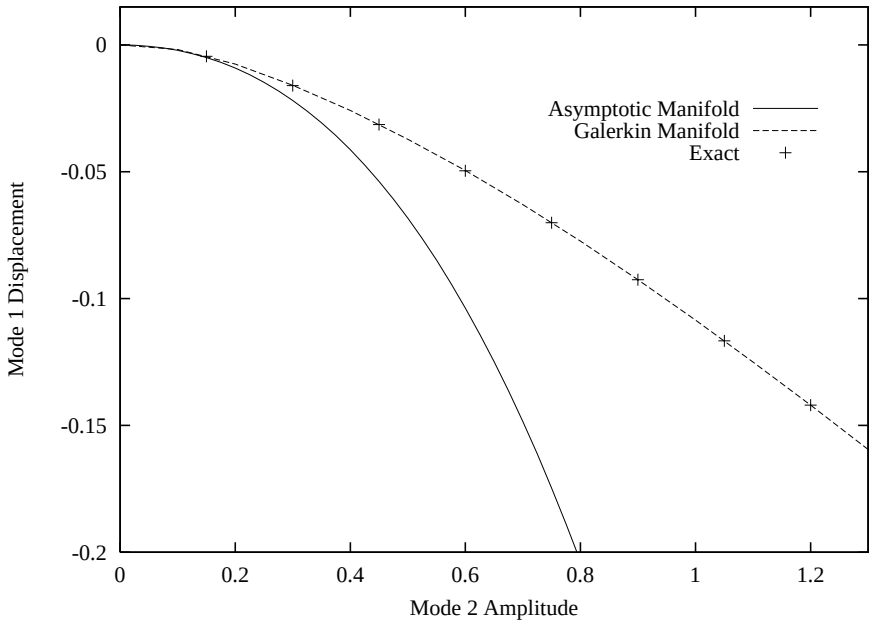

(a)

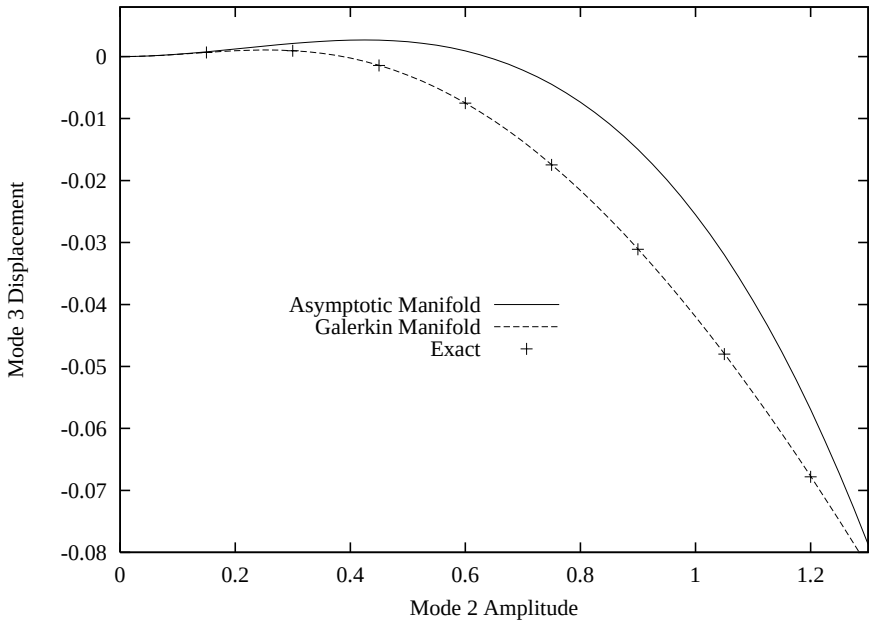

(b)

Figure 4.1: Exact, Asymptotic and Galerkin Manifolds (at $\phi = 0$) for the second nonlinear mode of the finite element system pictured in Fig. 4.12. The Asymptotic Manifold is of third order, while the Galerkin Manifold uses 80 piecewise linear segments in the amplitude, a, and $N_\phi = 8$ harmonics in ϕ.

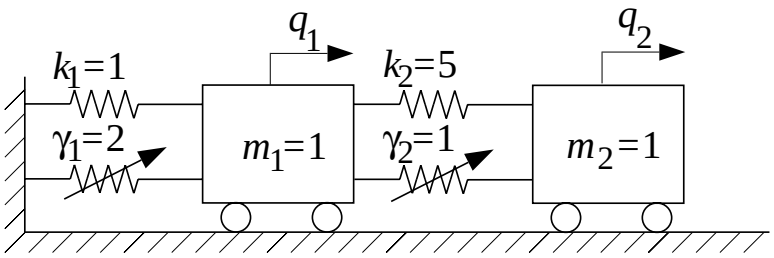

Figure 4.2: Two degree-of-freedom nonlinear system with hardening cubic springs of strength $\gamma_1 = 2$, and $\gamma_2 = 1$.

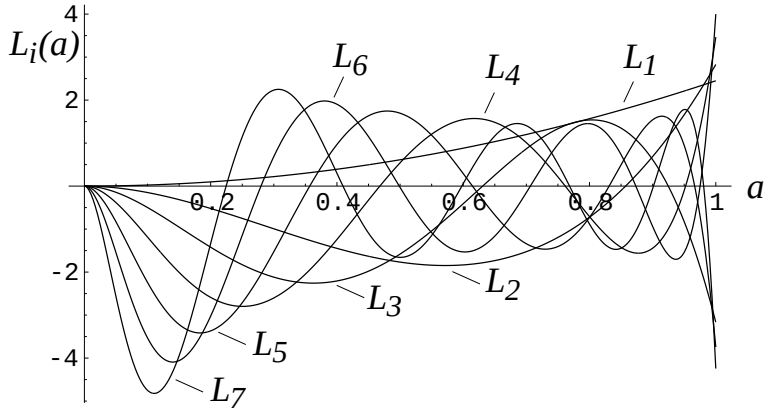

Figure 4.3: Orthogonal polynomials used for the a component of the manifold expansion, shown for $a_o = 1$.

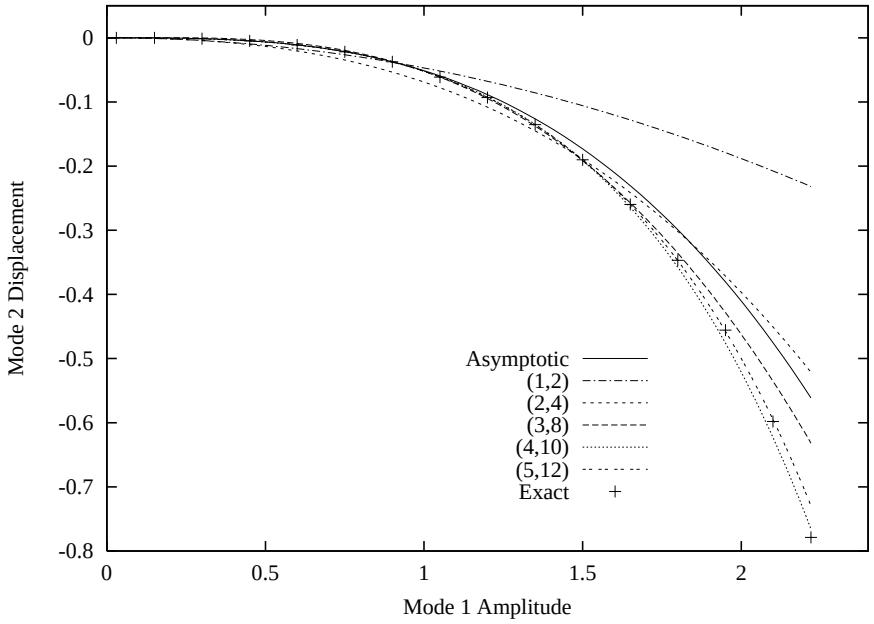

(a)

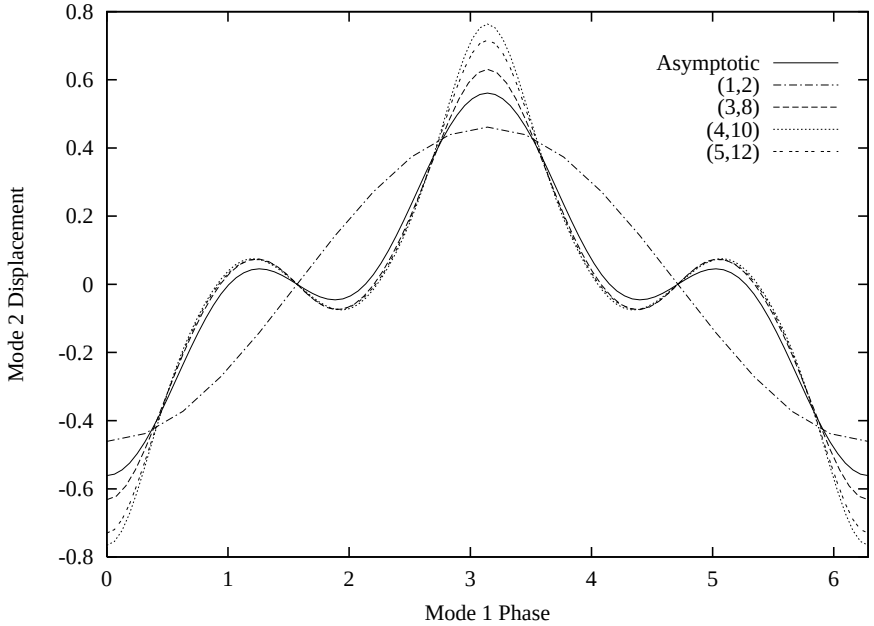

(b)

Figure 4.4: Convergence of the first mode invariant manifold. The parenthetical notation refers to the number of basis functions, (N_a, N_ϕ), used in the expansion. Plots (a) and (b) illustrate $P_2(a, 0)$, and $P_2(2.22, \phi)$ respectively.

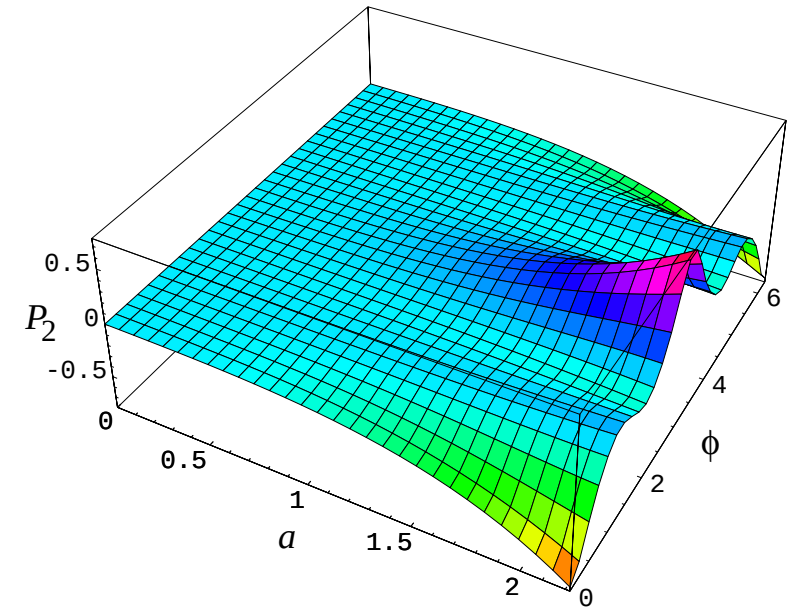

(a)

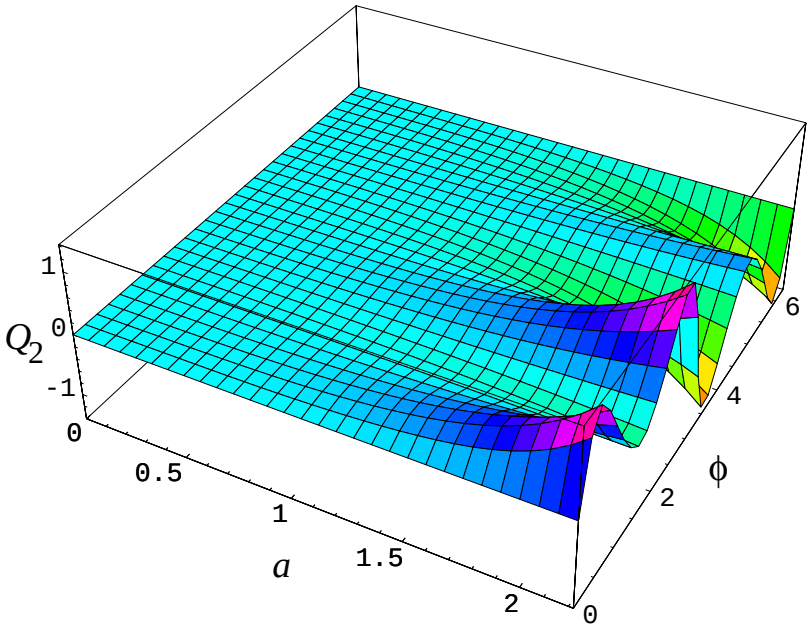

(b)

Figure 4.5: The first mode invariant manifold: The position (a), and velocity (b) of mode 2, as a function of the amplitude and phase of mode one (shown for $N_a = 5$, $N_\phi = 12$).

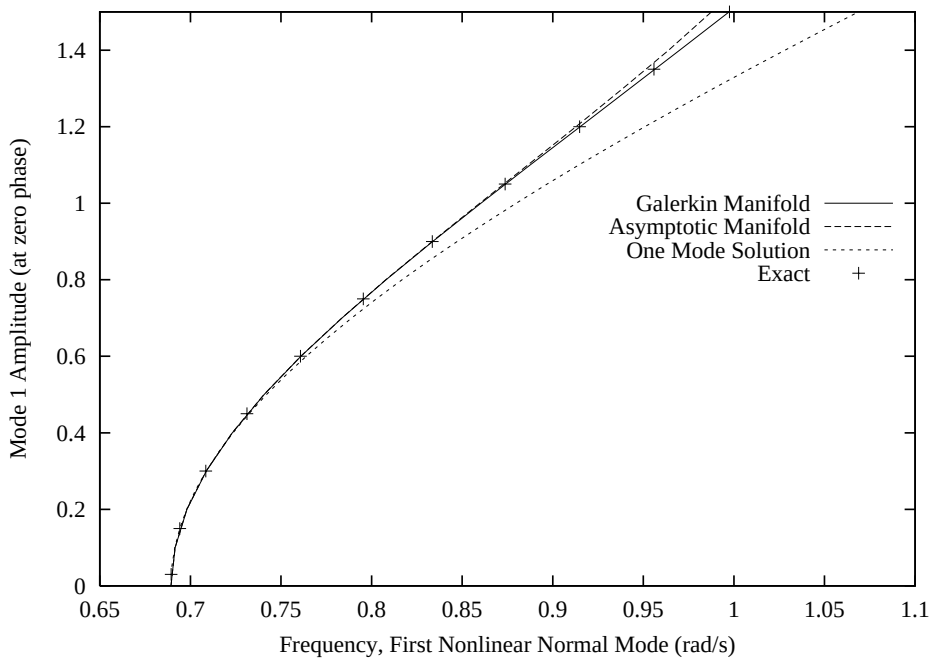

Figure 4.6: Response frequency for the first nonlinear normal mode versus the mode 1 amplitude, a, at $\phi = 0$. The Galerkin Manifold corresponds to the $N_a = 5$, $N_\phi = 12$ solution.

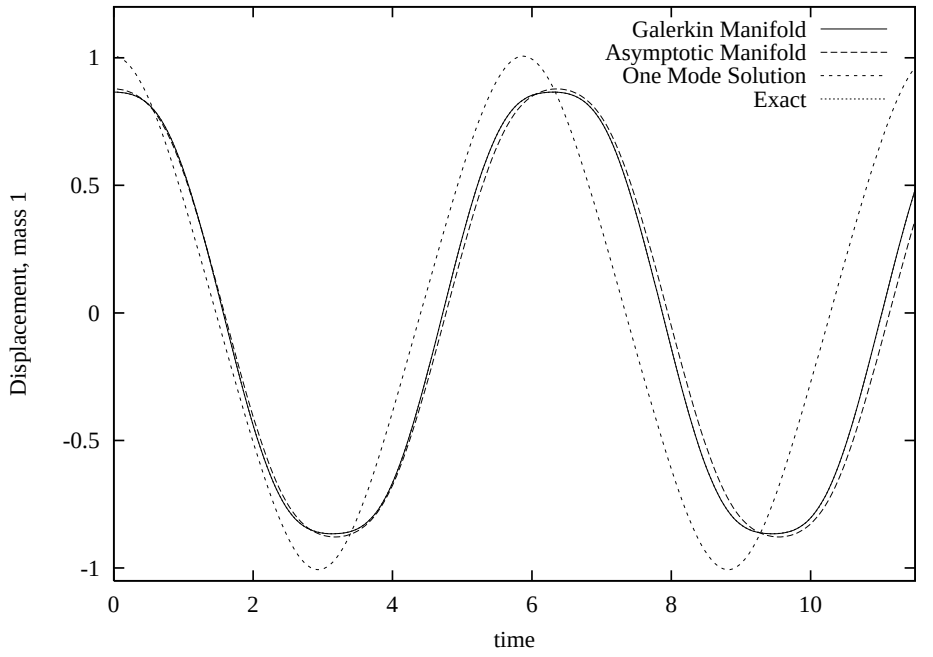

Figure 4.7: Response of the first mass, q_1, for periodic first-mode motions, using various reduced systems. The Exact and Galerkin Manifold ($N_a = 5$, $N_\phi = 12$) solutions are indistinguishable.

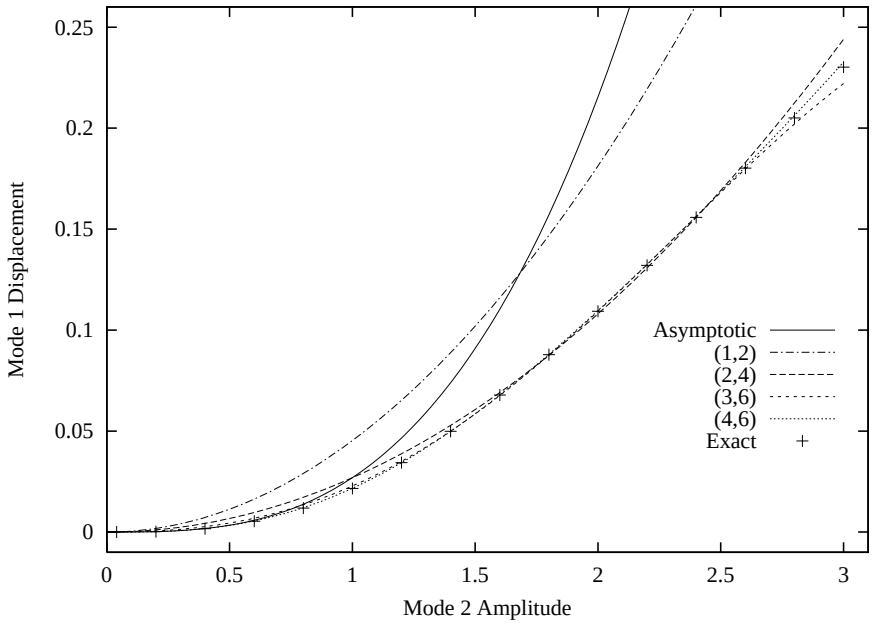

(a)

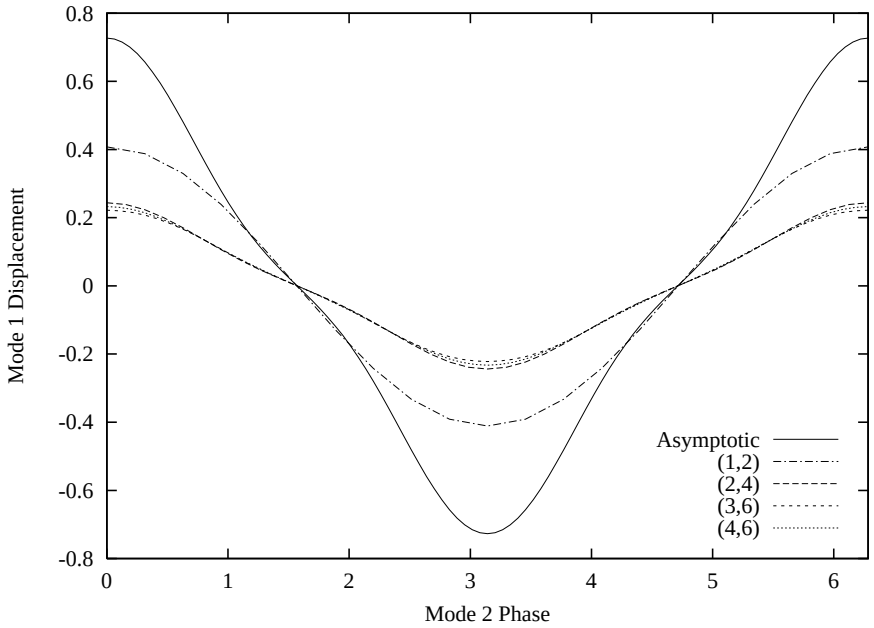

(b)

Figure 4.8: Convergence of the mode 2 invariant manifold. The parenthetical notation refers to the number of basis functions, (N_a, N_ϕ), used in the expansion. Plots (a) and (b) illustrate $P_1(a, 0)$ and $P_1(3.0, \phi)$, respectively.

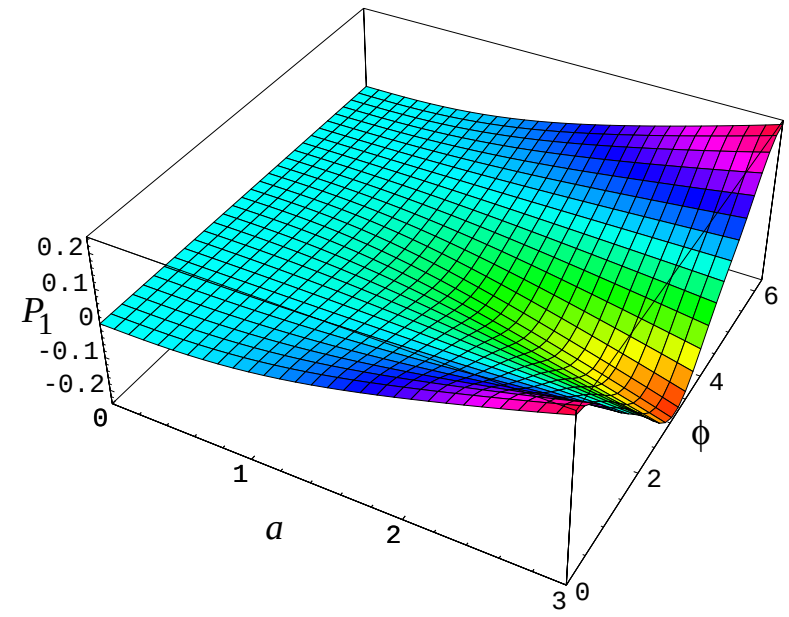

(a)

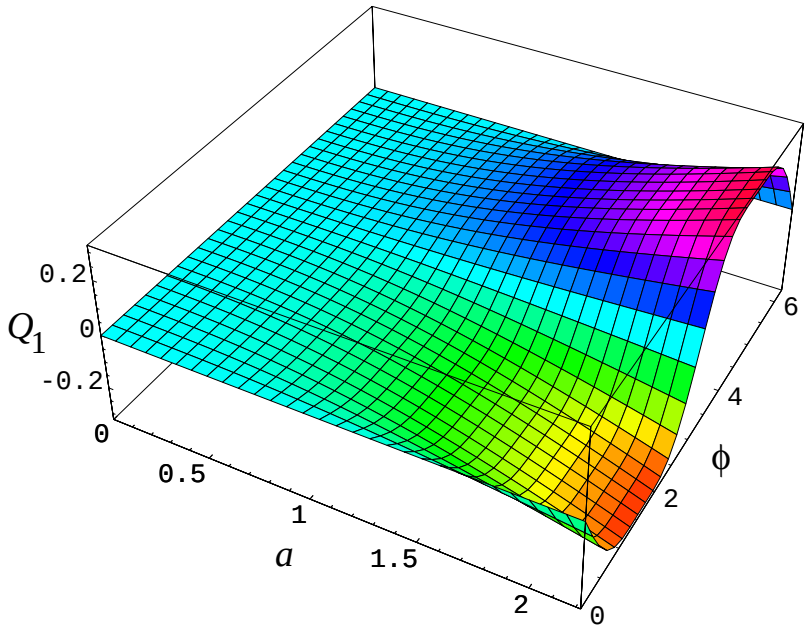

(b)

Figure 4.9: The second mode manifold: The position (a), and velocity (b) of mode 1, as a function of the amplitude and phase of mode 2 (shown for $N_a = 4$, $N_\phi = 6$).

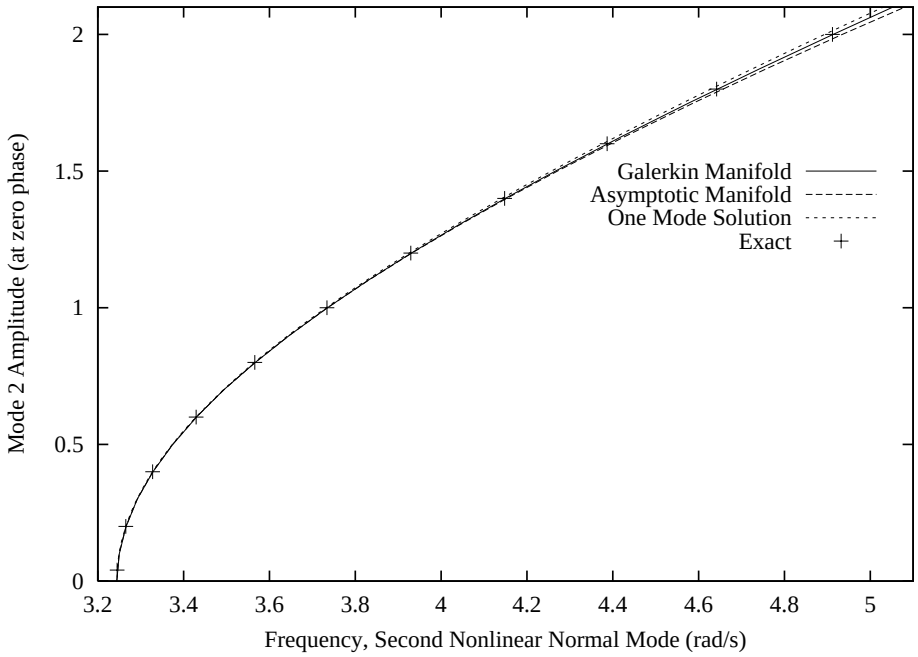

Figure 4.10: Response frequency for the second nonlinear normal mode versus the mode 2 amplitude, a, at $\phi = 0$. The Galerkin Manifold corresponds to the $N_a = 4$, $N_\phi = 6$ solution.

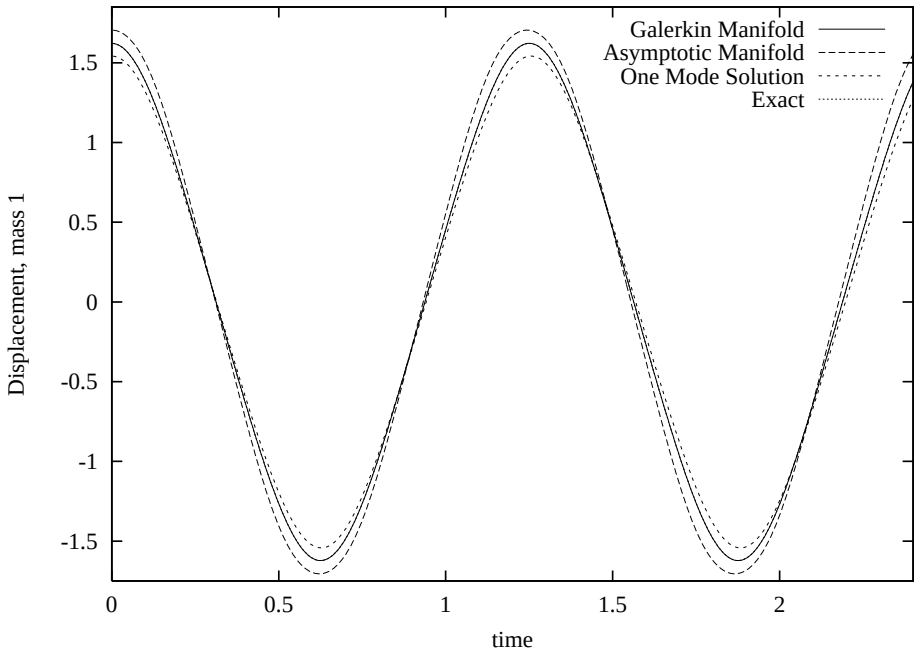

Figure 4.11: Response of the first mass, q_1, for periodic second-mode motions, using various reduced systems. The Exact and Galerkin Manifold ($N_a = 4$, $N_\phi = 6$) solutions are indistinguishable.

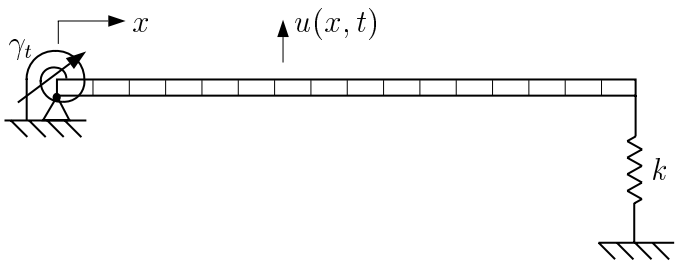

Figure 4.12: Schematic of finite element model: 200 linear beam elements were used to construct a beam with deflection $u(x,t)$, length $L = 1$ m, density $\rho = 7860\text{kg/m}^3$, Young's modulus $E = 2\times10^{11}\text{N/m}^2$, moment of inertia $I = 5 \times 10^{-8}\text{m}^4$, spring stiffness $k = 10^8\text{N/m}$, and nonlinear torsional stiffness $\gamma_t = 5000u'(0,t)^2 + 20000u'(0,t)^3\text{N}$. A $'$ indicates a partial derivative with respect to x.

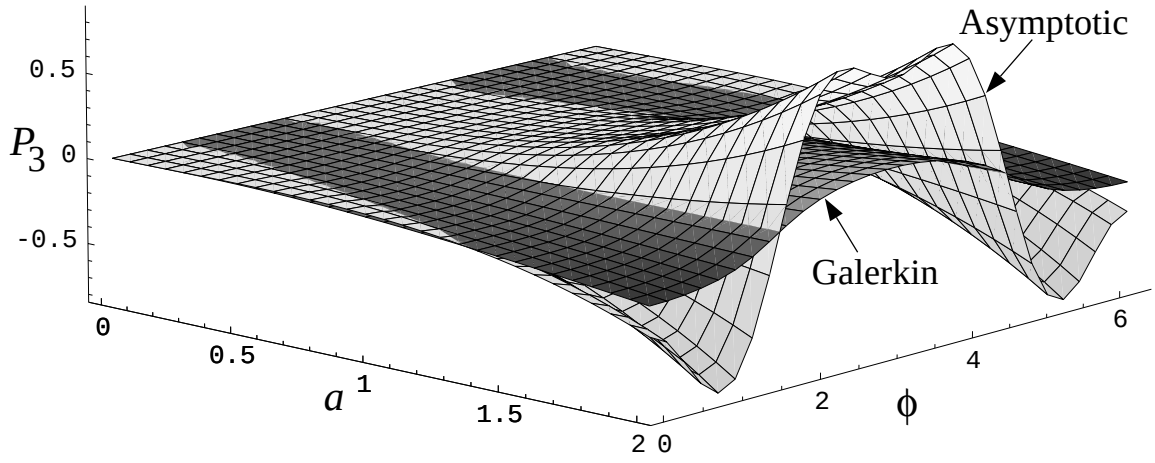

Figure 4.13: The asymptotic and Galerkin manifolds for the mode three displacement contribution to the second NNM. The asymptotic solution is of third order, while the Galerkin solution uses 80 piecewise linear segments in a, and $N_\phi = 8$ harmonics in ϕ.

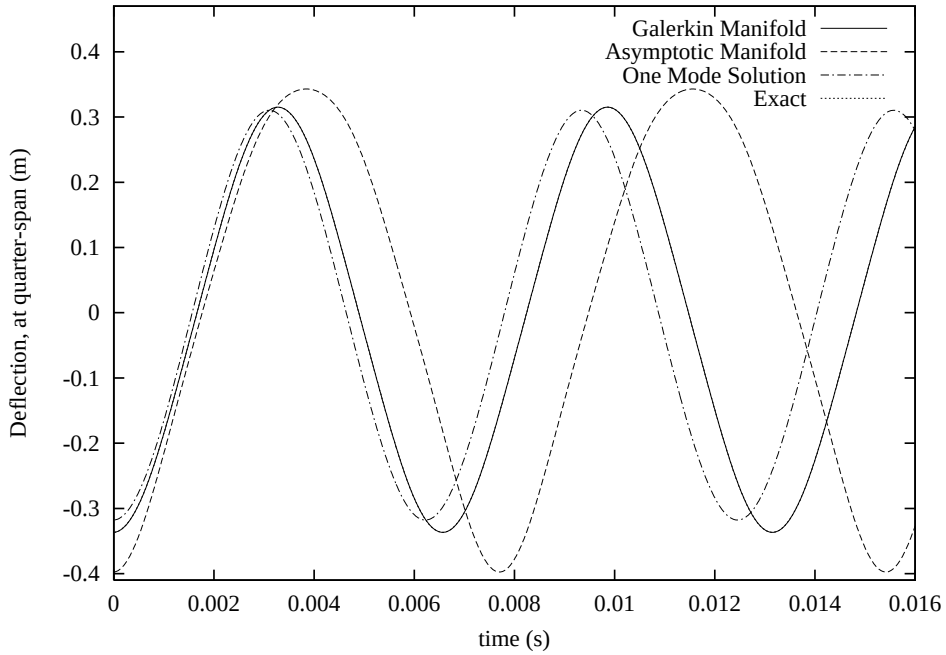

Figure 4.14: Time response for various second mode solutions. As before, the Galerkin Manifold and Exact solutions are indistinguishable.

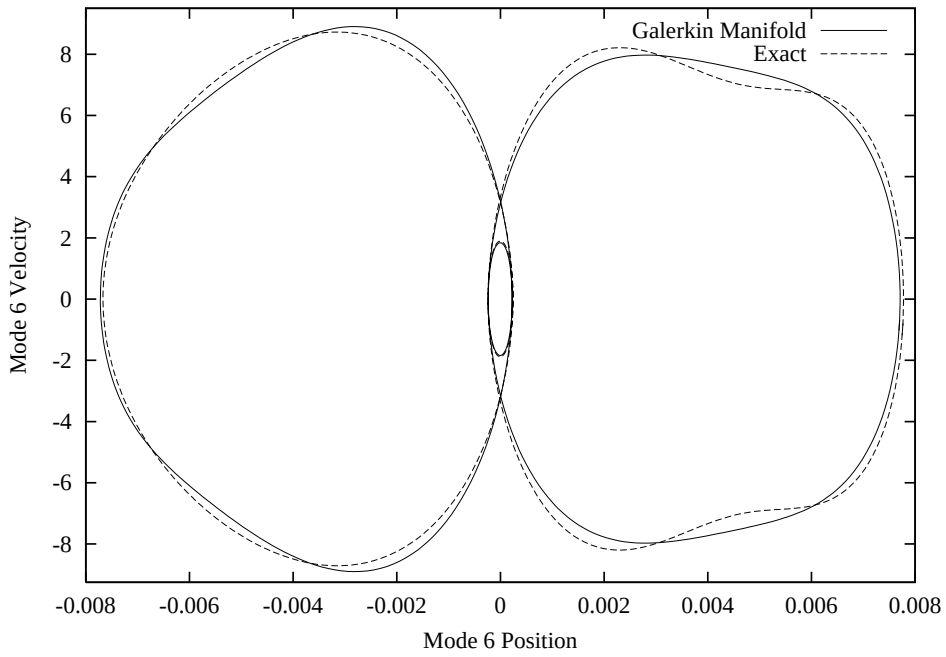

Figure 4.15: Phase space depiction of the periodic mode 6 contribution to the second NNM.

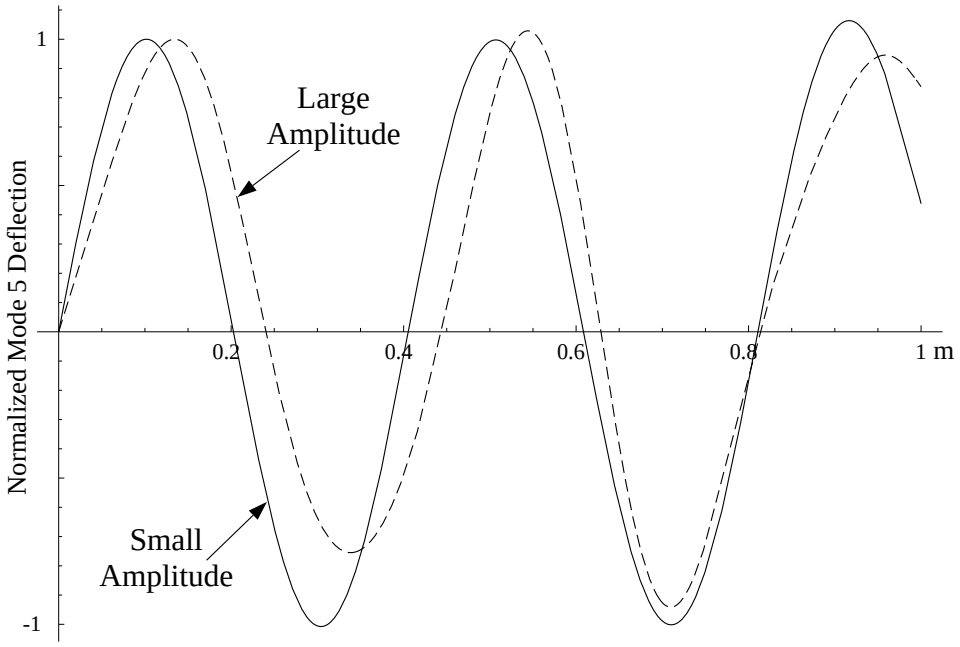

Figure 4.16: Normalized mode shape for the fifth NNM at small ($a = .01, \phi = 0$) and large ($a = 2.0, \phi = 0$) amplitudes, obtained through the Galerkin-based solution procedure.

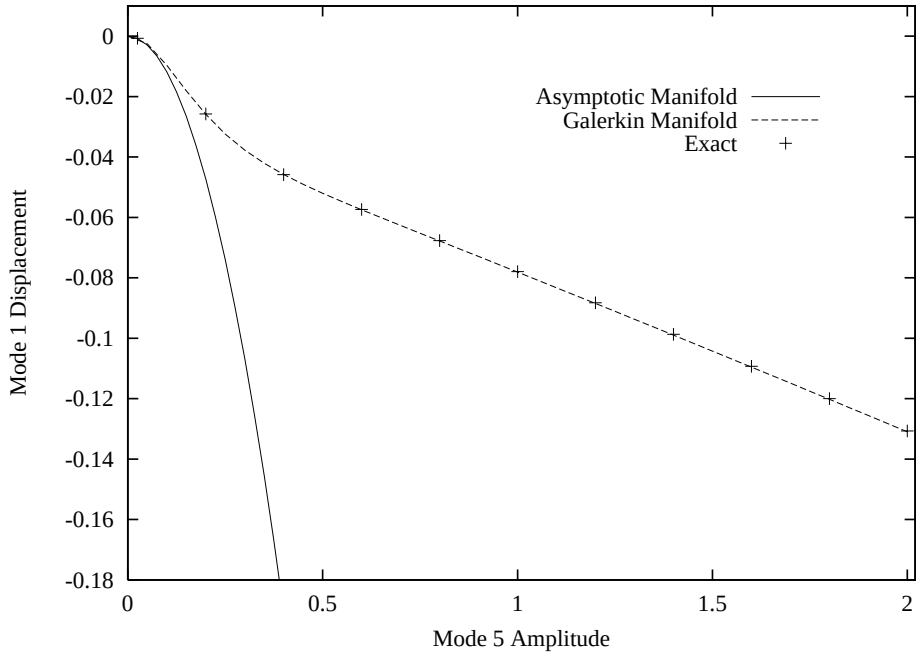

Figure 4.17: Mode 1 contribution to the fifth NNM (at $\phi = 0$). The asymptotic solution is third order, while the Galerkin solution uses $N_\phi = 8$ harmonics, and 40 linear segments in a.

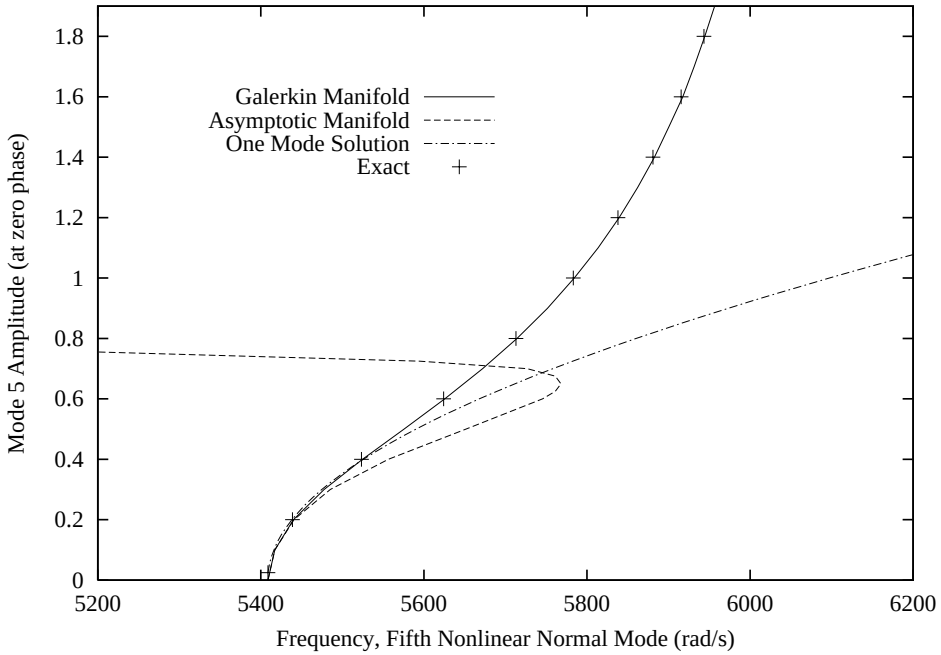

Figure 4.18: Response frequency versus amplitude for the fifth NNM, using various periodic solutions.

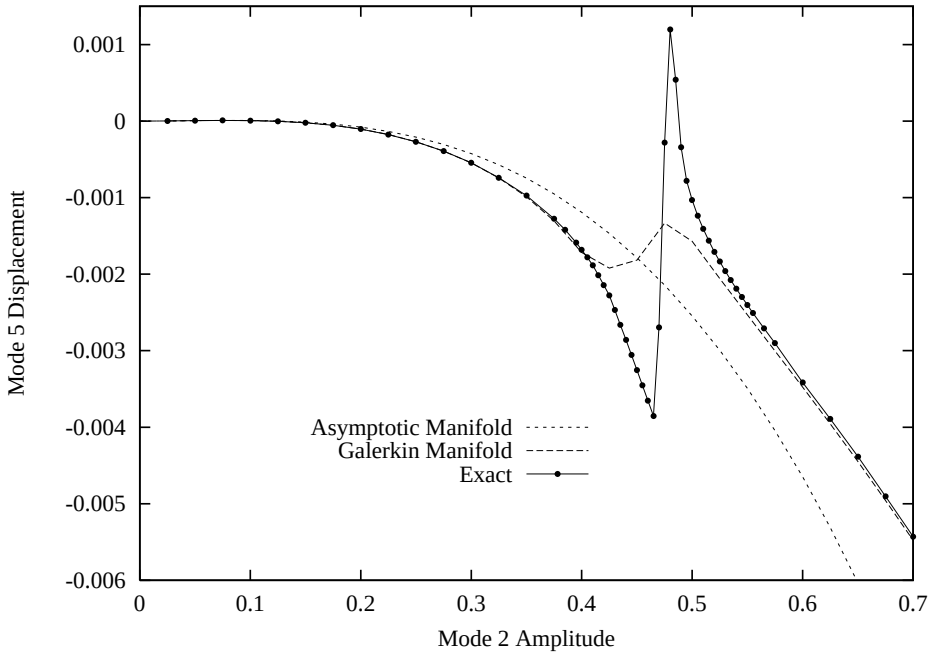

Figure 4.19: Manifold anomaly for the second NNM, indicating a 6:1 interaction with the fifth linear mode.

CHAPTER V

ACCURATE REDUCED ORDER MODELS FOR A SIMPLE ROTOR BLADE MODEL USING NONLINEAR NORMAL MODES

5.1 Introduction

The complex nature of rotorcraft dynamics and control has contributed to a design process which is often both slow and cumbersome. One of the sources of this complexity is the modeling and simulation of the rotor blade dynamics. Typically, accurate results have required models which are very complex, whether finite-element based [53–55], or analytic [56–58, 67], due to kinematic nonlinear effects which are amplified by blade rotation. However, the practical utility of such models has been limited by their large size and the corresponding computational effort required to achieve results. Some promising work has been done on the application of a mixed finite element method which is expected to reduce the blade model size necessary to achieve accurate simulation [68]. However, a need will remain for reduced order models (ROMs) which retain the accuracy of the original models, and allow for a more accurate and efficient design cycle.

Recently, some progress has been made toward meeting this need. The invariant manifold based nonlinear normal modes (NNMs) developed by Shaw and Pierre

[2, 3] were employed to reduce a simplified blade model from 18 nonlinearly coupled linear modes to a one or two degree of freedom (DOF) reduced order model [65] (there was no theoretical limitation to the number of linear modes in the original model). This work used automated procedures developed in reference [63] to generate asymptotic invariant manifolds to third order. Though these results were quite good, especially for internal resonances, they were restricted to modest amplitudes (peak to peak blade tip deflection of 2.5% blade length) due to the asymptotic nature of the manifolds. In addition, as is often true for asymptotic methods, it was difficult to ascertain the domain of validity of the ROM *a priori*. This compromises the effectiveness of the ROM, as extensive simulations are necessary to determine its applicable domain.

Herein, a new approach to generating NNMs is applied to the simplified blade model from reference [65]. This approach, recently developed by Pesheck *et al.* [69], produces a much more accurate and reliable invariant manifold, allowing the nonlinear effects of many coupled DOFs to be precisely captured within a minimal ROM over a selected amplitude range. This is accomplished through a procedure wherein the partial differential equations (PDEs) which govern the invariant manifold geometry are solved using a nonlinear Galerkin approach over a chosen domain. Though significant computational effort is necessary, the resultant ROM is shown to have extremely high integrity — even for large deflections and strong nonlinear effects. This reduction method is not specific to the simplified blade model employed here, and may easily be extended to more complex blade models. Further work is underway on the development of a finite element analog to the current model, which may then be extended to more realistic blade models. The application of this novel reduction method is shown to produce a single degree of freedom ROM which

successfully captures the critical nonlinear coupling between the linear modes of the blade model. This ROM is shown to be both more accurate and applicable than the previous asymptotic approach, while allowing analysis at much greater motion amplitudes.

5.2 Rotating Beam Formulation

The system under consideration, shown in Fig. 5.1, and much of the following formulation follow that in reference [65] — in which asymptotic manifold approximations for this system are generated and applied. In the formulation of this uniform rotating Euler-Bernoulli beam, we neglect rotatory inertia, restrict motion to a rotating plane (thus eliminating twist and lead-lag motion), and allow nonlinear axial strain. Hence, the potential energy, U, and kinetic energy, T, may be expressed as follows:

$$T = \frac{1}{2}\int_0^L m(\dot{u}^2 + \dot{w}^2) + m\Omega^2(h + x + u)^2 dx \tag{5.1}$$

$$U = \frac{1}{2}\int_0^L EI(w_{,xx})^2 + EA(u_{,x} + \frac{1}{2}(w_{,x})^2)^2 dx \tag{5.2}$$

where $u(x,t)$ and $w(x,t)$ are the axial and transverse displacements respectively, $(\cdot)_{,x}$ is a derivative with respect to the spatial variable x, an overdot represents a time derivative, h is the hub radius, Ω is the constant angular velocity of the beam, m is the mass per unit length, and E, A, I, and L are the usual beam parameters—Young's modulus, cross sectional area, moment of inertia, and length, respectively. These expressions, and Hamilton's principle, may be used to develop the following

weak formulation for the equations of motion:

$$\int_{t_1}^{t_2}\int_0^L \Big\{[-m\ddot{w}\delta w - EIw_{,xx}\,\delta w_{,xx} - EA(u_{,x}+\frac{1}{2}(w_{,x})^2)w_{,x}\,\delta w_{,x}]+ [-m\ddot{u}\delta u + m\Omega^2(x+h+u)\delta u - EA(u_{,x}+\frac{1}{2}(w_{,x})^2)\delta u_{,x}]\Big\}dxdt = 0 \tag{5.3}$$

where $\delta(\cdot)$ denotes the variation of a quantity.

With the foreknowledge that these equations will be discretized using the fixed-free axial bar modes and fixed-free transverse modes of the nonrotating linear beam (and their corresponding boundary conditions), these expressions may be reduced through integration by parts to:

$$\int_{t_1}^{t_2}\int_0^L \Big\{[-m\ddot{w} - EIw_{,xxxx}]\delta w - [EA(u_{,x}+\frac{1}{2}(w_{,x})^2)w_{,x}]\delta w_{,x} + [-m\ddot{u} + m\Omega^2(x+h+u) + EAu_{,xx}]\delta u - [EA\frac{1}{2}(w_{,x})^2]\delta u_{,x}\Big\}dxdt = 0 \tag{5.4}$$

At this point it is convenient to separate $u(x,t)$ into static and dynamic components, as follows:

$$u(x,t) = u_s(x) + u_d(x,t) \tag{5.5}$$

where $u_s(x)$ satisfies the equations of motion for $w(x,t) \equiv 0$ and $u(x,t) = u_s(x)$ as follows:

$$u_{s,xx} + \lambda^2 u = -\lambda^2(h+x)$$

Here, $\lambda^2 = m\Omega^2/EA$. Using the appropriate boundary conditions, it is found that

$$u_s(x) = \frac{1+\lambda h\sin(\lambda L)}{\lambda\cos(\lambda L)}\sin(\lambda x) + h\cos(\lambda x) - (h+x)$$

which represents the static elongation of the beam due to rotation (for $w(x,t) \equiv 0$). If Eq. (5.5) is substituted into Eq. (5.4) and the nonlinear terms are neglected (for now), we are left with two linear partial differential equations for the rotating beam, whose modal solutions will decouple the fully nonlinear equations of motion to linear order. These are:

$$m\ddot{u}_d - m\Omega^2 u_d - EAu_{d,xx} = 0 \tag{5.6}$$

$$m\ddot{w} + EIw_{,xxxx} - EA(u_{s,x}w_{,xx} + u_{s,xx}w_{,x}) = 0\,. \tag{5.7}$$

In the axial direction, the modes of the rotating beam, $\Phi_i(x)$, are simply the well known axial mode shapes for a uniform (fixed-free) nonrotating beam. However, the transverse mode shapes of the rotating beam, $\Psi_i(x)$, are approximated using a Rayleigh-Ritz procedure [20], as:

$$\Psi_i(x) = \sum_{j=1}^{N_c} \nu_{i,j}\Theta_j(x)$$

where the $\Theta_j(x)$ are the familiar modes of a (nonrotating) fixed-free beam. These modes are used for convenience, an alternative analytical formulation may be found in reference [59]. Once the modes of the linearized rotating beam are determined, modal solutions to the nonlinear equations are sought in the form:

$$u_d = \sum_{i=1}^{N_a} b_i(t)\Phi_i(x) \qquad\qquad w = \sum_{i=1}^{N_t} c_i(t)\Psi_i(x). \tag{5.8}$$

The integers N_a, N_t, and N_c are used to denote the number of modes included in each of the above expansions.

If these discretizations are substituted into the weak formulation, Eq. (5.4), projected onto the linear modes, and orthogonality is invoked, the resultant discretized

nonlinear equations are:

$$\ddot{b_j} + (\omega_{a,j})^2 b_j = -\frac{EA}{2} \sum_{k=1}^{N_t} \sum_{l=k}^{N_t} c_k c_l \int_0^L \gamma(k,l,x) \Phi_{j,x} dx \tag{5.9}$$

$$\text{for } j = 1 \ldots N_a$$

$$\ddot{c_j} + (\omega_{t,j})^2 c_j = -EA \Bigg[\sum_{k=1}^{N_a} \sum_{l=1}^{N_t} b_k c_l \int_0^L \Phi_{k,x} \Psi_{l,x} \Psi_{j,x} dx - \frac{1}{2} \sum_{k=1}^{N_t} \sum_{l=k}^{N_t} \sum_{i=l}^{N_t} c_k c_l c_i \int_0^L \sigma(k,l,i,x) \Psi_{j,x} dx \Bigg] \tag{5.10}$$

$$\text{for } j = 1 \ldots N_t$$

Here, γ and σ are defined as

$$\gamma(i,j,x) = \begin{cases} \Psi_{i,x}^2 & i = j \\ 2\Psi_{i,x}\Psi_{j,x} & i \neq j \end{cases} \tag{5.11}$$

$$\sigma(k,l,i,x) = \begin{cases} \Psi_{k,x}^3 & k = l = i \\ 3\Psi_{k,x}^2 \Psi_{i,x} & k = l \neq i \\ 3\Psi_{l,x}^2 \Psi_{k,x} & k \neq l = i \\ 6\Psi_{k,x}\Psi_{l,x}\Psi_{i,x} & k \neq l \neq i \end{cases} \tag{5.12}$$

and $\omega_{a,j}$ and $\omega_{t,j}$ are the natural frequencies associated with the jth mode in the axial and transverse directions, respectively. The transverse natural frequencies, $\omega_{t,j}$, were compared against those in reference [59] and found to be in good agreement. Small differences ($\approx .05\%$) were traced to different extensibility assumptions. Note that the nonlinearities dictate a particular form of nonlinear coupling between the two sets of differential equations. It is this nonlinear interaction which produces axial

shortening as a consequence of transverse bending, as well as the cubic stiffening due to nonlinear strains.

The accuracy of this system of equations depends primarily upon three parameters: N_c, the number of component (nonrotating fixed-free beam) modes used to assemble each transverse rotating mode; N_t, the number of transverse rotating modes in $w(x,t)$; and N_a, the number of axial modes in $u_d(x,t)$. In previous work [65], a convergence study was conducted to determine that the values $N_c = 18$, $N_t = 9$ and $N_a = 9$, were sufficient to produce a model which would accurately predict motions occurring primarily in the lower axial and transverse modes. This will be referred to as the *reference model*.

One should note that Eq. (5.9) may be (approximately) eliminated by employing a quasi-static assumption for the axial modes. That is, if the axial accelerations ($\ddot{b}_j$ in Eq. (5.9)) are neglected, each b_j may be determined as a quadratic function of the c_k's, and the b_j's may be eliminated from Eq. (5.10). Some results are shown where this procedure has been applied (labeled "quasi-static"). However, for more realistic geometries, more general nonlinear coupling will be present which makes this procedure much more difficult, if not impossible.

5.3 Galerkin-based ROM generation

In general, one is not particularly interested in the motions of all system modes, but only those that exhibit a large response or lie within a specific frequency range. However, in systems such as this, the linear modes are coupled to a degree which requires that their interactions be accounted for [63]. One way of including these effects in the ROM is the invariant manifold based nonlinear normal mode (NNM). Each NNM may be viewed as an extension of some corresponding linear mode and,

as with linear modes, motions initiated within an individual NNM must remain in that NNM for all time — a property known as invariance. A given NNM may be described as a nonlinear oscillator whose trajectory lies on a known surface within the state space of the original system. This surface, the invariant manifold, allows all linear modes to contribute to the motions of a given NNM. These contributions are incorporated into the dynamics of the NNM, allowing it to correctly account for the nonlinear interactions between linear modes, without requiring explicit simulation. In addition, the invariant manifold dictates the dynamic participation of the the various linear modes within a given NNM, allowing the corresponding nonlinear mode shape to vary with time. In effect, this manifold allows all system modes to contribute to the dynamics of a select few. An accurate determination of the invariant manifold produces an accurate ROM governing the mode (or modes) of choice.

The nonlinear Galerkin-based method used here was recently developed in reference [69], which also includes some illustrative examples. It expands the range of applicability considerably (to the large amplitude realm) over that available using the traditional asymptotic methods for invariant manifold generation. Currently, it is limited to the generation of single-mode, free-response, ROMs. However, no significant barrier has been found which limits its expansion into a multi-mode formulation, possibly including some type of external forcing in a rigorous manner.

Each single-mode invariant manifold exists as a surface within the ($2(N_a + N_t)$ dimensional) state space of the original model. This surface must be parameterized by a pair of variables and, in this work, a "master" amplitude, a, and phase, ϕ, are chosen. Given the formulation of our blade model, this amplitude and phase logically

correspond to a given "master" mode, here taken to be the kth mode, according to:

$$\eta_k = a\cos\phi$$
$$\dot{\eta}_k = -a\omega_k \sin\phi \tag{5.13}$$

where η_k, and $\dot{\eta}_k$ are a generalized modal position and velocity – corresponding to one of the b's and c's, and ω_k is the associated linear natural frequency. Given this definition, the "master" mode's equation of motion (from Eqs. (5.9) or (5.10)) may be recast as two first order ordinary differential equations (ODEs) in a and ϕ:

$$\dot{a} = \frac{-f_k \sin\phi}{\omega_k}$$
$$\dot{\phi} = \omega_k - \frac{f_k \cos\phi}{a\omega_k} \tag{5.14}$$

where f_k corresponds to the nonlinear portion (the right-hand side) of the kth equation of motion.

The remaining modal positions and velocities are required to depend on, or be "slaved" to a and ϕ as:

$$\eta_i = P_i(a,\phi)$$
$$\dot{\eta}_i = Q_i(a,\phi) \qquad \text{for } i = 1\ldots(N_a+N_t), i \neq k \tag{5.15}$$

This constraint may be met barring certain nonremovable modal interactions, such as internal resonances.

The relations above and the equations of motion may expanded through the chain rule and combined to produce nonlinear, time-independent, partial differential

equations which govern the geometry of the manifold:

$$Q_i = \frac{\partial P_i}{\partial a}\left(\frac{-f_k \sin\phi}{\omega_k}\right) + \frac{\partial P_i}{\partial \phi}\left(\omega_k - \frac{f_k \cos\phi}{a\omega_k}\right) \tag{5.16}$$

$$\text{for } i = 1 \ldots (N_a + N_t), i \neq k$$

$$-\omega_i^2 P_i + f_i = \frac{\partial Q_i}{\partial a}\left(\frac{-f_k \sin\phi}{\omega_k}\right) + \frac{\partial Q_i}{\partial \phi}\left(\omega_k - \frac{f_k \cos\phi}{a\omega_k}\right) \tag{5.17}$$

$$\text{for } i = 1 \ldots (N_a + N_t), i \neq k$$

Solving these for the P's and Q's results in the master/slave relations that satisfy the equations of motion. Note that these will represent an entire one-parameter family of solutions that are restricted to a two-dimensional surface (manifold) in the phase space.

Given these constraint relations (the P's and Q's), the c's and b's become known functions of (a, ϕ) and may be eliminated from the equations of motion. In particular, as these relations are used to evaluate the nonlinear coupling terms, f_k, Eq. (5.14) becomes a function of a and ϕ only. This pair of ODEs becomes the reduced-order model which governs the chosen nonlinear normal mode of the system. Numerical integration may be used to obtain time histories for both a and ϕ, from which the contributions of the linear modes may be determined. These modal motions may then be combined (using the known manifold coefficients) to determine the physical deflections of the system as a function of time.

In most previous work, similar manifold-governing equations have been solved through a polynomial expansion in $(\eta_k, \dot{\eta_k})$ whose coefficients are obtained through an order-matching routine, ultimately yielding an asymptotically-accurate ROM. Alternatively, the PDEs may be solved for the P's and Q's using an expansion which

is satisfied in an integral sense over a chosen domain, via a Galerkin projection. This yields a ROM with optimal accuracy for the chosen expansion, over a known domain. Reduced order models generated through this Galerkin-based procedure do not suffer from the uncertainties and convergence issues associated with the polynomial-based approach.

Here, this nonlinear Galerkin-based solution process is repeated over several adjacent subdomains to obtain a composite representation of the manifold for use over a larger domain. The periodic nature of ϕ (of period 2π) allows $P_i(a,\phi)$ and $Q_i(a,\phi)$ to be well represented in the ϕ direction by harmonic functions, but there is no such convenient basis for the a-dependence. Hence, the amplitude coordinate is divided into small sections, producing subdomains consisting of annular strips where $\phi \in [0, 2\pi]$ and $a \in [a_j, a_j + \Delta a]$. It has proven sufficient to represent each P and Q as locally linear in a, and with N_ϕ harmonics in ϕ [69]. This corresponds to the expansion:

$$\begin{aligned} P_i(a,\phi) &= \sum_{l,m} C_i^{l,m} T_{l,m}(a,\phi) \\ &= \sum_{m=1}^{N_\phi} \left[C_i^{1,m}(\frac{a-a_j}{\Delta a}) + C_i^{2,m}(1 - \frac{a-a_j}{\Delta a}) \right] \cos((m-1)\phi) \end{aligned}$$

$$\begin{aligned} Q_i(a,\phi) &= \sum_{l,m} D_i^{l,m} U_{l,m}(a,\phi) \\ &= \sum_{m=1}^{N_\phi} \left[D_i^{1,m}(\frac{a-a_j}{\Delta a}) + D_i^{2,m}(1 - \frac{a-a_j}{\Delta a}) \right] \sin(m\phi) \\ &\qquad\qquad \text{for } i = 1 \ldots (N_a + N_t), i \neq k \end{aligned} \quad (5.18)$$

for a given subdomain. This allows the expansion coefficients (the C's and D's) to govern the manifold geometry, and their determination defines the corresponding ROM.

This expansion is substituted into the manifold-governing equations (Eqs. (5.16) and (5.17)), which are multiplied through by a to remove the singularity at $a = 0$. Finally, all terms are moved to the right side of the equation, and a Galerkin projection is carried out using the individual shape functions over the chosen domain. This leaves:

$$0 = \int_{a,\phi} U_{p,q} \left[-a \sum_{l,m} D_i^{l,m} U_{l,m} + \sum_{l,m} C_i^{l,m} \frac{\partial T_{l,m}}{\partial a} \left(\frac{-f_k a \sin\phi}{\omega_k} \right) \right. \\ \left. + \sum_{l,m} C_i^{l,m} \frac{\partial T_{l,m}}{\partial \phi} \left[a\omega_k - \frac{f_k \cos\phi}{\omega_k} \right] \right] da\, d\phi \tag{5.19}$$

$$0 = \int_{a,\phi} T_{p,q} \left[\omega^2 a \sum_{l,m} C_i^{l,m} T_{l,m} - a f_i + \sum_{l,m} D_i^{l,m} \frac{\partial U_{l,m}}{\partial a} \left(\frac{-f_k a \sin\phi}{\omega_k} \right) \right. \\ \left. + \sum_{l,m} D_i^{l,m} \frac{\partial U_{l,m}}{\partial \phi} \left[a\omega_k - \frac{f_k \cos\phi}{\omega_k} \right] \right] da\, d\phi \tag{5.20}$$

for $i = 1 \ldots (N_a + N_t)$, $i \neq k$, $p = 1, 2$, and $q = 1 \ldots N_\phi$: a set of $68 \times N_\phi$ nonlinear equations in the C's and D's for $N_a + N_t = 18$. However, the fact that there are no velocity-dependent nonlinearities allows Eq. (5.19) to be reduced to the form:

$$D_i^{p,q} = F(\boldsymbol{C})$$

where $\boldsymbol{C}$ represents a vector containing all the $C_i^{l,m}$. As a consequence, for this application, only the C's need to be considered as independent variables, and $34 \times N_\phi$ independent nonlinear equations remain. One should note that the independent solution of neighboring subdomains (in a) generally yields a slight discontinuity at the subdomain intersection. In practice, this discrepancy has been found to be quite small, and slight modifications to the manifold coefficients may be made to reflect the mean value at these locations — producing a continuous composite manifold.

For the results presented here, Eqs. (5.19) and (5.20) are solved numerically using Powell's Hybrid method [66]. This approach simply evaluates the expressions for various sets of C's to develop an approximate Jacobian, which is then used and updated iteratively to make progress toward a solution. At each iteration, the evaluation requires that the entire set of equations be numerically integrated. This computational expense could be avoided by completing the integration analytically for a general set of coefficients. However, the effort necessary to achieve such a specialized set of equations is not warranted here. The most likely way to improve the efficiency of the approach is by eliminating the harmonic functions from the expansions of P and Q, and using a locally linear approximation in ϕ as well as a. This would retain the generality of the formulation, while reducing the number of coefficients required to represent each local section of the manifold.

Once the manifold coefficients are determined, the P's and Q's may be assembled to obtain expressions for all the modal positions and velocities in term of the variables (a, ϕ). These may then be used to evaluate f_k in Eq. 5.14, which represents a single degree of freedom oscillator. Numerical integration produces values for $a(t)$ and $\phi(t)$, from which the corresponding modal dynamics may be determined.

5.4 Results

The results presented here correspond to a rotating beam with the following properties: $L = 9\,\mathrm{m}$, $m = 10\,\mathrm{kg/m}$, $EI = 3.99 \times 10^5\,\mathrm{N \cdot m^2}$, $EA = 2.23 \times 10^8\,\mathrm{N}$, $\Omega = 30$ rad/s, and $h = 0.5\,\mathrm{m}$. These values are chosen to correspond roughly to a rotorcraft blade with nearly transonic blade tip velocity. The procedure outlined above was applied to generate an invariant manifold for the first flapping mode ($c_1(t)$) which is piecewise linear in a, and uses $N_\phi = 8$ harmonics in ϕ. For the results shown, 48

piecewise linear manifold segments of width $\Delta a = 0.05$ are used to achieve a total manifold domain of $a \in [0, 2.4]$, $\phi \in [0, 2\pi]$. This corresponds to a peak-to-peak amplitude of nearly one meter at the beam tip — a considerable deflection. At greater amplitudes the manifold solution fails to converge. This could indicate that a manifold bifurcation or modal interaction is present, that more harmonics are necessary in the solution, or that more modes are necessary in the original reference model. However, at this large amplitude, additional questions arise regarding the precision of the original beam formulation and the magnitude of higher-order (previously neglected) effects.

Figure 5.2 shows the contribution of the second flapping mode, c_2, to the manifold (for $\phi = 0$), and illustrates the agreement between the Galerkin-based manifold solution and a numerical solution produced using the reference model. This numerical solution is obtained through an extensive simulation of the original equations of motion, which searches for initial conditions that yield periodic responses in the vicinity of the first flapping mode. The two solutions agree quite well, with almost no discrepancies throughout the domain. However, as all the modes are represented in terms of the first, there are 16 more sets of results to compare. Not all agree as well as those seen here but, in general, there are only minor discrepancies toward the high amplitude portion of the domain. Although more segments in a, and harmonics in ϕ could be used to improve these results, it will be seen that those used here are sufficient to produce an accurate reduced-order model for the first nonlinear flapping mode.

Figure 5.2 is simply a "slice" of the manifold, corresponding to $\phi = 0$, projected into a plane. A more complete projection of the manifold is shown in Fig. 5.3 for the entire solution domain. This surface dictates the contribution of the second

linear flapping mode required to achieve the correct periodic response of the chosen nonlinear normal mode. A similar surface governing the participation of the first linear axial mode is shown in Fig. 5.4. Note that the two surfaces indicate different harmonic content: c_2 is primarily third order in ϕ, while b_1 is primarily second (and zeroth) order. This even-order dependence for b_1 (as well as the rest of the b's) corresponds to an axial response which is identical for both positive and negative transverse deflections.

Given the manifold geometry, the equations of motion governing the ROM may be evaluated and numerically integrated to yield time history results. Some such results are shown in Figs. 5.5 and 5.6 for a motion occurring in the first nonlinear normal mode of the system, which corresponds to the system's fundamental flapping mode. Figure 5.5 shows the predicted tip motion in the w-direction (flap) for both the reduced-order model (Galerkin NNM), and the original model (Reference Solution). As with the results from Fig. 5.2, the reference results are obtained numerically by searching for motions which must lie on the manifold of interest. The results shown correspond to the initial condition $a(0) = 2.375$, $\phi(0) = 0$, which produces an initial tip deflection of about 0.47m. The two solutions are nearly identical, indicating that the ROM accurately represents the fundamental flapping motion of the beam. Though the agreement is excellent, there are still slight discrepancies present. Figure 5.6 illustrates the eighth linear flapping mode's contribution to the deflections of Fig. 5.5, as predicted by both the reference solution and the Galerkin NNM. The reference solution is simply a result of the original initial conditions and the ensuing interactions between the modes, whereas the Galerkin NNM solution is a reconstruction based on the values of $a(t)$, $\phi(t)$, and $P_8(a, \phi)$. The discrepancies may largely be attributed to the restricted harmonic content of the Galerkin-based results.

Though eight harmonics are used in the solution, the odd harmonics dominate the flapping mode results. Hence, only four harmonics contribute to the results shown. It is assumed that additional harmonics would eliminate this (small) error. However, this degree of precision is not necessary, as the ROM is already sufficiently accurate.

The transverse and axial deflections associated with the motions in Figs. 5.5 and 5.6 are illustrated in Fig. 5.7. Here, the deflections are shown for several instants of time, spaced evenly within a quarter-period of motion. The dashed line for $u(x)$ corresponds to the static extension of the beam, $u_s(x)$, due to the rotation, and the departure from this line is a consequence of the axial shortening due to transverse bending. Hence, the uppermost line for $w(x)$ corresponds to the lowest line for $u(x)$. Note that, for $u(x,t)$, the shapes shown are representative of the entire periodic behavior. That is, while $w(x,t)$ would become symmetric about the x-axis with further time sampling, the corresponding axial motion, $u(x,t)$, would simply repeat, but at twice the frequency of $w(x,t)$. Also, the nonsimilar nature of the NNM is apparent here, as the deflection shapes obviously change through the course of the motion. This key component of nonlinear structural vibrations is automatically embedded within the invariant manifold formulation.

Lastly, Fig. 5.8 depicts the amplitude-frequency relationship for a number of reduced-order models, as well as the reference solution. Here, the Galerkin NNM is shown to be extremely accurate, while all other methods diverge from the correct solution. The "One Linear Mode" results correspond to the assumption that only the first linear flapping mode participates, while all other modes remain quiescent. This overly constrains the system (by not allowing shortening, or any other coupling effects), and the corresponding nonlinear effects are entirely wrong. The "One Quasi-Static Mode" curve is from a similar model, where the longitudinal inertia is

neglected, and the axial modes are condensed out. The remaining transverse modes are assumed to be quiescent. This approximates the nonlinear influence of the axial shortening, and produces results which are quite good at low amplitudes, but increasingly less accurate as the amplitude grows. Furthermore, this approach becomes considerably more difficult for more realistic rotorcraft models, as additional nonlinear coupling terms are present. The two NNM-based models are both accurate at low amplitude, but the "Asymptotic NNM", constructed from a third-order manifold from reference [65], fails to maintain convergence due to its polynomial nature. Only the "Galerkin NNM" accurately follows the reference solution and, unlike the quasi-static results, it may easily be extended to more realistic rotorcraft models. As a group, these results highlight the critical role of the modal interactions in determining the proper system response.

5.5 Conclusion

The nonlinear behavior of rotorcraft blades has made it difficult to produce low-order models which are both accurate and efficient. As a means of investigating this fundamental issue, the nonlinear equations of motion for a simple rotating Euler-Bernoulli beam model were reduced using a procedure based on the invariant manifold formulation of nonlinear normal modes.

The approach used here allows accurate numerical computation of the invariant manifolds associated with a particular nonlinear normal mode. This nonlinear Galerkin method yields reduced-order models which account for the nonlinear interactions between the linear modes in a manner which is both rigorous and precise. Applied to the rotating beam, this approach accurately models the critical dynamic coupling between the axial and transverse modes, as well as the coupling within the

set of transverse modes through amplitudes of considerable magnitude.

The results shown for the nonlinear normal mode associated with the first flapping mode of the system illustrate the power and accuracy of the method. The invariant manifold solution is shown to be quite accurate, and the corresponding single degree of freedom reduced-order model yields results which agree nearly exactly with those of the original system. The computational cost associated with generating the manifold solution is not trivial, but the efficiency of the resultant model justifies this investment. In addition, the reduced-order model allows one to focus on the motions of interest, without devoting attention to the entire original model.

Furthermore, the nature of the reduction procedure outlined here does not restrict it to problems with simple geometries or nonlinearities. It may easily be applied to more accurate (and complex) rotorcraft blade models, including those based on finite elements, and work on such models is currently underway. Furthermore, the current formulation may be expanded to produce reduced-order models which include several modal degrees-of-freedom [63]. Such a generalization will allow the rigorous treatment of internal resonances, as well as more practical low-order models. Additional work will focus on the optimal strategy for the application of forcing to these reduced-order models.

5.6 Figures

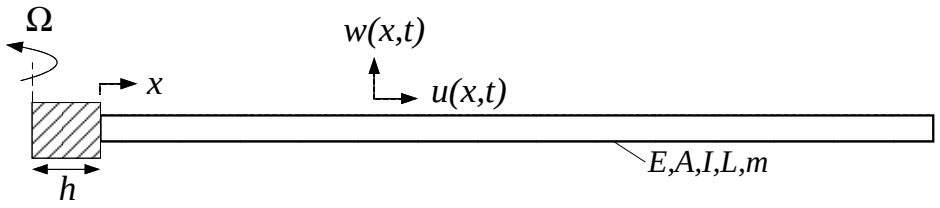

Figure 5.1: Rotating beam system, for Ω =Constant

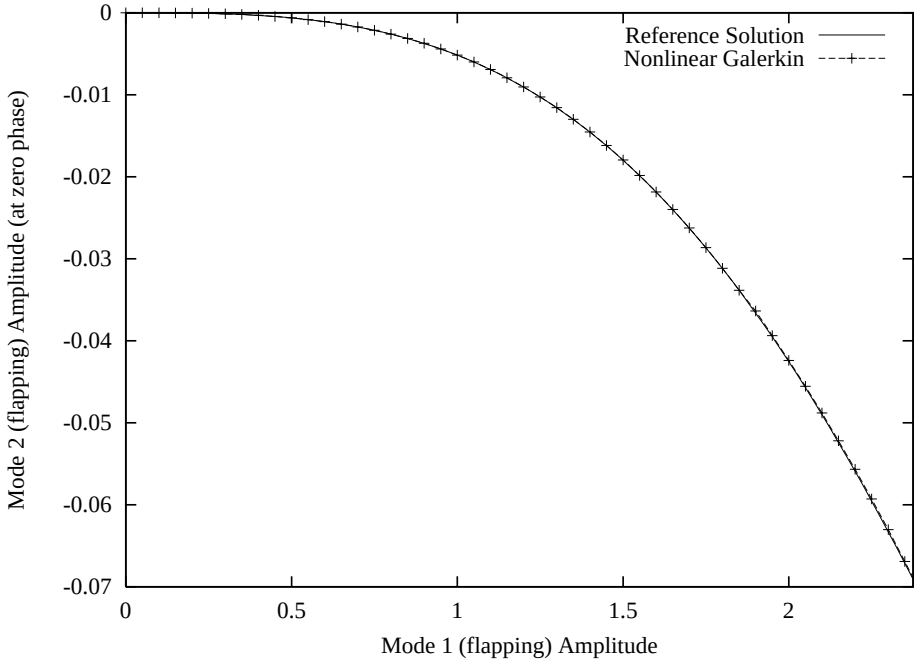

Figure 5.2: The invariant manifold corresponding to the first flapping mode, at $\phi = 0$, indicating agreement between the Nonlinear Galerkin and Reference Solution through a large amplitude. The manifold corresponding to the reference solution is obtained through numerical simulation.

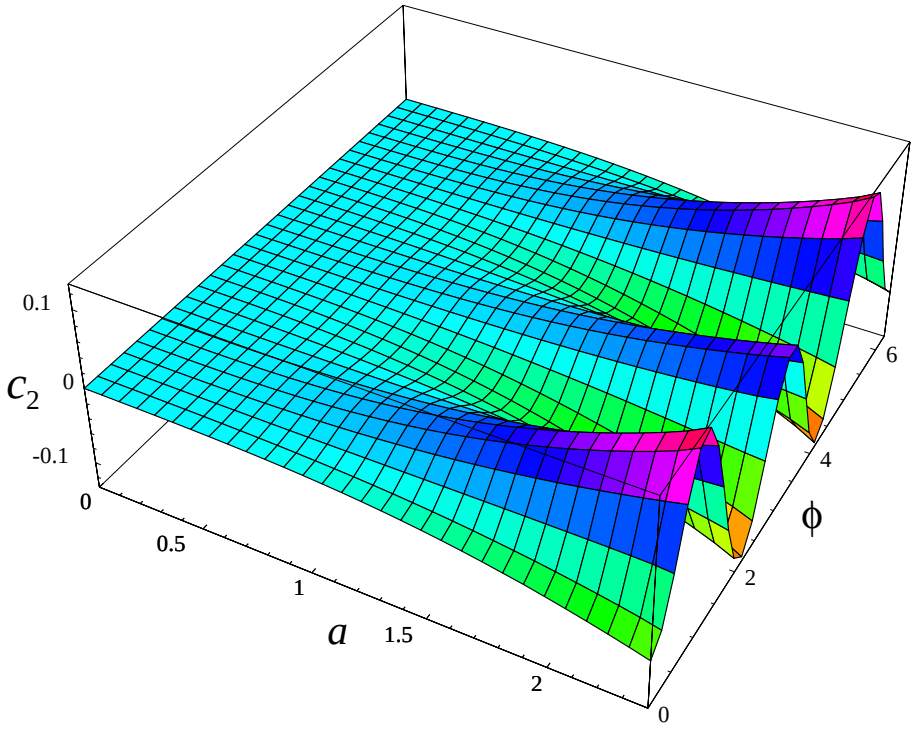

Figure 5.3: Projection of the first-mode manifold depicting the contribution of the second flapping mode (c_2), as a function of the first flapping mode's amplitude and phase.

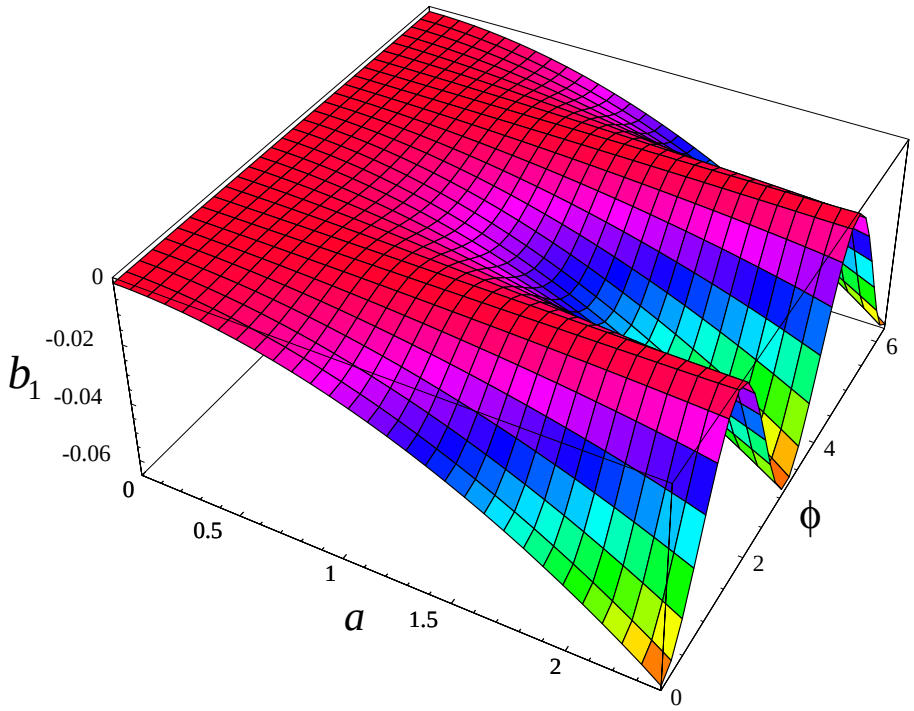

Figure 5.4: Projection of the first-mode manifold depicting the contribution of the first axial mode (b_1), as a function of the first flapping mode's amplitude and phase.

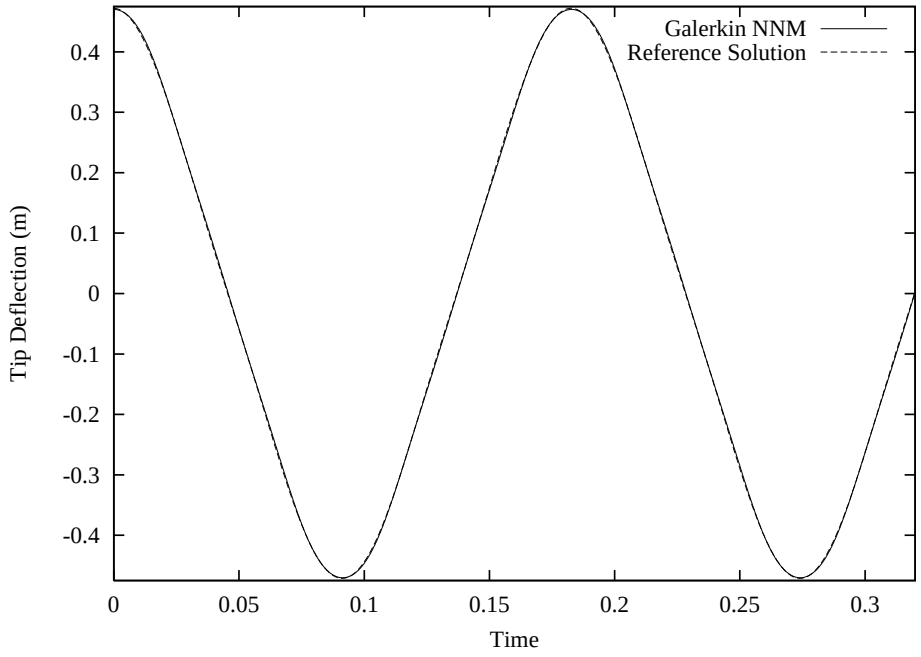

Figure 5.5: Transverse deflection at the beam tip, $w(L,t)$, for the Galerkin NNM and the reference solution. The responses are nearly identical.

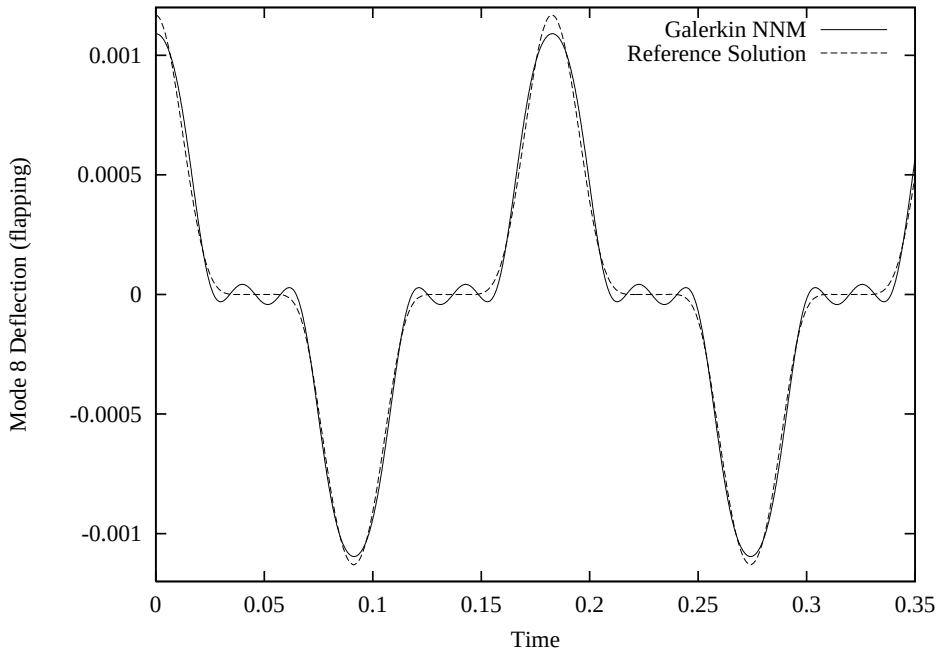

Figure 5.6: Modal contribution of the eighth flapping mode to the motion of Fig. 5.5. Presumably, agreement would improve with the inclusion of more harmonics in the Galerkin solution.

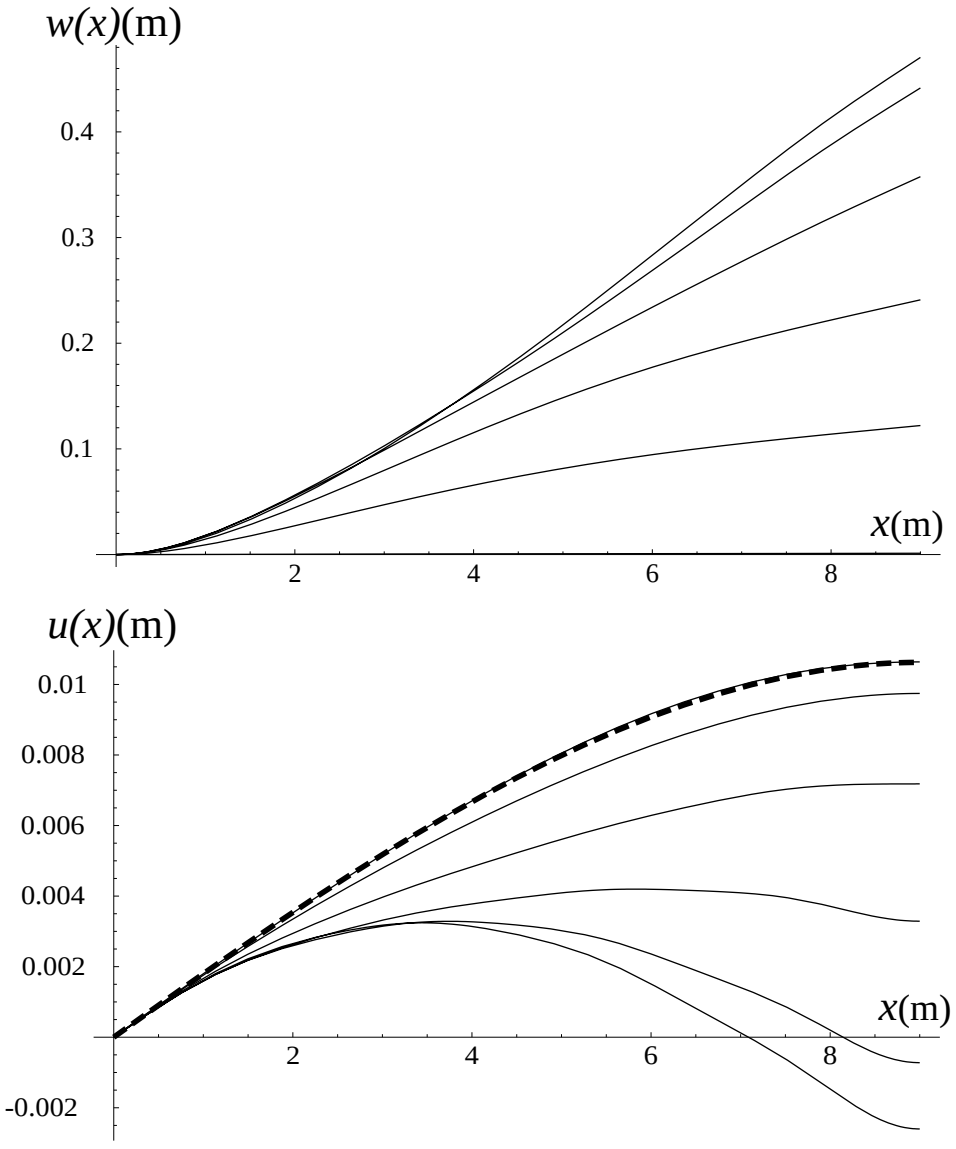

Figure 5.7: Transverse and axial deflections, $w(x,t)$ and $u(x,t)$, for a quarter-period of motion in the first nonlinear mode. The dashed line denotes the static deflection, $u_s(x)$, and the top curve for $w(x)$ corresponds to the bottom $u(x)$ curve.

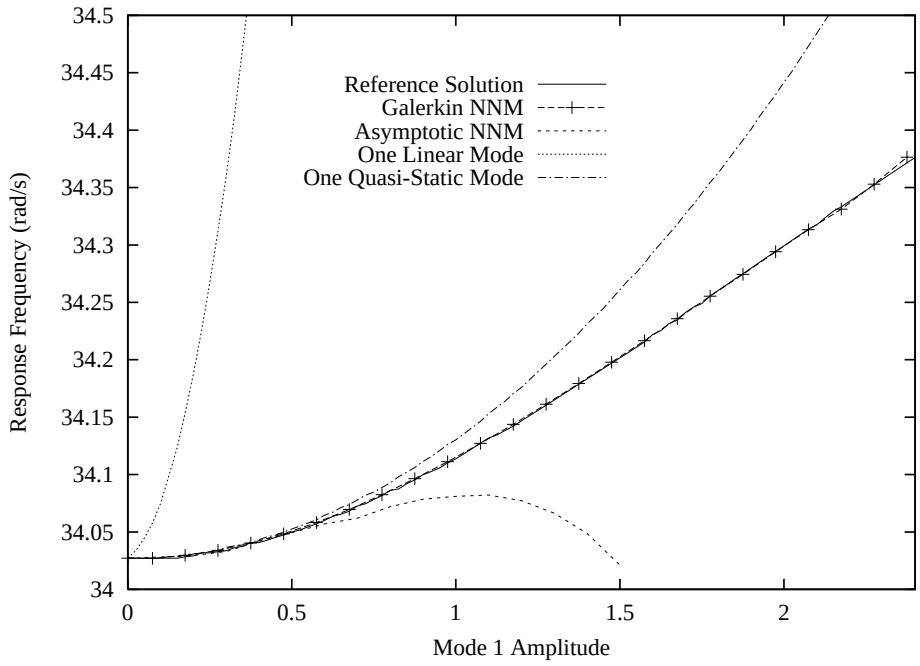

Figure 5.8: Response frequency as a function of modal amplitude for several one-mode models, as well as the Reference Solution, for the first nonlinear mode.

CHAPTER VI

CONCLUSIONS

6.1 Introduction

The numerical and analytical results summarized within this work contain several contributions to the field of nonlinear dynamics and rotating beam dynamics. These contributions, as a whole, enable the systematic generation of reduced-order models (ROMs) for a general class of nonlinear structural systems. This is accomplished through methodical, expansion-based solutions for the invariant manifolds which govern the nonlinear normal modes of the structure. These solutions allow the practical application of the invariant manifold formulation to a wide variety of structures, including discrete, finite element, and continuous dynamic systems. The nonlinear Galerkin-based formulation developed in Chapters IV and V is particularly promising, and may be expanded into a number of problem domains, such as external forcing, sub-structuring, and multi-mode solutions. The generality and numerical nature of this approach makes it ideal for producing high-fidelity ROMs for many types of nonlinear systems.

6.2 Contributions

The contributions contained within this dissertation are most easily described by examining each chapter individually:

• Chapter II utilizes a standard formulation to produce analytical solutions for the invariant manifold coefficients (through third order), based on the asymptotic, polynomial-based, approach developed in earlier works. This general solution has been computationally implemented, and allows the generation of ROMs of arbitrary size for a certain class of systems, with little or no additional analytical work. Previous to this work, no general multi-mode solutions existed, and the existing single-mode solutions were considerably more limited in scope.

• In Chapter III, these automated solutions are applied to a discretized model of a rotating, Euler-Bernoulli beam. This beam model results in a unique modal formulation, with critical nonlinear terms coupling the axial and transverse beam motions. These critical coupling terms are shown to be well captured (within a limited amplitude) by the asymptotic approach for both single-mode and internally resonant multi-mode motions.

• A new procedure for determining accurate invariant manifolds is developed in Chapter IV. This method uses a Galerkin projection to produce manifolds which are locally accurate in an integral sense. This approach relies on a coordinate transformation to obtain new manifold-governing equations, which are then solved numerically. This solution, though computationally demanding, is shown to produce ROMs which realize the full potential of the invariant manifold formulation — yielding models which remain precise, even for large-amplitude, strongly nonlinear motions. In addition, the generality of the formulation makes it a good foundation for further

research opportunities.

• The rotating beam formulation and Galerkin-based manifold solution method are brought together in Chapter V. The results indicate that ROMs generated in this manner are both practical and extremely accurate. These results encourage the use of this approach for the analysis of more rigorous rotorcraft blade models, as well as other complex nonlinear structural systems.

6.3 Future Work

As is mentioned above, the methods developed in this dissertation provide many potential avenues for future work. Due to the effectiveness of the Galerkin-based reduced-order models, this section focuses on the improvement, extension, and application of this approach. The likely improvements to the current approach lie primarily in the computational domain, whereas analytical refinements will most likely include substructure analysis, multi-mode ROMs, and time-dependent forcing. The current capabilities, combined with these forthcoming developments will enable the generation of sophisticated reduced-order models for a wide variety of nonlinear systems.

6.3.1 Theoretical Development

There are several ways in which the current implementation of the Galerkin-based solution may be improved. The most significant of these is the addition of manifold discretization in the ϕ direction. It is expected that this change would improve the solution speed by a factor of two (or so) without reducing the accuracy. Though approximate, this calculation is detailed in Appendix D. Further improvements could be achieved by simply improving the computational efficiency of the code. Also, the solution procedure could be made more robust by allowing the manifold "mesh" to

become finer in areas where convergence problems are encountered.

The analytical formulation may also be adjusted to improve the computational efficiency of the solution. The most promising adjustment is to move toward a component mode formulation, where the nonlinear effects are concentrated entirely on a set of constraint modes, using a formulation similar to that in reference [70]. Though this is not possible for distributed nonlinearities (such as those in the rotating beam problem), it is practical for many structures containing discrete nonlinearities. If such a constraint mode is used as the "master" mode, the partial differential equations governing the invariant manifolds for the remaining modes are simplified considerably. This change may make it practical to integrate the Galerkin projection analytically (or numerically) only once to produce an explicit set of nonlinear equations for the manifold expansion coefficients. Essentially, this approach allows a specific type of linear modal coupling in exchange for isolating the effects of the nonlinearity. Another advantage of this modification is that it logically leads to a substructuring implementation. That is, a manifold-based ROM for a nonlinear substructure may be coupled to a linear substructure to produce similar equations of motion. These may then be reduced to obtain a ROM for the combined structure. Similarly, it may be advantageous to formulate the ROM for a given substructure in terms of the amplitude and phase of one or more points lying on the substructure boundary.

The practical application of the methods developed within this dissertation would be aided considerably by a rigorous understanding of the stability and bifurcation conditions for the manifold. A system's ROM should represent a unique and stable reduction of the original system, and with the current solution procedure there is no guarantee of these properties. However, these properties are well understood for the corresponding linearized systems, and it is primarily the unprecedented range of

the Galerkin-based ROMs which make the issue significant. Ideally, some analytical measure of the manifold PDE could be monitored to indicate the presence of a manifold bifurcation, and this information could be incorporated into the ROM.

Another useful addition to this work would be the addition of time-dependent forcing. Some results have been achieved previously for the asymptotic approach, with moderate success. In general, the manifold generation process may either ignore or include the forcing. If the forcing is ignored in the manifold solution, it still may be applied to the resulting ROM. Though this compromises the invariance of the system, it is expected that some accuracy will be maintained. This should be especially true when the forcing is small relative to the response — as when near resonance. Of course, more accurate results could be obtained through including time-dependence in the manifold itself. This would have the effect of changing the double expansion in a and ϕ into a triple expansion with t as well. The addition of forcing will, of course, allow multiple solutions to exist. These solutions may correspond to a unique ROM with several possible responses, but manifold bifurcations could also result in multiple ROM's for some forcing conditions. Regardless of the approach, a method for generating forced ROMs is necessary for the practical application of this method in an industrial setting.

Furthermore, practical use of this method requires the ability to generate ROMs which contain more than one nonlinear normal mode. As with the asymptotic solutions, this simply involves using additional variables to parameterize the invariant manifold. Though this will add analytical complexity and incur additional computational costs, it will greatly expand the applicability of the method. This approach is necessary in the instance of internal resonance, but its utility extends much farther. Often it is attractive to include all modes within a certain frequency range in a ROM,

or allow particular modes to dynamically interact. As with linear systems, there are many practical applications for an accurate, multi-mode, reduced-order model.

6.3.2 Applications

The general nature of the Galerkin-based, NNM reduction method allows it to be applied to great effect for a wide variety of engineering systems. It is ideally suited for the analysis of structural dynamic systems with nonlinearities which introduce complex modal interactions. Such behavior is observed in the idealized rotating beam problem examined in Chapters III and V, as well as in the analysis of actual rotorcraft blades. In addition, as the model becomes more complex, the reduction procedure remains largely unchanged. Consequently, the advantage over other analytical approaches will only increase with model complexity. The basic analytical foundation of this approach, and its computational solution procedure allow efficient application to complex systems with very little analytical work.

As the method has shown considerable promise on the rotating beam problem, work will most likely continue toward the goal of ROM generation for more realistic rotorcraft system models. The current rotating beam model must be refined to more closely resemble a rotorcraft blade. Currently, work is underway on the development of a finite-element analog to the continuous blade model used previously. This discretized model will allow more general blade properties, and may eventually include additional degrees-of-freedom (such as twist and lead-lag). Once such a model has been obtained, the current theory would be sufficient to gain considerable insight into the blade dynamics. However, with further theoretical work, the approach may become much more applicable.

The development of accurate forced ROMs allows the individual blade models to

be coupled to the driving forces as well as the aerodynamic loads. Given the proper substructuring approach, these blade models may then be assembled to obtain a composite nonlinear ROM for the entire rotor assembly. A model such as this would be of considerable aid in the design cycle. Of course, achieving such an ambitious goal is dependent on the development of additional theoretical techniques. These techniques may be evaluated as the blade model advances, leading to a progression such as:

- Generation and evaluation of forced ROMs for the analytic rotating beam model.
- Generation and evaluation of forced Multi-Mode ROMs for a simple finite-element rotating beam model.
- Application of substructure methods to ROM's corresponding to several blades connected by a rigid hub.
- Forced analysis of a simple multi-blade hub assembly.
- In depth dynamic analysis of a detailed nonlinear rotor assembly model.

In parallel with this development there are topics which deserve exploration, but are not convenient to study in the context of rotorcraft. These include systems with nonsmooth nonlinearities, and those containing nonlinearities at discrete locations. Though some examples of discrete nonlinearities were discussed in this dissertation, they provide an ideal testbed for the component mode formulation discussed earlier. Nonsmooth nonlinearities have been difficult to study in this context previously, as the asymptotic methods did not apply, and other approaches required extensive analytical work. However, the Galerkin-based solution makes their study much more accessible.

These topics could be combined to great effect using either a continuous or finite

element beam with a nonsmooth nonlinearity along its length, such as a clearance or dry friction damper. A formulation such as that in reference [70], which uses a continuous beam and a flexible friction damper, could be used to obtain both free response and forced response ROMs. Conceivably, this work could be extended to several nonlinearly coupled subsystems (with or without nonsmooth nonlinearities) for the development of substructure methods.

Of course, many more systems could be found which would benefit from the application of the methods developed within this work. The above systems are mentioned only because they offer ideal domains for the further conceptual development of the approach. The limitations of this method lie primarily in the accuracy of the original model, and the computational effort necessary to obtain a solution. Given these resources and the need for accurate, efficient reduced-order models, the potential applicability of this approach is considerable.

APPENDICES

APPENDIX A

ALTERNATIVE FORMULATION FOR THE SECOND-ORDER MANIFOLD EQUATIONS

If the original equations of motion are expressed in the following second order form:

$$\ddot{\mathbf{x}} = \boldsymbol{f}$$

where $\mathbf{x}$ is a vector of N displacements (modal or otherwise), and $\boldsymbol{f}$ is a vector containing the linear and nonlinear forces on the system, the assumptions from Chapter II may still be applied. That is,

$$x_k = u, \text{ and } \dot{x_k} = v$$

and

$$x_i = X_i(u, v) \qquad \text{where } i \neq k.$$

If these relations are applied to the above equations of motion, the kth equation simply becomes:

$$\dot{v} = f_k$$

while the chain rule may be used to expand the remaining equations as:

$$\frac{d}{dt}\left(\frac{\partial X_i}{\partial u} v + \frac{\partial X_i}{\partial v} f_k\right) = f_i$$

Further expansion results in a set of second order partial differential equations, which are independant of time:

$$\frac{\partial^2 X_i}{\partial u^2}v^2 + 2\frac{\partial^2 X_i}{\partial u \partial v}v f_k + \frac{\partial^2 X_i}{\partial v^2}f_k^2 + \frac{\partial X_i}{\partial u}f_k + \frac{\partial X_i}{\partial v}(\frac{\partial f_k}{\partial u}v + \frac{\partial f_k}{\partial v}f_k) = f_i$$

Note that $\boldsymbol{f}$ is, in general, a function of all positions and velocities. Consequently, its partial derivatives may require further expansion. As with the first order formulation, all velocities may be expressed in terms of u, v, f_k, and the X_i's. However, if f_k contains velocity terms, the velocities may never be entirely eliminated from the above formulation. Further investigation is necessary to determine the consequences of this limitation.

APPENDIX B

ADDITIONAL FORMULAS FOR THE GENERATION OF MULTI-MODE MANIFOLDS

The constants from the two and three mode problems are as follows:

$$C^{3,k,l}_{1,i} = 2\sum_{q\in S_M} \alpha^{q}_{k,k} a^{q,l}_{5,i}$$

$$C^{3,k,l}_{2,i} = 2\sum_{q\in S_M} \alpha^{q}_{k,l} a^{q,k}_{5,i}$$

$$C^{3,k,l}_{5,i} = 2\sum_{q\notin S_M} \alpha^{i}_{k,q} a^{k,l}_{5,q}$$

$$C^{3,k,l}_{6,i} = \sum_{q\notin S_M} \alpha^{i}_{l,q} a^{k,k}_{5,q}$$

$$C^{3,k,l}_{7,i} = \beta^{i}_{k,k,l} + \sum_{q\notin S_M} (2\alpha^{i}_{k,q} a^{k,l}_{3,q} + \alpha^{i}_{l,q} a^{k,k}_{3,q}) - \sum_{q\in S_M} (\alpha^{q}_{k,k} b^{l,q}_{4,i} + \alpha^{q}_{k,l} b^{k,q}_{4,i})$$

$$C^{3,k,l,m}_{8,i} = 2\sum_{q\in S_M} \alpha^{q}_{k,l} a^{q,m}_{5,i}$$

$$\begin{aligned} C^{3,k,l,m}_{9,i} \;=\; & \sum_{q\notin S_M} (\alpha^{i}_{k,q} a^{l,m}_{3,q} + \alpha^{i}_{m,q} a^{k,l}_{3,q} + \alpha^{i}_{l,q} a^{m,k}_{3,q}) \\ & + \frac{1}{2}\sum_{q\in S_M} (\alpha^{q}_{m,k} b^{l,q}_{4,i} + \alpha^{q}_{l,k} b^{m,q}_{4,i} + \alpha^{q}_{m,l} b^{k,q}_{4,i}) + \frac{1}{2}\beta^{i}_{m,l,k} \end{aligned}$$

$$C^{3,k,l,m}_{10,i} = 2\sum_{q\notin S_M} \alpha^{i}_{k,q} a^{l,m}_{5,q}$$

APPENDIX C

MANIFOLD EXPANSION POLYNOMIALS

The expansion polynomials used in the first example of Chapter IV are as follows:

$$L_1(a) = \sqrt{6}(a/a_o)^2$$

$$L_2(a) = \sqrt{2}\,[-12(a/a_o)^2 + 14(a/a_o)^3]$$

$$L_3(a) = \sqrt{10}\,[-21(a/a_o)^2 + 56(a/a_o)^3 - 36(a/a_o)^4]$$

$$L_4(a) = \sqrt{3}\,[-112(a/a_o)^2 + 504(a/a_o)^3 - 720(a/a_o)^4 + 330(a/a_o)^5]$$

$$L_5(a) = \sqrt{14}\,[-126(a/a_o)^2 + 840(a/a_o)^3 - 1980(a/a_o)^4 + 1980(a/a_o)^5 - 715(a/a_o)^6]$$

$$L_6(a) = -1008(a/a_o)^2 + 9240(a/a_o)^3 - 31680(a/a_o)^4 + 51480(a/a_o)^5 - 40040(a/a_o)^6 + 12012(a/a_o)^7$$

$$L_7(a) = \sqrt{2}\,[-1386(a/a_o)^2 + 16632(a/a_o)^3 - 77220(a/a_o)^4 + 180180(a/a_o)^5 - 225225(a/a_o)^6 + 144144(a/a_o)^7 - 37128(a/a_o)^8]$$

APPENDIX D

ESTIMATED COMPUTATIONAL EFFORT

The approximate computational effort necessary to determine a manifold solution may roughly be expressed as:

$$E = (\#\text{ of iterations/subproblem})(\#\text{ of operations/iteration})(\#\text{ of subproblems})$$

The information on Powell's Hybrid method indicates that, for N_c coefficients, the number of iterations necessary may approach N_c^2. However, in practice, this has seldom been the case. On average, observations have indicated that about $1.25N_c$ iterations are necessary to reach a solution. When polynomials are used to approximate the a-dependence of the manifold, it has been necessary to use $100N_a$ points in the a direction of the numerical integration (more for $N_a > 5$). This is presumably due to the large values of the polynomial coefficients (seen in Appendix C). The number of points necessary on the ϕ direction is much more reasonable, and $10N_\phi$ has provided good results. This difference makes switching to local domains in a much more crutical than the same transition in ϕ.

If we represent the number of modes which need to be approximated by N (one less than the number of DOF), the number of coefficients, N_c, may be written as:

$$N_c = N \cdot N_a \cdot N_\phi.$$

Hence, the effort, E_o, correponding to the original approach of using both polynomials and harmonics, may be written as:

$$\begin{aligned} E_o &= (1.25N \cdot N_a \cdot N_\phi)(100N_a \cdot 10N_\phi)(1) \\ &= 1250NN_a^2N_\phi^2 \end{aligned}$$

When the a-dependence is discretized into locally linear domains, six points per domain were found to give accurate results. Also, it is assumed that 30 segments in a will accurately capture the manifold. Hence, the effort associated with this approach, E_a, may be expressed as:

$$\begin{aligned} E_a &= (1.25N \cdot 2 \cdot N_\phi)(6 \cdot 10N_\phi)(30) \\ &= 4500NN_\phi^2 \end{aligned}$$

Lastly, it is expected that 30 sements, with 6 points in each will be sufficient in the ϕ direction. This allows the effort for a solution which is discretized in both a and ϕ, $E_{a,\phi}$, to be written as:

$$\begin{aligned} E_{a,\phi} &= (1.25N \cdot 2 \cdot 2)(6 \cdot 6)(30 \cdot 30) \\ &= 162000N \end{aligned}$$

If a solution is sought which requires $N_a = 5$ polynomials, and $N_\phi = 8$ harmonics, we find the following:

$$\frac{E_a}{E_o} = 0.144,$$

indicating that a discretized solution in a reqires %14 of the effort associated with the original approach. Furthermore, discretization in ϕ produces:

$$\frac{E_{a,\phi}}{E_a} = 0.5625,$$

a solution which requires %56 of E_a. Consequently, shifting from the original approach to an entirely discretized solution should, for this case, yield a computational savings of %92.

Of course, there are many assumptions embedded in these calculations, but they are believed to represent the essential factors found in a typical problem.

BIBLIOGRAPHY

BIBLIOGRAPHY

[1] S. W. Shaw and C. Pierre. Non-linear normal modes and invariant manifolds. *Journal of Sound and Vibration*, 150(1):170–173, 1991.

[2] S. W. Shaw and C. Pierre. Normal modes for non-linear vibratory systems. *Journal of Sound and Vibration*, 164(1):85–124, 1993.

[3] S. W. Shaw and C. Pierre. Normal modes of vibration for non-linear continuous systems. *Journal of Sound and Vibration*, 169(3):319–347, 1994.

[4] S. W. Shaw. An invariant approach to nonlinear normal modes of vibration. *Journal of Nonlinear Science*, 4:419–448, 1994.

[5] A. H. Nayfeh and D. T. Mook. *Nonlinear Oscillations*. John Wiley & Sons, 1979.

[6] J. A. Stricklin and W. E. Haisler. Formulations and solution procedures for nonlinear structural analysis. *Computers and Structures*, 7:125–136, 1977.

[7] V. N. Shah, G. J. Bohm, and A. N. Nahavandi. Modal superposition method for computationally economical nonlinear structural analysis. *Journal of Pressure Vessel Technology, Transactions of the ASME*, 101:134–141, 1979.

[8] A. K. Noor. Recent advances in reduction methods for nonlinear problems. *Computers and Structures*, 13:31–44, 1981.

[9] K. Watanabe and H. Sato. Development of nonlinear building block approach. *Journal of Vibration, Acoustics, Stress, and Reliability in Design*, 110:36–41, 1988.

[10] C. J. Chang and B. Mohraz. Modal analysis of nonlinear systems with classical and non-classical damping. *Computers and Structures*, 36(6):1067–1080, 1990.

[11] M. I. Friswell, J. E. T. Penny, and S. D. Garvey. The application of the irs and balanced realization methods to obtain reduced models of structures with local nonlinearities. *Journal of Sound and Vibration*, 196(4):453–468, 1996.

[12] C. P. Atkinson and Beverly Tasket. A study of the nonlinearly related modal solutions of coupled nonlinear systems by superposition techniques. *Journal of Vibration and Acoustics, Transactions of the ASME*, 32:359–364, 1965.

[13] R. H. Rand. Nonlinear normal modes in two-degree-of-freedom systems. *Journal of Applied Mechanics, Transactions of the ASME*, 38:561, 1971.

[14] T. K. Caughey and A. F. Vakakis. A method for examining steady state solutions of forced discrete systems with strong nonlinearities. *International Journal of Non-Linear Mechanics*, 26(1):89–103, 1991.

[15] L. Jezequel and C. H. Lamarque. Analysis of non-linear dynamical systems by the normal form theory. *Journal of Sound and Vibration*, 149(3):429–459, 1991.

[16] A. H. Nayfeh, J. F. Nayfeh, and D. T. Mook. On methods for continuous systems with quadratic and cubic nonlinearities. *Nonlinear Dynamics*, 3:145–162, 1992.

[17] J. Aubrecht and A. F. Vakakis. Localized and non-localized nonlinear normal modes in a multi-span beam with geometric nonlinearities. *Journal of Applied Mechanics, Transactions of the ASME*, 118:533–542, 1996.

[18] M. Chati, R. Rand, and S. Mukherjee. Modal analysis of a cracked beam. *Journal of Sound and Vibration*, 207(2):249–270, 1997.

[19] G. Chakraborty, A. K. Mallik, and H. Hatwal. Normal modes and near-resonance response of beams with non-linear effects. *Journal of Sound and Vibration*, 210(1):19–36, 1998.

[20] L. Meirovitch. *Analytical Methods in Vibrations*. MacMillan Publishing Co., Inc., 1967.

[21] R. M. Rosenberg. On nonlinear vibrations of systems with many degrees of freedom. *Advances in Applied Mechanics*, 9:155–242, 1966.

[22] R. H. Rand. A direct method for non-linear normal modes. *International Journal of Non-linear Mechanics*, 9:363–368, 1974.

[23] M. E. King and A. F. Vakakis. An energy based approach to computing resonant nonlinear normal modes. *Journal of Applied Mechanics, Transactions of the ASME*, 63:810–819, 1996.

[24] Y. V. Mikhlin. Normal vibrations of a general class of conservative oscillators. *Nonlinear Dynamics*, 11:1–15, 1996.

[25] M. I. Qasi. Nonlinear normal modes of a lumped parameter system. *Journal of Sound and Vibration*, 205(2):205–211, 1997.

[26] M. E. King and A. F. Vakakis. An energy based formulation for computing nonlinear normal modes in undamped continuous systems. *Journal of Vibrations and Acoustics, Transactions of the ASME*, 116:332–340, 1994.

[27] M. I. Qasi. A power series solution for the non-linear vibration of beams. *Journal of Sound and Vibration*, 199(4):587–594, 1997.

[28] M. I. Qasi. Nonlinear normal modes of a continuous system. *Journal of Sound and Vibration*, 209(4):561–569, 1998.

[29] N. Boivin, C. Pierre, and S. W. Shaw. Non-linear modal analysis of structural systems using multi-mode invariant manifolds. In *Proceedings of the AIAA Dynamics Specialists Conference, Paper No. 94-1672*, Hilton Head, South Carolina, 1994.

[30] N. Boivin, C. Pierre, and S. W. Shaw. Non-linear normal modes, invariance, and modal dynamics approximations of non-linear systems. *Nonlinear Dynamics*, 8:315–346, 1995.

[31] N. Boivin, C. Pierre, and S. W. Shaw. Non-linear modal analysis of structural systems featuring internal resonances. *Journal of Sound and Vibration*, 182(2):336–341, 1995.

[32] J. Carr. *Applications of Center Manifold Theory*. Springer-Verlag, 1981.

[33] R. Temam. Inertial manifolds. *The Mathematical Intelligencer*, 12:68–74, 1990.

[34] N. Boivin. *Non-linear Modal Analysis of Structural Systems Using Invariant Manifolds*. PhD thesis, The University of Michigan, Ann Arbor, MI., 1995.

[35] A. J. Roberts. The invariant manifold of beam deformations. *Journal of Elasticity*, 30:1–54, 1993.

[36] I. T. Georgiou and I. B. Schwartz. Slaving the in-plane motions of a nonlinear plate to its flexural motions: An invariant manifold approach. *Journal of Applied Mechanics, Transactions of the ASME*, 64:175–182, 1997.

[37] I. T. Georgiou, A. K. Bajaj, and M. Corless. Slow and fast invariant manifolds, and normal modes in a two degree-of freedom structural dynamical system with multiple equilibrium states. *International Journal of Non-linear Mechanics*, 33(2):275–300, 1998.

[38] T. B. Burton and M. N. Hamdan. On the calculation of non-linear normal modes in continuous systems. *Journal of Sound and Vibration*, 197(1):117–130, 1996.

[39] A. H. Nayfeh, C. Chin, and S. A. Nayfeh. On nonlinear normal modes of systems with internal resonance. *Journal of Vibrations and Acoustics, Transactions of the ASME*, 118:340–345, 1996.

[40] J. C. Slater. A numerical method for determining nonlinear normal modes. *Nonlinear Dynamics*, 10:19–30, 1996.

[41] Shyh-Leh Chen and S. W. Shaw. Normal modes for piecewise linear vibratory systems. *Nonlinear Dynamics*, 10:135–164, 1996.

[42] A. Y. T. Leung and T. Ge. Normal multi-modes of non-linear euler beams. *Journal of Sound and Vibration*, 202(2):145–160, 1997.

[43] J. C. Slater and D. J. Inman. On the effect of weak non-linearities on linear controllability and observability norms, an invariant manifold approach. *Journal of Sound and Vibration*, 199(3):417–429, 1997.

[44] A. F. Vakakis, L. I. Manevitch, Y. V. Mikhlin, V. N. Pilipchuck, and A. A. Zevin. *Normal Modes and Localization in Nonlinear Systems.* John Wiley & Sons, 1996.

[45] A. F. Vakakis. Non-linear normal modes (nnms) and their applications in vibration theory: An overview. *Mechanical Systems and Signal Processing*, 11(1):3–22, 1997.

[46] A. Stiendl, H. Troger, and J. Zemann. Improved galerkin method in the dimension reduction of nonlinear dynamical systems. In Francis C. Moon, editor, *IUTAM Symposium on New Applications of Nonlinear and Chaotic Dynamics in Mechanics. Proceedings of the IUTAM Symposium held in Ithica, NY, July 27-August 1, 1997*, 1999.

[47] B. F. Feeny. Interpreting proper orthogonal modes in vibrations. In *Proceedings of DET'97, 1997 ASME Design Engineering Technical Conferences, September 14-17, 1997, Paper No. VIB-3955*, Sacramento, California, 1997.

[48] N. Boivin, C. Pierre, and S. W. Shaw. Non-linear modal analysis of the forced response of structural systems. In *Proceedings of the AIAA Dynamics Specialists Conference, Paper No. 96-1250*, Salt Lake City, Utah, 1996.

[49] R. H. Rand. Personal Communication, 1995.

[50] Shang-Rou Hsieh, S. W. Shaw, and C. Pierre. Normal modes for large amplitude vibration of a cantilever beam. *International Journal of Solids and Structures*, 31(14):1981–2014, 1994.

[51] A. H. Nayfeh. On direct methods for constructing nonlinear normal modes of continuous systems. *Journal of Vibration and Control*, 1(4):389–430, 1995.

[52] C. E. N. Mazzilli. Personal Communication, 1997.

[53] P. P. Friedmann. Recent developments in rotary-wing aeroelasticity. *Journal of Aircraft*, 14(11):1027–1041, 1977.

[54] D. H. Hodges, A. S. Hopkins, and D. L. Kunz. Analysis of structures with rotating, flexible substructures applied to rotorcraft aeroelasticity. *AIAA Journal*, 27(2):192–200, 1989.

[55] J. B. Kosmatka and P. P. Friedmann. Vibration analysis of composite turbopropellers using a nonlinear beam-type finite-element approach. *AIAA Journal*, 27(11):1606–1614, 1989.

[56] D. H. Hodges and E. H. Dowell. Nonlinear equations of motion for the elastic bending and torsion of twisted nonuniform rotor blades. TN D-7818, NASA, 1974.

[57] M. R. M. Crespo Da Silva and D. H. Hodges. Nonlinear flexure and torsion of rotating beams, with application to helicopter rotor blades—I. formulation. *Vertica*, 10(2):151–169, 1986.

[58] J. C. Simo and L. Vu-Quoc. On the dynamics in space of rods undergoing large motions — a geometrically exact approach. *Computer Methods in Applied Mechanics and Engineering*, 66:125–161, 1988.

[59] A. D. Wright, C. E. Smith, R. W. Thresher, and J. L. C. Wang. Vibration modes of centrifugally stiffened beams. *Journal of Applied Mechanics*, 49:197–202, 1982.

[60] H. Du, M. K. Lim, and K. M. Liew. A power series solution for vibration of a rotating timoshenko beam. *Journal of Sound and Vibration*, 175(4):505–523, 1994.

[61] S. Naguleswaran. Lateral vibration of a centrifugally tensioned uniform euler-bernoulli beam. *Journal of Sound and Vibration*, 176(5):613–624, 1994.

[62] H. H. Yoo and S. H. Shin. Vibration analysis of rotating cantilever beams. *Journal of Sound and Vibration*, 212(5):807–828, 1998.

[63] E. Pesheck, C. Pierre, S. W. Shaw, and N. Boivin. Nonlinear modal analysis of structural systems using multi-mode invariant manifolds. *Nonlinear Dynamics*, Accepted for publication, 1999.

[64] S. W. Shaw, C. Pierre, and E. Pesheck. Modal analysis-based reduced-order models for nonlinear structures—an invariant manifold approach. *Shock and Vibration Digest*, 31(1):3–16, 1999.

[65] E. Pesheck, C. Pierre, and S. W. Shaw. Modal reduction of a nonlinear rotating beam through nonlinear normal modes. *Journal of Vibration and Acoustics, Transactions of the ASME*, Submitted for publication, 1999.

[66] W. H. Press, S. A. Teukolsky, W. T. Vetterling, and B. P. Flannery. *Numerical Recipies in C: The Art of Scientific Computing*. Cambridge University Press, 1992.

[67] A. Hopkins, G. Ruzicka, and R. Ormiston. Analytical investigations of coupled rotorcraft/engine/drive train dynamics. In *Proceedings of the American Helicopter Society 2nd International Aeromechanics Specialists Conference*, Bridgeport, Connecticut, 1995.

[68] G. Ruzicka and D. Hodges. Application of the mixed finite element method to rotor blade modal reduction. In *Proceedings of the Eighth ARO Workshop on Aeroelaticity of Rotorcraft Systems*, Penn State University, 1999.

[69] E. Pesheck, C. Pierre, and S. W. Shaw. Accurate nonlinear modal analysis through optimized invariant manifolds. *Journal of Sound and Vibration*, Submitted for publication, 2000.

[70] E. Pesheck and C. Pierre. Analysis of a friction damped system using two component mode methods. *Journal of Vibration and Acoustics, Transactions of the ASME*, Submitted for publication, 2000.

ABSTRACT

REDUCED ORDER MODELING OF NONLINEAR STRUCTURAL SYSTEMS USING NONLINEAR NORMAL MODES AND INVARIANT MANIFOLDS

by

Eric Pesheck

Co-Chairs: Christophe Pierre, Steve Shaw

The generation of reduced-order models of nonlinear systems is particularly difficult, due to the complex interactions of the system components. This work applies the invariant manifold formulation for nonlinear normal modes to create rigorous reduced-order models of a wide variety of nonlinear structures, including discrete, finite element, and continuous dynamic systems. This is accomplished through two types of expansion-based solutions for the invariant manifolds which govern the nonlinear normal modes of the structure.

The first expansion is polynomial-based and produces analytic, third-order, invariant manifolds which are asymptotically accurate. The solution obtained is applicable to a subclass of weakly nonlinear structural systems with quadratic and cubic nonlinearities in displacement. The second method uses a Galerkin projection and numerical solver to determine the invariant manifold over a chosen domain. This approach is shown to be accurate for strong nonlinear effects as well as being more

adaptable than the polynomial-based approach. Both methods are applied to various nonlinear structural systems, and the results indicate that, in general, the high accuracy of the Galerkin-based solution compensates for the additional computational effort.

One field in which nonlinear interactions play a critical role, and are difficult to capture, is rotorcraft dynamics. In particular, blade simulations are cumbersome due to the large models which have been necessary to achieve accurate results. Equations of motion are developed for a uniform nonlinear Euler-Bernoulli beam, rotating at constant velocity, and constrained to move in only the transverse and axial directions. In the interest of improving the rotorcraft design process, the above reduction methods were applied to this simplified blade model. The results indicate that, although both methods capture the critical nonlinear coupling terms at low amplitudes, the Galerkin-based solution achieves excellent results, allowing accurate analysis for tip deflections as large as one meter (peak-to-peak), for a nine meter blade. However, the polynomial-based solutions remain applicable, as they allow investigations of internal resonances which are currently not possible using the present Galerkin-based formulation.